

DTIC FILE COPY

4

AFGL-TR-88-0112

A Wind Dependent Desert Aerosol Model:
Radiative Properties

David R. Longtin
Eric P. Shettle
John R. Hummel
James D. Pryce

OptiMetrics, Inc
50 Mill Road
Burlington, MA 01803

DTIC
ELECTE
DEC 29 1988
S D
&D

19 April 1988

Scientific Report No. 6

APPROVED FOR PUBLIC RELEASE; DISTRIBUTION UNLIMITED

AIR FORCE GEOPHYSICS LABORATORY
AIR FORCE SYSTEMS COMMAND
UNITED STATES AIR FORCE
HANSCOM AIR FORCE BASE, MASSACHUSETTS 01731-5000

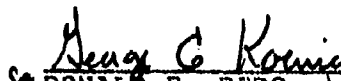
AD-A201 951

88 12 27 151

"This technical report has been reviewed and is approved for publication"

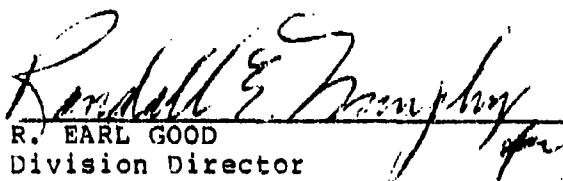


ERIC P. SHETTLE
Contract Manager



DONALD E. BEDO
Branch Chief

FOR THE COMMANDER



R. EARL GOOD
Division Director

This report has been reviewed by the ESD Public Affairs Office (PA) and is releasable to the National Technical Information Service (NTIS).

Qualified requestors may obtain additional copies from the Defense Technical Information center. All others should apply to the National Technical Information Service.

If your address has changed, or if you wish to be removed from the mailing list, or if the addressee is no longer employed by your organization, please notify AFGL/DAA, Hanscom AFB, MA 01731. This will assist us in maintaining a current mailing list.

Do not return copies of this report unless contractual obligations or notices on a specific document requires that it be returned.

DISCLAIMER NOTICE

THIS DOCUMENT IS BEST QUALITY PRACTICABLE. THE COPY FURNISHED TO DTIC CONTAINED A SIGNIFICANT NUMBER OF PAGES WHICH DO NOT REPRODUCE LEGIBLY.

ADA 201 951

REPORT DOCUMENTATION PAGE

1a. REPORT SECURITY CLASSIFICATION Unclassified		1b. RESTRICTIVE MARKINGS	
2a. SECURITY CLASSIFICATION AUTHORITY		3. DISTRIBUTION/AVAILABILITY OF REPORT Approved for public release; distribution unlimited	
2b. DECLASSIFICATION/DOWNGRADING SCHEDULE		4. PERFORMING ORGANIZATION REPORT NUMBER(S) OMI-221	
4. PERFORMING ORGANIZATION REPORT NUMBER(S)		5. MONITORING ORGANIZATION REPORT NUMBER(S) AFGL-TR-88-0112	
6a. NAME OF PERFORMING ORGANIZATION OptiMetrics, Inc.	6b. OFFICE SYMBOL (if applicable)	7a. NAME OF MONITORING ORGANIZATION Air Force Geophysics Laboratory	
6c. ADDRESS (City, State, and ZIP Code) 50 Mall Road Burlington, Massachusetts 01803		7b. ADDRESS (City, State, and ZIP Code) Hanscom Air Force Base Massachusetts 01731	
8a. NAME OF FUNDING/SPONSORING ORGANIZATION Air Force Geophysics Lab	8b. OFFICE SYMBOL (if applicable)	9. PROCUREMENT INSTRUMENT IDENTIFICATION NUMBER F19628-85-C-0178	
8c. ADDRESS (City, State, and ZIP Code) Hanscom AFB, MA 01731		10. SOURCE OF FUNDING NUMBERS	
		PROGRAM ELEMENT NO 6210F 6210F	PROJECT NO 7670 7670
		TASK NO. 15 15	WORK UNIT ACCESSION NO. AI 16*
11. TITLE (Include Security Classification) A Wind Dependent Desert Aerosol Model: Radiative Properties			
12. PERSONAL AUTHOR(S) David R. Longtin, Eric P. Shettle,* John R. Hummel and James D. Pryce			
13a. TYPE OF REPORT Scientific #6	13b. TIME COVERED FROM 11/86 to 04/88	14. DATE OF REPORT (Year, Month, Day) April 19, 1988.	15. PAGE COUNT 114
16. SUPPLEMENTARY NOTATION *This work was partially accomplished under Inhouse Work Unit #7670 15 16 **AFGL/OPA, Hanscom AFB, MA 01731			
17. COSATI CODES		18. SUBJECT TERMS (Continue on reverse if necessary and identify by block number)	
FIELD	GROUP	Indices of Refraction, Desert Aerosol, Aerosol Modeling, Single Scattering Albedo, Radiative Transfer, Optical Properties. (11411) ←	
19. ABSTRACT (Continue on reverse if necessary and identify by block number)			
<p>This report presents a desert aerosol model that predicts aerosol radiative properties during background and severe dust storm conditions. The model treats the desert aerosol as an external mixture of natural carbon, water soluble and sand particles. The sand consists of two kinds of particles, pure quartz and quartz contaminated with a small amount of hematite. Mie calculations are performed using different size distributions and indices of refraction for each type of particle, and then a volume-weighting scheme is used to obtain the radiative properties of the aerosol as a whole.</p> <p>Attenuation coefficients, single scattering albedo and asymmetry parameter are given for 68 wavelengths between 0.2 and 300 μm. The results indicate that extinction is wavelength dependent for background conditions, but increases and becomes nearly constant for dust storm conditions. (over)</p>			
20. DISTRIBUTION/AVAILABILITY OF ABSTRACT <input type="checkbox"/> UNCLASSIFIED/DUNLIMITED <input type="checkbox"/> SAME AS RPT <input type="checkbox"/> DTIC USERS		21. ABSTRACT SECURITY CLASSIFICATION Unclassified	
22a. NAME OF RESPONSIBLE INDIVIDUAL Eric P. Shettle		22b. TELEPHONE (Include Area Code)	22c. OFFICE SYMBOL AFGL/OPA

19. Abstract (cont.)

Also, hematite in the sand particles leads to selective absorption at visible wavelengths, which becomes more pronounced as the wind speed increases.

The radiative properties of the present model are then compared with other desert aerosol formulations. The comparisons suggest that the absorption at wavelengths between about 0.6 and 2.0 μm is less than that calculated by previous models.



Accession For	
NTIS CRA&I	<input checked="" type="checkbox"/>
DTIC TAB	<input type="checkbox"/>
Unannounced	<input type="checkbox"/>
Justification	
By	
Distribution	
Availability Codes	
Dist	Availability Codes
A-1	

Contents

1.	INTRODUCTION	1
1.1	Organization of Report	2
2.	PHYSICAL PROPERTIES OF DESERT AEROSOLS	3
2.1	Source Regions and Transport Characteristics	5
2.2	Size Distributions	6
2.3	Composition	8
2.4	Effects of Wind	10
2.5	Indices of Refraction	12
2.5.1	An Assessment of the Available Measurement Techniques	13
2.5.1.1	In Situ Measurements	13
2.5.1.2	An Aerosol Sample Suspended in a KBr Disk	14
2.5.1.3	Diffuse Reflection Techniques	15
2.5.2	Reported Values of the Indices of Refraction for Desert Aerosols	15
2.5.2.1	Real Part	15
2.5.2.2	Imaginary Part	16
2.5.3	Concerns Over the Reported Values	18
2.6	Radiative Impacts	20
2.7	Conclusions That Can Be Drawn From Previous Studies	22
3.	THE PRESENT DESERT AEROSOL MODEL	23
3.1	Overview	23
3.2	Wind Speed Dependence On Aerosol Loading	24
3.3	Indices of Refraction	30
3.3.1	Carbonaceous and Water Soluble Components	30

		Contents
3.3.2	Sand Component	30
3.3.3	Discussion of the Indices of Refraction	47
3.4	Method of Determining the Optical Properties of Multicomponent Mixtures	47
4.	RESULTS	49
4.1	Results for Various Concentrations of Hematite in the Sand Component	49
4.2	Choosing a Sand Component for the Desert Aerosol Model	52
4.3	General Discussion of the Desert Aerosol Model	52
4.4	Comparison with Other Researchers	59
4.5	Comparison with Observations	68
5.	SUMMARY AND CONCLUSIONS	69
REFERENCES		70
APPENDIX A:	AEROSOL FRACTIONS BY VOLUME AS A FUNCTION OF WIND SPEED	A-1
APPENDIX B:	MIE SCATTERING CALCULATIONS FOR THE THREE COMPONENTS	B-1
APPENDIX C:	RADIATIVE PROPERTIES OF THE DESERT AEROSOL AS A FUNCTION OF WIND SPEED	C-1

Illustrations

1.	Values of the Imaginary Index of the Desert Aerosol Reported by Other Researchers (From Carlson and Benjamin ³⁰)	17
2.	Number Density Distribution of the Desert Aerosol for Four Wind Speeds	28
3.	Area Distribution of the Desert Aerosol for Four Wind Speeds	29
4.	Indices of Refraction of Carbonaceous Material and Ammonium Sulfate, (a) Real part and (b) Imaginary Part	33
5.	Indices of Refraction of Quartz, (a) Real part and (b) Imaginary Part	38

Illustrations

6. Indices of Refraction of Hematite, (a) Real part and (b) Imaginary Part	40
7. Real Part of the Index of Refraction for Sand Having Hematite Concentrations of 0, 5, and 10%, (a) O-Ray and (b) E-Ray	44
8. Imaginary Part of the Index of Refraction for Sand Having Hematite Concentrations of 0, 5, and 10%, (a) O-Ray and (b) E-Ray	45
9. Desert Aerosol Model (a) Absorption Coefficient and (b) Single Scattering Albedo using Cases 1, 3 and 5 for the Sand Component with 0 ms^{-1} Wind Speeds	51
10. Desert Aerosol Model (a) Absorption Coefficient and (b) Single Scattering Albedo using Cases 1, 3 and 5 for the Sand Component with 10 ms^{-1} Wind Speeds	51
11. Desert Aerosol Model (a) Absorption Coefficient and (b) Single Scattering Albedo using Cases 1, 3 and 5 for the Sand Component with 20 ms^{-1} Wind Speeds	53
12. Desert Aerosol Model (a) Absorption Coefficient and (b) Single Scattering Albedo using Cases 1, 3 and 5 for the Sand Component with 30 ms^{-1} Wind Speeds	53
13. Desert Aerosol Model Attenuation Coefficients Versus Wavelength for 0 ms^{-1} Wind Speed Conditions	54
14. Desert Aerosol Model Attenuation Coefficients Versus Wavelength for 10 ms^{-1} Wind Speed Conditions	54
15. Desert Aerosol Model Attenuation Coefficients Versus Wavelength for 20 ms^{-1} Wind Speed Conditions	55
16. Desert Aerosol Model Attenuation Coefficients Versus Wavelength for 30 ms^{-1} Wind Speed Conditions	55
17. Single Scattering Albedo of the Desert Aerosol Model Versus Wavelength for 0 and 30 ms^{-1} Wind Speed Conditions	58
18. Asymmetry Parameter of the Desert Aerosol Model Versus Wavelength for 0 and 30 ms^{-1} Wind Speed Conditions	60

Illustrations

19. Number Density Distributions for the Present Desert Aerosol Model and Those of d'Almeida ³⁴	61
20. Area Distributions for the Present Desert Aerosol Model and Those of d'Almeida	62
21. Comparison of Extinction Coefficients for the Desert Aerosol Model With Those of (a) Shettle ¹ and (b) d'Almeida ³⁴	64
22. Comparison of Scattering Coefficients for the Desert Aerosol Model With Those of (a) Shettle ¹ and (b) d'Almeida ³⁴	64
23. Comparison of Absorption Coefficients of the Desert Aerosol Model with (a) ³⁴ Those of Shettle ¹ and (b) Those of d'Almeida	65
24. Comparison of Single Scattering Albedos for the Desert Aerosol Model With Those of Shettle ¹ and d'Almeida ³⁴ , (a) Background and (b) Dust Storm Conditions	67
25. Comparison of Asymmetry Parameters for the Desert Aerosol Model With Those of Shettle ¹ and d'Almeida ³⁴ , (a) Background and (b) Dust Storm Conditions	67
C-1. Normalized Angular Scattering Function of the Desert Aerosol for a Wavelength of 0.55 μm	C-11
C-2. Normalized Angular Scattering Function of the Desert Aerosol for a Wavelength of 1.06 μm	C-13
C-3. Normalized Angular Scattering Function of the Desert Aerosol for a Wavelength of 10.591 μm	C-15

Tables

1. Summary of Measurements of Aerosols from Arid or Semi-arid Environments	4
2. Parameters Used in the Background Desert and Desert Dust Storm Aerosol Models	7

Tables

3.	Variation of Elemental Concentrations in Middle Eastern Desert Aerosols As (a) A Function of Source Region and (b) Averaged Over Meteorological Conditions	10
4.	Density of Each Component of the Desert Aerosol Model and Aerosol Fraction by Volume for Background Conditions	24
5.	Wind Speed Dependence of the Desert Aerosol Size Distribution Parameters	25
6.	Mass Loading of the Desert Aerosol as a Function of Wind Speed	27
7.	Indices of Refraction for Carbonaceous Material	31
8.	Indices of Refraction for Ammonium Sulfate	32
9.	Indices of Refraction for the O-Ray of Quartz	35
10.	Indices of Refraction for the E-Ray of Quartz	36
11.	Indices of Refraction for Hematite	39
12.	Indices of Refraction for Sand Having a Volume Fraction of Hematite of 5%	42
13.	Indices of Refraction for Sand Having a Volume Fraction of Hematite of 10%	43
14.	Various Compositions of the Sand Component Investigated in this Report	49
B-1.	Mie Scattering Results for the Carbonaceous Component Normalized to 1 Particle cm^{-3}	B-2
B-2.	Mie Scattering Results for the Water Soluble Component Normalized to 1 Particle cm^{-3}	B-4
B-3.	Mie Scattering Results for the Sand Component With a 0 ms^{-1} Wind Normalized to 1 Particle cm^{-3}	B-6
B-4.	Mie Scattering Results for the Sand Component With a 10 ms^{-1} Wind Normalized to 1 Particle cm^{-3}	B-8
B-5.	Mie Scattering Results for the Sand Component With a 20 ms^{-1} Wind Normalized to 1 Particle cm^{-3}	B-10
B-6.	Mie Scattering Results for the Sand Component With a 30 ms^{-1} Wind Normalized to 1 Particle cm^{-3}	B-12

Tables

B-7. Surface Area and Volume of Each Aerosol Component of the Desert Aerosol Model per Unit Volume of Air for a Number Density of 1 Particle cm^{-3}	B-14
C-1. Radiative Properties of the Desert Aerosol for 0 ms^{-1} Wind Speed Conditions	C-2
C-2. Radiative Properties of the Desert Aerosol for 10 ms^{-1} Wind Speed Conditions	C-4
C-3. Radiative Properties of the Desert Aerosol for 20 ms^{-1} Wind Speed Conditions	C-6
C-4. Radiative Properties of the Desert Aerosol for 30 ms^{-1} Wind Speed Conditions	C-8
C-5. Normalized Angular Scattering Function for the Desert Aerosol Model as a Function of Wind Speed for a Wavelength of $0.55 \mu\text{m}$	C-10
C-6. Normalized Angular Scattering Function for the Desert Aerosol Model as a Function of Wind Speed for a Wavelength of $1.06 \mu\text{m}$	C-12
C-7. Normalized Angular Scattering Function for the Desert Aerosol Model as a Function of Wind Speed for a Wavelength of $10.591 \mu\text{m}$	C-14

1. INTRODUCTION

Aerosols can be found throughout the atmosphere. They can have a role in cloud formation and precipitation processes and plus they can have an impact on the radiation balance of the earth-atmosphere system. The radiative impact will depend on the size, shape and composition of the aerosols, as well as their spatial distribution in the atmosphere and the nature of the underlying surface.

Aerosols can be separated into a set of generic categories based primarily on their (spatial) location in the atmosphere. Each aerosol "type" has its own characteristic optical properties that distinguish it from other aerosols. For most aerosol types, a set of parameters exist for calculating aerosol radiative properties with reasonable accuracy.

An important aerosol type is the desert aerosol which is representative of arid and semi-arid regions. This category has been added because about one-third of the earth's land surface area consists of arid and semi-arid terrain and because the radiative effects of desert aerosols are important during dust storm conditions. In addition, the source regions of desert aerosols have high solar insolation and strong convective processes that enable the particles to be lifted to altitudes where synoptic-scale air motions can transport the particles well beyond their source regions.

A tentative desert aerosol model was developed¹ for use in the Air Force Geophysics Laboratory (AFGL) model atmospheres. This model was based primarily on recommendations from a meeting of experts conducted by the World Climate Research Programme². It is the purpose of the present study to examine the features of that formulation and to present improvements to it.

1.1 Organization of Report

Chapter 2 reviews the literature pertaining to the physical properties of desert aerosols. Chapter 3 presents a model that can be used to calculate desert aerosol radiative properties. Chapter 4 discusses the implications of the new desert aerosol model and compares it against observed data and models used by other researchers. Finally, Chapter 5 summarizes our results.

-
1. Shettle, E. P. (1984) Optical and radiative properties of a desert aerosol model, IRS '84: Current Problems in Atmospheric Radiation, G. Flocco, Ed., A. Deepak Publishing, Hampton, VA, 74-77.
 2. World Climate Research Programme (1983) Report of the Experts Meeting on Aerosols and Their Climatic Effects, Deepak, A., and H. E. Gerber, eds. World Climate Program Publication WCP-55, December 1983.

2. PHYSICAL PROPERTIES OF DESERT AEROSOLS

The desert aerosol model that has been recommended by the World Climate Research Programme² and utilized by Shettle¹ is based on a limited data set. The formulation uses data that were obtained primarily in the Middle East, although measurements from other arid and desert locations have been included. Table 1 provides a partial listing of measurements³⁻¹³ that

3. d'Almeida, G. and Schutz, L. (1983) Number, mass and volume distributions of mineral aerosol and soils of the Sahara, J. Climate and Appl. Meteor., 22:233-243.
4. Patterson, E. M. and Gillette, D. A. (1977) Commonalities in measured size distributions for aerosols having a soil-derived component, J. Geophys. Res., 82:2074-2082.
5. Schutz, L. and Jaenicke, R. (1974) Particle number and mass distributions above 10^{-4} cm radius in sand and aerosols of the Sahara Desert, J. Appl. Meteor., 13:863-870.
6. Levin, Z. and Lindberg, J. D. (1979) Size distribution, chemical composition, and optical properties of urban and desert aerosols in Israel, J. Geophys. Res., 84:6941-6950.
7. Kushelevsky, A., Shani G. and Haccoun A. (1983) Effect of meteorologic conditions on total suspended particulate (TSP) levels and elemental concentration of aerosols in a semi-arid zone (Beer-Sheva, Israel), Tellus, 35B:55-64.
8. Cahill, T. A., Kusko, B. H., Ashbaugh, L. L., Barone, J. B., Eldred, R. A. and Walther, F. G. (1981) Regional and local determinations of particulate matter and visibility in the southwestern United States during June and July, 1979, Atmospheric Environment, 15:2011-2016.
9. Annegarn, H. J., Van Greiken, R. E., Bibby, D. M. and Von Blottnitz, F (1983) Background aerosol composition in the Namib Desert, south west Africa (Namibia), Atmospheric Environment, 17:2045-2053.
10. Pinnick, R. G., Jennings, S. G and Fernandez, G. (1987) Volatility of aerosols in the arid southwestern United States, J. Atmos. Sci., 44:562-576.
11. Levin, Z., Joseph, J. H. and Mekler, Y (1980) Properties of Sharav (Khamsin) Dust - Comparison of optical and direct sampling data, J. Atmos. Sci., 37:882-891.

relate to the physical properties of aerosols in arid or desert environments.

Table 1. Summary of Measurements of Aerosols from Arid or Semi-arid Environments

LOCATION	PERIOD OF MEASUREMENTS	MEASUREMENT TYPE	REFERENCE
Central Sahara	Feb 1979 - Feb 1982	SD	d'Almeida and Schutz ³
Haskell, Colorado	Unknown	SD	Patterson and Gillette ⁴
Plains, Texas	Unknown	SD	Patterson and Gillette ⁴
Camp Dery and Sebha, Libya	Unknown	SD	Schutz and Jaenicke ⁵
Mitzpe Ramon (Negev Desert), Israel	Winter and Early Spring 1976	SD, RAD Comp	Levin and Lindberg ⁶
Beer-Sheva, Israel	June 1977 - May 1978	Comp, TML	Kushelevaky et al. ⁷
Arizona and Utah	June - July 1979	Comp, TML	Cahill et al. ⁸
Namib Desert	Nov 1976 - April 1977	Comp	Annegarn et al. ⁹
Tularosa Basin, NM	Aug 1984 - Aug 1985	Comp, SD	Pinnick et al. ¹⁰
Mitzpe Ramon (Negev Desert), Israel	Dust Storm on 6 June 1977	SD, RAD	Levin et al. ¹¹
Grand Canyon, Arizona	Dec 1979 - Nov 1981	TML, RAD	Malm and Johnson ¹²
Iran and Pakistan	Unknown	RAD	Ottorman et al. ¹³

Key: SD - Size Distributions, Comp - Composition, RAD - Radiative Measurements
TML - Total Mass Loadings

12. Malm, W. C. and Johnson, C. E. (1984) Optical characteristics of fine and coarse particulates at Grand Canyon, Arizona, Atmospheric Environment, 18:1231-1237.
13. Ottorman, J., Fraser, R. S., and Bahethi, O. P. (1982) Characterization of tropospheric desert aerosols at solar wavelengths by multispectral radiometry from Landsat, J. Geophys. Res., 87:1270-1278.

2.1 Source Regions and Transport Characteristics

Desert aerosols have been measured at great distances from their source regions. Saharan aerosols have been measured well into the tropical North Atlantic^{14,15} and in Mediterranean countries^{16,17,18}. Desert aerosols originating from Asian deserts have been measured in the Hawaiian Islands¹⁹. The bulk aerosols in the lower few kilometers of the troposphere over the tropical North Atlantic consist primarily of sea-salt aerosols and mineral aerosols originating from the arid and semi-arid regions of West Africa¹⁴.

These measurements indicate that the aerosols at a given location are not necessarily representative of the underlying soils. d'Almeida and Schutz³ have shown from their data of soil samples and aerosol samples from across the Sahara that the aerosols are largely made up of crustal material that are representative of loose and finely grained soils. They state

-
14. Junge, C. and Jaenicke, R. (1971) New results in background aerosols studies from the Atlantic expedition of the R. V. Meteor, Spring 1969, Aerosol Science, 2:305-314.
 15. Savoie, D. L. and Prospero, J. M. (1977) Aerosol concentration statistics for the Northern Tropical Atlantic, J. Geophys. Res., 82:5954-5964.
 16. Schmidt, M., Specht, H. and Fabian, P. (1978) Aerosol measurements at the Algarve Coast of Portugal, Tellus, 30:449-457.
 17. Ganor, E. and Mamane, Y. (1982) Transport of Saharan dust across the Eastern Mediterranean, Atmospheric Environment, 16:581-587.
 18. Chester, R., Sharples, E. J., Sanders, G. S. and Saydam, A. C. (1984) Saharan dust incursion over the Tyrhenian Sea, Atmospheric Environment, 18:929-935.
 19. Shaw, G. E. (1980) Transport of Asian desert aerosol to the Hawaiian Islands, J. Appl. Meteor., 19:1254-1259.

that wadis and floodplains near mountains offer probable production source areas for desert aerosols rather than dune-like deposits. These results are consistent with those of Chester et al.¹⁸ who performed an elemental analysis of aerosols from over the Tyrrhenian Sea. Their data indicated that the aerosols are characteristic of crystal material rather than from dune areas.

2.2 Size Distributions

Aerosol size distributions are often modeled by the sum of two or three log normal distributions,

$$\frac{dN(r)}{d \log r} = \sum_{i=1}^{2,3} \frac{N_i}{(2\pi)^{1/2} \log \sigma_i} \exp\left(-\frac{[\log(r/R_i)]^2}{2(\log \sigma_i)^2}\right) \quad (1)$$

where $N(r)$ is the particle concentration for particles greater than a given radius r , N_i is the total number of particles for the distribution i , σ_i is the geometric standard deviation and R_i is the geometric mean radius. The individual distributions are often meant to represent different size classifications that are representative of different production processes. Three size ranges², $10^{-7} < r < 10^{-5}$ cm, $10^{-5} < r < 10^{-4}$ cm and $r > 10^{-4}$, cm are typically used to describe aerosols in the atmosphere. The size ranges are referred to, respectively, as the Aitken or nucleation mode, the large or accumulation mode and the giant or coarse mode.

Based on an analysis of tropospheric aerosol measurements, Patterson and Gillette⁴ characterized the distributions with three modes that they referred to as (respectively),

modes C, A and B. Mode C represents particles centered at about 0.02 - 0.5 μm and is representative of background aerosols. Mode A particles cover the radius range 1 - 10 μm and consist of particles produced from the parent soil by a sandblasting process. This component of the size distribution is determined by the lifting force of the local winds. Mode B particles peak at about 30 μm radius and are primarily found when the wind speed is high and the dustloading is significant. Under heavy dust loading conditions, Patterson and Gillette found that only modes A and B were present as a result of soil erosion and sandblasting plus the subsequent injection of this material into the atmosphere. These results suggest that different size distribution formulations were needed to describe background desert and duststorm conditions.

The size distributions used in the tentative AFGL desert aerosol model, which were based on recommendations from the World Climate Research Programme², are shown in Table 2.

Table 2. Parameters Used^{1,2} in the Background Desert and Desert Dust Storm Aerosol Models^{1,2}

MODEL	i	N_i (cm^{-3})	$\log(\sigma_i)$	R_i (μm)
Background	1	997	0.328	0.0010
	2	842	0.505	0.0218
	3	7.10×10^{-4}	0.277	6.24
Dust Storm	1	726	0.247	0.0010
	2	1,140	0.770	0.0188
	3	1.78×10^{-1}	0.438	10.8

These values are based primarily on measurements^{14,20,21} from the Sahara. For calm (or background) conditions, the parameters are similar to those for "remote continental aerosols." The parameters for the dust storm conditions are based on the work of Schutz and Jaenicke⁵, Jaenicke and Schutz²⁰ and d'Almeida and Jaenicke²¹. The major difference between the model for background and dust storm conditions is in the number of large particles in mode 3, the component associated with large particles that are injected by high winds. Therefore, the values for the dust storm model represent extreme values and should be linked to wind velocity.

2.3 Composition

Compositional measurements indicate that desert aerosols are a mixture of different kinds of materials. Desert aerosols consist of a background component and a component representative of local soil sources. Depending upon location, desert aerosols can also have an anthropogenic component.

Simple visual examination of desert dust reveals many of the particles to have a light brown to tan appearance⁶ unlike urban aerosols that are generally gray or black. Elements commonly found in desert aerosols^{6,7,8,9,10} include sodium, calcium, silicon, aluminum and sulfur. Silicon, presumably in

20. Jaenicke, R., and Schutz, L. (1978) A comprehensive study of physical and chemical properties of the surface aerosols in the Cape Verde Islands region, J. Geophys. Res., 83:3583-3598.

21. d'Almeida, G. A. and Jaenicke, R. (1981) The size distribution of mineral dust, J. Aerosol Sci., 12:160-162.

the form of quartz, and calcium, appear to be the most common elements in the desert aerosol^{6,7}. The five most common elements found by Kushelevsky et al.⁷ were calcium, silicon, sulfur, iron and chlorine. Calcium, silicon and iron are primarily crustal in nature while sulfur and chlorine can have both crustal and industrial sources. Chlorine can also be derived from sea spray⁹.

Particles with radii less than about 0.4 μm appear to have a large ammonium sulfate and ammonium bisulfate component while larger particles have quartz, clay components and other elements associated with soil or crustal sources^{8,9,10,18}. Generally speaking, desert aerosols are not hygroscopic. The only exception to this is a "well aged" desert aerosol in which the background component has acted as a condensation nuclei as a result of numerous trips up and down through the desert atmosphere.

Abundances of the elements can vary from sample to sample as a function of wind speed (i.e., increased mass loading) and wind direction (i.e., source region). Cahill et al.⁸ observed a seasonal variation in the amount of silicon particulate in samples collected in Arizona and Utah. Their results, which consisted of one year of data, indicated that for particles in the range 3.5 to 15 μm , the silicon abundance increased to a maximum in the spring and then decreased to a minimum in the winter. Table 3, from Kushelevsky et al.⁷, summarizes how the abundances of these elements can vary on a day-to-day basis and when averaged over different meteorological conditions.

Carbon is generally found in very small abundances in desert aerosols. However, due to its strong absorption, a small increase in the carbon amount, as little as 1%, can lead to a large increase in the total absorption properties of desert aerosols.

Table 5. Variation of Elemental Concentrations in Middle Eastern Desert Aerosols as (a) A Function of Source Region and (b) Averaged Over Meteorological Conditions. Measurements were made by Kushelevsky et al. at Beer-Sheva, Israel using Instrumental Neutron Activation Analysis and X-ray Fluorescence

(a)

WIND DIRECTION	MEAN WIND SPEED (m s ⁻¹)	TOTAL SUSPENDED PARTICULATE (g m ⁻³)	NOTES	ELEMENTAL CONCENTRATIONS (%)				
				Ca	Si	S	Fe	Cl
W-E	2.04	291		10	9	2	2	2
N-W	2.01	243		18	13	2	2	1
N-W	1.85	160		14	13	4	2	2
W-E	1.67	36	Rain	1	5	4	1	4
NW-E	2.29	104	Rain	9	11	3	2	2
W-SE	1.83	50	Rain	19	20	5	4	7
N-E	4.59	581	Dust Storm	18	21	1	3	0.4
W-EW	2.00	610	Dust Storm	17	18	1	2	1
W	2.73	1600	Dust Storm	22	17	0.3	2	0.1
N-E	2.25	613	Sharav	15	14	1	2	1
E-SE-E	2.87	412	Sharav	17	2	1	3	1
W Variable	3.16	5080	Sharav	16	18	0.2	3	0.2

(b)

METEOROLOGICAL CONDITIONS	ELEMENTAL CONCENTRATIONS (%)				
	Ca	Si	S	Fe	Cl
Normal	17.2	11.5	3.1	1.9	2.5
Rain	12.6	14.6	4.5	2.4	3.6
Dust Storm	16.8	18.0	0.6	2.4	0.5

Note: Sharav, or Khamsin, is a Dust Storm Characterised by Hot Winds from the North African Desert. It Typically Occurs During the Period Between Easter and Pentecost

2.4 Effects of Wind

Enormous amounts of clay and sand can be loaded into the desert atmosphere during windy conditions. During calm condi-

tions the desert aerosol resembles aerosols other than that which would be produced from the underlying soil. In particular, Patterson and Gillette⁴ have studied the composition of the desert aerosol in light, medium and heavy mass loading conditions and have found that particles having radii between 0.02 and 0.5 μm were generally grey or black and represented the global background aerosol. Furthermore, these particles were always present in the same amount regardless of the amount of mass loading. Similar findings reported in the World Climate Programme² study confirmed that under very calm conditions the composition of the desert aerosol resembles that of a remote continental aerosol.

Local wind conditions provide the mechanism to inject and transport aerosols. Wind also provides a mechanism for the generation of additional aerosols via a sandblasting process. The amount of aerosol injection and generation depends upon factors such as wind speed^{22,23}, soil moisture, and the extent

22. Gillette, D. A., Blifford, Jr., I. H. and Fryrear, D. W. (1974) The influence of wind velocity on the size distributions of aerosols generated by the wind erosion of soils, J. Geophys. Res., 79:4068-4075.

23. Gillette, D. A. (1978) Tests with a portable wind tunnel for determining wind erosion threshold velocities, Atmospheric Environment, 12:2309-2313.

of vegetation²⁴, soil texture and the amount of soil crusting²⁵.

Soil movement as a result of aerodynamic forces occurs for wind speeds above a given threshold value. This wind speed threshold will vary as a function of soil condition and on the amounts of nonerodible elements, such as rocks and pebbles, on top of the soil. Utilizing a portable wind tunnel, Gillette²³ examined the threshold velocities for three different kinds of soils, two types of desert soil and one farmland soil. A relatively smooth desert soil had a threshold velocity of 34.2 cm s^{-1} while one with a pebble covering had a threshold velocity of 121.9 cm s^{-1} .

The size distribution of the aerosols that are injected into the air as a result of wind erosion has been found to be similar to that of the underlying soil²⁴.

2.5 Indices of Refraction

The index of refraction characterizes the optical properties of a particular material. It can be expressed as the complex number,

$$m = n + ik, \quad (2)$$

-
24. Gillette, D. A., Blifford, Jr., I. H. and Fenster, C. R. (1972) Measurements of aerosol size distributions and vertical fluxes of aerosols on land subject to wind erosion, J. Appl. Meteor., 11:977-987.
25. Gillette, D. A. (1978) A wind tunnel simulation of the erosion of soil: Effect of soil texture, sandblasting, wind speed, and soil consolidation on dust production, Atmospheric Environment, 12:1735-1743.

where n and k are related to the phase velocity and attenuation, respectively, of an electromagnetic wave as it passes through the material. In general, the index of refraction of a material will not be the same for all wavelengths of radiation.

2.5.1 An Assessment of the Available Measurement Techniques

Measuring the optical properties of any material is not a trivial job. Three techniques are commonly used to determine the index of refraction of aerosols: in situ measurements, laboratory measurements made on a compressed disk of the collected sample and KBr pellets and laboratory measurements of diffuse reflectance. The laboratory measurements usually involve collecting the aerosol on a filter and must avoid evaporation of volatile compounds and contamination from the admixture of other aerosols, such as clouds or gases.

2.5.1.1 In Situ Measurements

In situ measurements of particle size distribution and the angular dependence of scattering can be used to predict the optical properties of aerosols (Grams et al.²⁶). The index of refraction is then equal to the value, which when used in Mie calculations, replicates the observed scattering pattern. Unfortunately, this technique involves a few assumptions that may be risky. First, the particles are assumed to be spherical. This assumption is valid for some aerosols,

26. Grams, G. W., Blifford, Jr., I. H., Gillette, D. A. and Russell, P. B. (1974) Complex index of refraction of airborne soil particles, J. Appl. Meteor., 13:459-471.

such as those found near oceans, but not for desert aerosols, especially fresh ones. A second point to keep in mind is that this technique may not be appropriate for materials in which scattering dominates over absorption. That is, small errors in the measured scattered intensity can lead to large errors in the inferred absorption²⁷. Finally, inaccurate representation of the particle size distribution, when used in the Mie calculations, can give rise to erroneous values for the imaginary index.

2.5.1.2 An Aerosol Sample Suspended in a KBr Disk

The optical constants of desert aerosols have been determined by Levin and Lindberg⁶ and by Volz²⁸ by compressing the particles into a disk with pellets of KBr and then measuring the reflectance and transmittance. Next these measurements are interposed with solutions to electromagnetic boundary value problems for plane surfaces to infer the optical properties of the aerosol. Unfortunately, it is sometimes difficult or questionable to determine the optical constants of desert aerosols using this technique. That is, the technique cannot be used for visible wavelengths because scattering dominates over absorption. Also, the underlying electromagnetic theories used to calculate the optical properties are only valid for homogeneous materials; however, the airborne desert

27. Bohren, C. F., Private Communication.

28. Volz, F. E. (1973) Infrared optical constants of ammonium sulfate, Sahara dust, volcanic pumice and flyash, Appl. Opt., 12:564-568.

aerosol is composed of discrete particles, each having its own composition.

2.5.1.3 Diffuse Reflection Techniques

The method of diffuse reflection involves mixing the aerosol with a barium sulfate powder and measuring the diffuse reflectance with a spectrophotometer. With these measurements and the diffuse reflectance of pure barium sulfate, the imaginary part of the index of refraction is then determined using the equations of the Kubelka-Munk theory of diffuse reflectance. This technique has been used by Patterson et al.²⁹ and by Levin and Lindberg⁶ to determine k of desert aerosols.

2.5.2 Reported Values of the Indices of Refraction for Desert Aerosols

2.5.2.1 Real Part

All available measurements report the n of desert aerosols to be between about 1.5 and 1.6 for visible wavelengths. These values are referred to rather casually because, for spheres at least, the specific choice of n will not significantly affect the absorption, scattering and extinction coefficients. In fact, some of the experimental techniques must assume a real index in order to determine the imaginary part.

Values for n approach a minimum in the 5 - 8 μm region and a local maxima around 10 μm and 25 μm . These peaks of the real part roughly correspond to the peaks in the absorption.

29. Patterson, E. M., Gillette, D. A. and Stockton, B. H.
(1977) Complex index of refraction between 300 and 700
nm for Saharan aerosols, J. Geophys. Res., 82:3153-3160.

This is expected because the behavior of n is related to the behavior of k .

2.5.2.2 Imaginary Part

The measurements of k for desert aerosols are given in Figure 1 from Carlson and Benjamin³⁰. Most measurements, regardless of technique, place the imaginary index for visible wavelengths between about 0.001 and 0.04. Generally speaking, absorption is slightly less at red wavelengths than at blue wavelengths and reaches a minimum near 1.0 μm . Unfortunately at many wavelengths in the visible, the various measurements of k are different from each other. These large discrepancies are a problem because when the different values are used in radiative transfer calculations, they can give rise to a wide range of values for the absorption of solar radiation.

The measurements of k suggest that it is quite variable in the infrared. The magnitude of k is smallest at the shorter IR wavelengths and reaches a local maxima at wavelengths within the 8 - 12 μm atmospheric window and around 20 μm . These peaks in the window region are due to the absorption by quartz and the various clays present in the aerosol. Although most sets of measurements place the peaks near the same wavelengths, there are striking differences in the magnitudes of absorption.

30. Carlson, T. N. and Benjamin, S. G. (1980) Radiative Heating Rates for Saharan Dust, J. Atmos. Sci., 37:193-213.

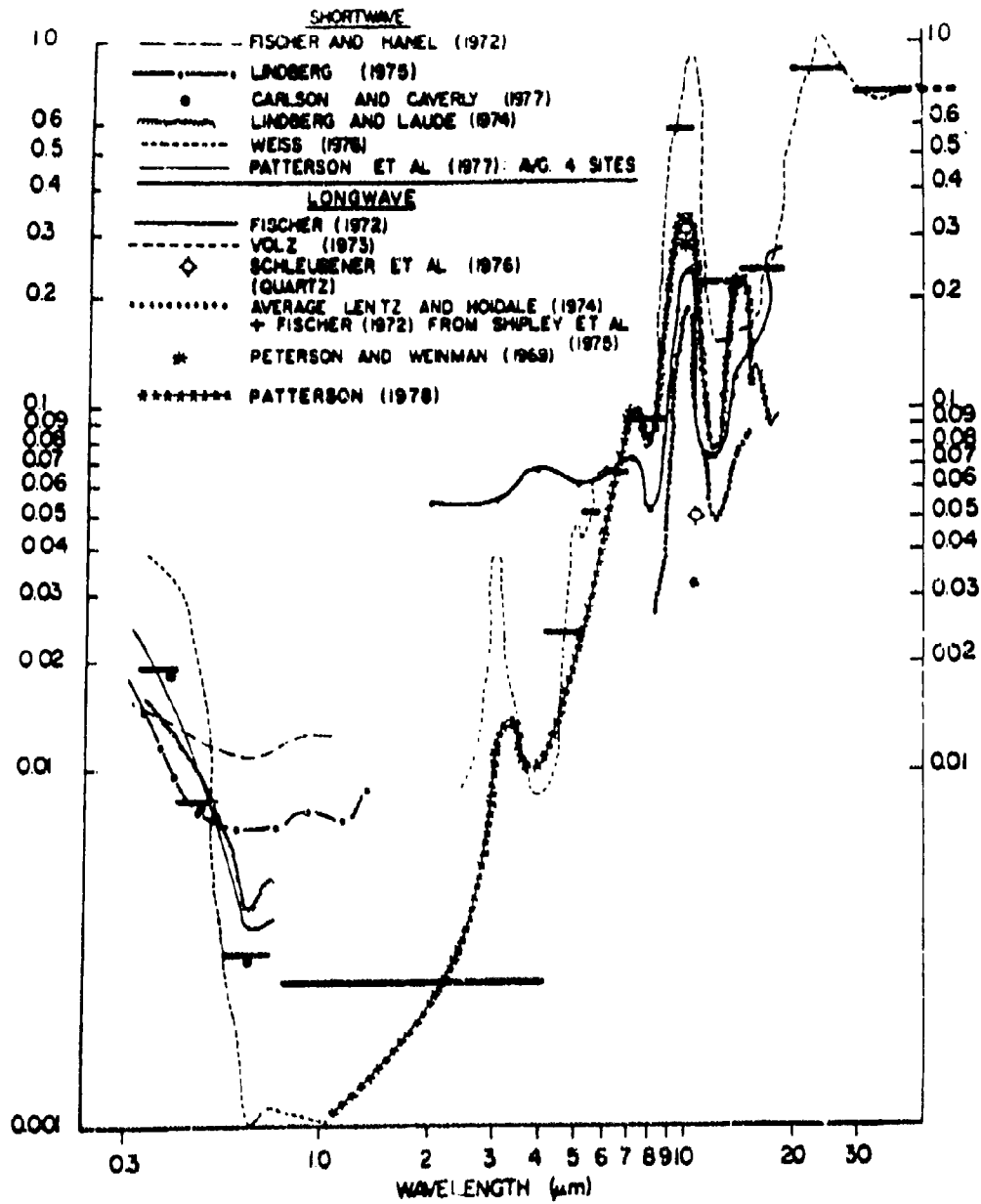


Figure 1. Values of the Imaginary Index of the Desert Aerosol Reported by Other Researchers (From Carlson and Benjamin³⁰). See Carlson and Benjamin³⁰ for the references cited in this figure

2.5.3 Concerns Over the Reported Values

It is generally agreed that the optical constants of desert aerosols reported in the literature probably represent average or effective values because the desert aerosol is an inhomogeneous material. The problem with using average values is that they do not accurately describe the radiative properties of desert aerosols. The radiative properties of any multicomponent material depend on how the components are mixed. In the case of desert aerosols, most of the absorption is due to the small, discrete carbon-based particles from the background global aerosol. The problem is that when the average indices of refraction are used in radiative transfer calculations, each particle is treated as though it has the same optical parameters, which is clearly not true. In high wind conditions when greater amounts of less absorbant, local dust and sand are lofted, the relative contributions of the highly absorbant carbon particles to the total radiative impact of the desert aerosols are lessened.

It is important to examine the consequences of using the values cited in the literature. Because the typical desert aerosol does contain a small amount of highly absorbing material, such as carbon or hematite, one would expect the values for k (in the visible), to be greater than those for pure quartz or various clays, which have values of k of about 10^{-6} . However, all of the values for k in Figure 1 are too high. To demonstrate this, let us calculate the "penetration depth" of a $0.55 \mu\text{m}$ wave as it passes through a single desert aerosol

particle. (This argument is taken from Bohren and Huffman³¹.) For the purposes of the argument, the penetration depth will be defined as the distance where the transmission through the particle T is reduced to 1%. A value of 1% transmission is chosen because it defines a particle as appearing black when placed in front of a light source. If reflection effects are ignored (which is a reasonable assumption), then the wave will be attenuated exponentially

$$T = \exp(-az) \quad (3)$$

where the absorption coefficient, a , equals $4\pi k/\lambda$. Solving this expression for z gives

$$z = -\ln(T)/(4\pi k/\lambda) \quad (4)$$

Now, letting $T = 0.01$, $k = 0.001$, and $\lambda = 0.55 \mu\text{m}$, the resulting penetration depth is $200 \mu\text{m}$. Desert aerosol particles with diameters of $200 \mu\text{m}$ are common in the desert atmosphere during dust storms, but our penetration depth calculation implies that the desert aerosol is black, which observations show not to be the case (See Section 2.3). Therefore, the quoted values for k must be approached cautiously. Since all measurement techniques yield physically unrealistic values for k , our dilemma may be due to the nature of the desert aerosol itself. Specifically, an atmosphere containing a desert aerosol is an inhomogeneous and "dirty" medium and, therefore,

31. Bohren, C. F. and Huffman, D. (1983) Absorption and Scattering of Light by Small Particles, Wiley-Interscience, New York.

using a single value for the index of refraction at each wavelength is not the best way to approach the problem. It would be better to treat the aerosol as a heterogeneous mixture of different types of particles.

2.6 Radiative Impacts

Desert aerosols have been studied extensively due to their pervasiveness in the atmosphere and due to their potentially significant radiative impacts. The desert dusts are speculated to have an impact on the radiative balance of the tropical North Atlantic and on the climatology of the desert areas themselves.

Carlson and Benjamin³⁰ have studied the effects of Saharan dust on the radiative fluxes and heating/cooling rates in the atmosphere over the ocean, as well as for cloud-free cases over the desert. Their study showed that the downward radiative flux into the ocean or desert surface decreased in the presence of desert dust and that the heating of the atmosphere increased, leading to a stabilizing effect on the temperature lapse rate. Over the ocean (for conditions representative of the summertime eastern Atlantic), the increased heating amounted to about 1 K day^{-1} , averaged between 1000 mb and 500 mb.

In terms of the net radiative impact at the top of the atmosphere, Carlson and Benjamin found that desert dust had little impact over a cloud free ocean. The surface cooling resulting from the decreased downward infrared flux was nearly compensated for by the increased atmospheric heating. How-

ever, over highly reflecting surfaces such as clouds or the desert floor, the presence of desert dust in the atmosphere leads to a net system warming as a result of a decrease in the earth-atmosphere system albedo.

Guedalia et al.³² demonstrated that the presence of a desert dust layer at night increases the downward infrared flux at the surface and the radiative cooling rate at the top of the haze layer. Within the first few hundred meters of the haze layer, the radiative cooling rate first increases with the increasing dust concentration but eventually reaches a limiting value. However, the increases in radiative effects with increasing dust concentrations that occur at the top of the haze layer and the surface could give rise to vertical instabilities.

The radiative impact of desert aerosols changes during dust storm conditions. Levin et al.¹¹ reported that in the wavelength region 0.3 - 1.7 μm , the imaginary part of the index of refraction of desert dust in the Negev desert was lower by a factor of 3 - 5 during a Sharav period as compared to a normal weather period. This was due to the increased contributions of local dust, which is less absorbant to the total aerosol burden than much of the background aerosol. Malm and Johnson¹² observed similar decreases in total aerosol absorption with increases in windblown dust in measurements made at the Grand Canyon. These conclusions are also consistent with results of Otterman et al.¹³ who used Landsat data to characterize desert aerosols over Iran and Pakistan.

2.7 Conclusions That Can Be Drawn From Previous Studies

Measurements of size distributions and mass loadings indicate that local wind speed controls the numbers of large particles. Therefore, this mode of the distribution should be wind speed dependent.

The compositional data indicate that desert aerosols consist of a mixture of different sized particles with different compositions. Small particles ($r < 0.5 \mu\text{m}$) tend to be associated with the generally observed background aerosol. Larger particles are associated with soil and crustal sources. Therefore, a model for desert aerosols would need to include different size distributions for each aerosol component.

The studies of the radiative impact of desert aerosols indicate that desert aerosols can have an impact in the atmosphere in desert regions as well as in air masses in which the dust is imbedded. The radiative impact is not easily established due to the radiative effects of the underlying surface. The studies of radiative effects of desert aerosols also point out that the radiative impacts change during dust storm conditions as a result of the less absorbant, locally produced dust taking up a larger share of the total aerosol burden. This result requires that not only must a separate set of size distributions be considered, but also for an associated set of indices of refraction for each of the aerosol components.

3. THE PRESENT DESERT AEROSOL MODEL

3.1 Overview

The present model separates the desert aerosol into its three major components by composition and uses a different log normal size distribution and set of indices of refraction for each component. The components represent carbonaceous particles, water soluble particles and sand. The sand component consists of two kinds of particles, pure quartz and quartz contaminated with a small amount of hematite (iron oxide, Fe_2O_3). Mie calculations are performed separately for each component and then weighted according to their volume fraction of the total aerosol. The following radiative parameters were calculated:

- 1) extinction coefficient in km^{-1}
- 2) scattering coefficient in km^{-1}
- 3) absorption coefficient in km^{-1}
- 4) single scattering albedo
- 5) asymmetry parameter.

The calculations were performed for 68 wavelengths between 0.2 and 300 μm . The density and aerosol fraction by volume for background conditions of each component is summarized in Table 4. The aerosol fractions by volume in Table 4 are the same as those for a remote continental aerosol (see page 83 of the World Climate Research Programme²).

Table 4. Density of Each Component of the Desert Aerosol Model and Aerosol Fraction by Volume for Background Conditions

AEROSOL COMPONENT	DENSITY (g/cm ³)	AEROSOL FRACTION BY VOLUME
Carbonaceous	2.000	0.001
Water Soluble	1.769	0.299
Sand	2.650	0.700
Total	-	1.00

3.2 Wind Speed Dependence On Aerosol Loading

The present model assumes that the volume (or mass) of the water soluble and carbonaceous components remains the same as that for background conditions. Consequently all extra mass loading due to the wind is from sand. The mass loading equation of Jaenicke³³ is the basis for the wind speed dependence

$$c = 52.77 \exp(0.30 u) \quad (5)$$

where c is the mass concentration in $\mu\text{g m}^{-3}$ of air and u is the wind speed in ms^{-1} at a height of 10 meters. This equation is an average based on values in the literature gathered

33. Jaenicke, R. (1984) Aerosol Physics and Chemistry, Meteorology Volume, Landolt-Boernstein Numerical Data and Functional Relationships in Science and Technology, to be published by Springer-Verlag.

by Jaenicke. It is meant to represent a generic desert aerosol and is valid only within the mixing layer.

As mentioned in Section 3.1, the present model uses a different size distribution for each component of the desert aerosol. For reference, these size distributions and the range of the Mie calculations are given in Table 5. It is

Table 5. Wind Speed Dependence of the Desert Aerosol Size Distribution Parameters

AEROSOL COMPONENT	WIND SPEED (m/s)	SIZE DISTRIBUTION PARAMETERS			RADIUS RANGE USED IN MIE CALCULATIONS (μm)
		r ₁ (μm)	log(σ ₁)	COMMENTS	
Carbonaceous	0 - 30	0.0118	0.301	WMO ² (p. 31)	0.0005 - 100
Water Soluble	0 - 30	0.0285	0.350	WMO ² (p. 31)	0.0005 - 100
Sand	0	6.24	0.277	Coarse Mode of the Remote Continental Model of Jaenicke	0.05 - 100
	10	7.76	0.331	Linear Interpolation of the Values at 0 and 30 m/s	0.05 - 300
	20	9.28	0.384		0.05 - 750
	30	10.80	0.438	Coarse Mode of the Dust Storm Model of Jaenicke	0.05 - 1000

important to note that the mode radius and the standard deviation of the sand component increase as the wind speed increases. The standard deviation is increased so that the smaller sand particles are retained.

Values for the aerosol fractions by volume, absolute volumes and absolute masses as a function of wind speed are given in Table 6. (The method of determining the values in Table 6 is described in Appendix A.) The total particle concentration for each component, N_i , is then equal to the absolute volume in Table 6 divided by the volume for 1 particle (the latter is known from the Mie calculations). These "inferred" values of N_i can then be used to generate number density and area distributions for the present desert aerosol model (see Figs. 2 and 3). Figure 3 shows not only that the amount of scattering material increases as the wind speed increases, but the peak of the area distribution curve, which indicates the range of particles that contribute most to the radiative properties of the aerosol, shifts toward larger particle sizes. Here it should be reemphasized that values of N_i used in Figs. 2 and 3 are not based on direct measurements but give total aerosol masses that are consistent with Eq. 5. The present model has adopted this approach instead of using the observed size distributions recently reported by d'Almeida³⁴. This is because his size distribution parameters do not behave consistently as a function of wind speed; that is, in going from background to wind blown dust conditions, the number density for the middle mode of the d'Almeida model decreases, which is not realistic.

34. d'Almeida, G. A. (1987) On the variability of desert aerosol radiative characteristics, J. Geophys. Res., 92:3017-3026.

Table 6. Mass Loading of the Desert Aerosol as a Function of Wind Speed. The parameters C_i , V_i and m_i are the aerosol fraction by volume, volume concentration and mass per unit volume of air, respectively

AEROSOL COMPONENT	0 ms ⁻¹			10 ms ⁻¹			20 ms ⁻¹			30 ms ⁻¹		
	C_i	V_i	m_i **	C_i	V_i	m_i	C_i	V_i	m_i	C_i	V_i	m_i
Carbonaceous	0.001	0.022	0.044	5.50×10^{-5}	0.022	0.044	2.75×10^{-6}	0.022	0.044	1.37×10^{-7}	0.022	0.044
Water Soluble	0.299	6.613	11.69	0.0164	6.613	11.69	8.23×10^{-4}	6.613	11.69	4.09×10^{-5}	6.613	11.69
Sand	0.700	15.2	41.07	0.9835	395.5	1046.1	0.9992	8029.1	21277.1	0.9999	161353.9	427587.8
Total	1.000	22.1	52.7	1.000	402.2	1057.8	1.000	8035.7	21280.9	1.000	161360.5	427589.5

* The units are μm^3 of Aerosol cm^{-3} of Air

** The units are μgms of Aerosol m^{-3} of Air

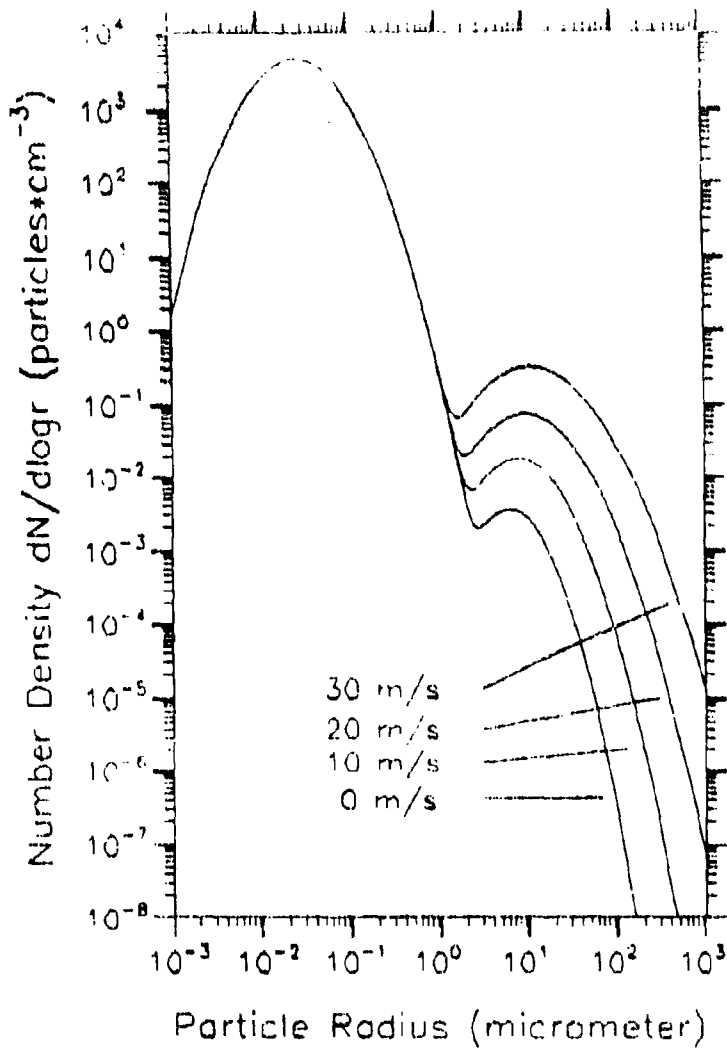


Figure 2. Number Density Distribution of the Desert Aerosol for Four Wind Speeds

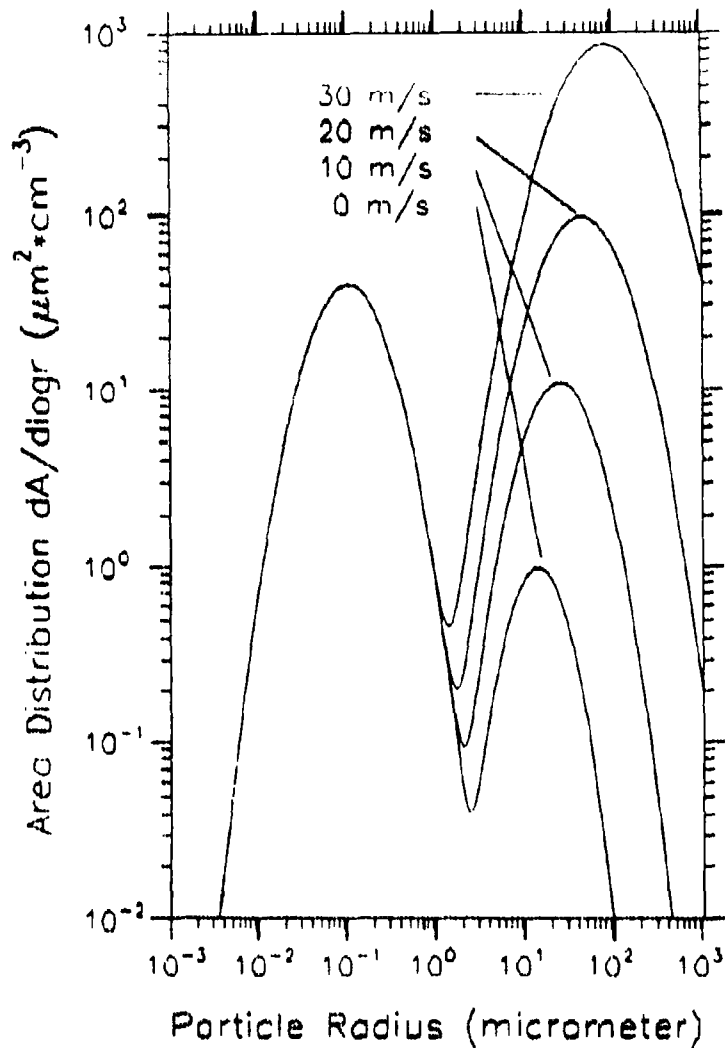


Figure 3. Area Distribution of the Desert Aerosol for Four Wind Speeds

3.3 Indices of Refraction

3.3.1 Carbonaceous and Water Soluble Components

The indices of refraction for the carbonaceous and water soluble components are listed in Tables 7 and 8 respectively. Figure 4 presents these values in pictorial form. (The values at 40 μm have been used for the 50 to 300 μm region because indices of refraction were not available for these wavelengths.) The values for the carbonaceous component are taken from the work of Shettle and Fenn³⁵, and they represent various types of carbon blacks and soots. The water soluble component utilizes the index of refraction measurements made by Toon, Pollock and Khare³⁶ for pure crystalline ammonium sulfate.

3.3.2 Sand Component

The hematite in the sand particles is assumed to be in the form of discrete pigments embedded within the quartz. This assumption is reasonable based on the visual examination of sand. An equation originally proposed by Maxwell-Garnett³⁷ is then used to obtain average indices of refraction for sand. The expression is given by

-
35. Shettle, E. P. and Fenn, R. W. (1979) Models for the Aerosols of the Lower Atmosphere and the Effects of Humidity Variations on Their Optical Properties, AFGL-TR-79-0214, 20 Sept 1979, ADA085951.
 36. Toon, O. B., Pollock, J. B. and Khare, B. N. (1976) The optical constants of several atmospheric aerosols species: Ammonium sulfate, aluminum oxide and sodium chloride, J. Geophys. Res., 81:5733-5748.
 37. Maxwell-Garnett, J.C. (1904) Colours in metal glasses and in metallic films, Philo. Trans. R. Soc., A203:385-420.

Table 7. Indices of Refraction for Carbonaceous Material. The numbers in parentheses in the k columns are the power of 10 following the value of k (if no value given, then the previous power of 10 is implied)

WAVELENGTH (μm)	INDEX OF REFRACTION		WAVELENGTH (μm)	INDEX OF REFRACTION	
	n	k		n	k
0.200	1.50	0.350(0)	8.500	2.15	0.690(0)
0.250	1.62	0.450	8.700	2.16	0.690
0.300	1.74	0.470	9.000	2.17	0.700
0.337	1.75	0.470	9.200	2.18	0.700
0.400	1.75	0.460	9.500	2.19	0.710
0.488	1.75	0.450	9.800	2.20	0.715
0.515	1.75	0.450	10.000	2.21	0.720
0.550	1.75	0.440	10.591	2.22	0.730
0.633	1.75	0.430	11.000	2.23	0.730
0.694	1.75	0.430	11.500	2.24	0.740
0.860	1.75	0.430	12.500	2.27	0.750
1.060	1.75	0.440	13.000	2.28	0.760
1.300	1.76	0.450	14.000	2.31	0.775
1.536	1.77	0.460	14.800	2.33	0.790
1.800	1.79	0.480	15.000	2.33	0.790
2.000	1.80	0.490	16.400	2.36	0.810
2.250	1.81	0.500	17.200	2.38	0.820
2.500	1.82	0.510	18.000	2.40	0.825
2.700	1.83	0.520	18.500	2.41	0.830
3.000	1.84	0.540	20.000	2.45	0.850
3.200	1.86	0.540	21.300	2.46	0.860
3.392	1.87	0.550	22.500	2.48	0.870
3.500	1.88	0.560	25.000	2.51	0.890
3.750	1.90	0.570	27.900	2.54	0.910
4.000	1.92	0.580	30.000	2.57	0.930
4.500	1.94	0.590	35.000	2.63	0.970
5.000	1.97	0.600	40.000	2.69	1.000
5.500	1.99	0.610	50.000	2.69	1.000
6.000	2.02	0.620	60.000	2.69	1.000
6.200	2.03	0.625	80.000	2.69	1.000
6.500	2.04	0.630	100.000	2.69	1.000
7.200	2.06	0.650	150.000	2.69	1.000
7.900	2.12	0.670	200.000	2.69	1.000
8.200	2.13	0.680	300.000	2.69	1.000

Table 8. Indices of Refraction for Ammonium Sulfate. The numbers in parentheses in the k columns are the power of 10 following the value of k (if no value given, then the previous power of 10 is implied)

WAVELENGTH (μm)	INDEX OF REFRACTION		WAVELENGTH (μm)	INDEX OF REFRACTION	
	n	k		n	k
0.200	1.55	1.0(-)	8.500	0.90	2.9(-1)
0.250	1.55	1.0	8.700	0.71	6.5
0.300	1.54	1.0	9.000	0.98	1.7(0)
0.337	1.54	1.0	9.200	2.10	1.9
0.400	1.54	1.0	9.500	2.70	5.9(-1)
0.488	1.54	1.0	9.800	2.39	2.3
0.515	1.53	1.0	10.000	2.19	1.3
0.550	1.53	1.0	10.591	1.97	5.6(-2)
0.633	1.52	1.0	11.000	1.90	4.3
0.694	1.52	1.0	11.500	1.84	2.7
0.860	1.52	1.5	12.500	1.75	2.0
1.060	1.51	1.8(-6)	13.000	1.72	2.0
1.300	1.50	1.7(-5)	14.000	1.65	2.0
1.536	1.49	7.7	14.800	1.56	2.4
1.800	1.48	7.6	15.000	1.53	2.6
2.000	1.47	1.0(-3)	16.400	2.77	5.8(-1)
2.250	1.46	1.1	17.200	2.13	5.8(-2)
2.500	1.44	3.5(-4)	18.000	1.82	2.5
2.700	1.41	2.0(-3)	18.500	1.76	2.0
3.000	1.30	9.6(-2)	20.000	1.69	2.0
3.200	1.49	2.6(-1)	21.300	1.65	2.5
3.392	1.61	1.7	22.500	1.61	3.2
3.500	1.61	1.4	25.000	1.55	5.0
3.750	1.58	3.6(-2)	27.900	1.45	9.4
4.000	1.55	1.4	30.000	1.35	1.7(-1)
4.500	1.50	7.3(-3)	35.000	1.42	5.8
5.000	1.46	6.5	40.000	2.14	1.12(0)
5.500	1.41	8.0	50.000	2.14	1.12
6.000	1.35	1.3(-2)	60.000	2.14	1.12
6.200	1.31	1.8	80.000	2.14	1.12
6.500	1.19	4.9	100.000	2.14	1.12
7.200	1.93	5.4(-1)	150.000	2.14	1.12
7.900	1.36	7.5(-2)	200.000	2.14	1.12
8.200	1.16	1.2(-1)	300.000	2.14	1.12

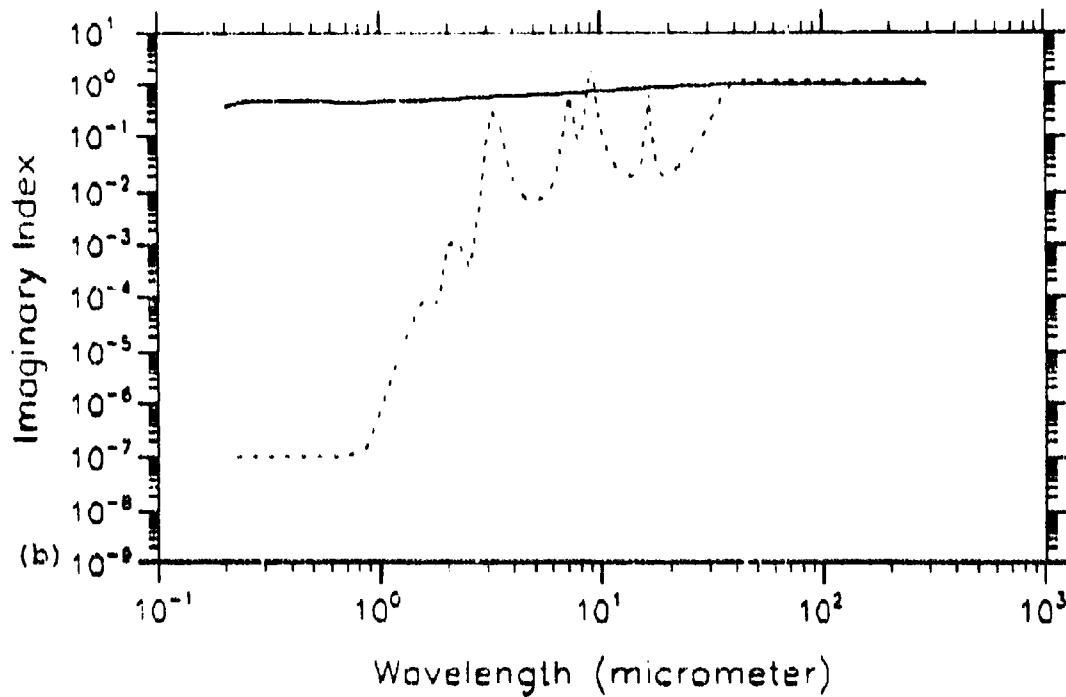
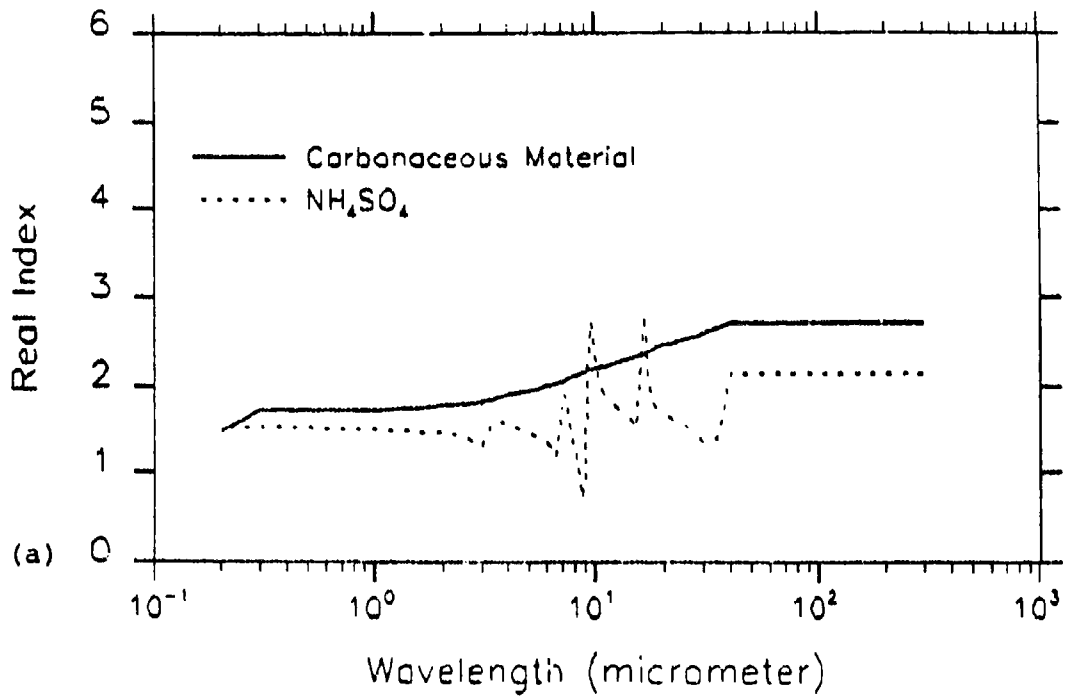


Figure 4. Indices of Refraction of Carbonaceous Material and Ammonium Sulfate, (a) Real part and (b) Imaginary Part

$$e_{av} = e_m \left[1 + \frac{3f \left(\frac{e - e_m}{e + 2e_m} \right)}{1 - f \left(\frac{e - e_m}{e + 2e_m} \right)} \right] \quad (6)$$

where for our problem, e_{av} , e and e_m are the complex dielectric constants of sand, hematite and quartz respectively, and f is the volume fraction of hematite in the sand particles. The complex dielectric constant of a material is related to its complex index of refraction by

$$\text{Re}(e) = n^2 - k^2 \quad (7)$$

and

$$\text{Imag}(e) = 2nk \quad (8)$$

A recent comparison of different effective media theories by Chylek et al.³⁸ showed that the Maxwell-Garnett approximation gave acceptable results.

The use of Maxwell-Garnett theory requires indices of refraction for quartz and hematite. To account for anisotropic behavior of quartz, separate index of refraction data have been obtained for the ordinary ray (o-ray) and extraordinary ray (e-ray) of pure crystalline quartz. The values are listed in Tables 9 and 10, and come from five sources:

38. Chýlek, P., Srivastava, V., Pinnick, R. G. and Wang, R. T. (1988) Scattering of electromagnetic waves by composite spherical particles; experiment and effective medium approximations, Appl. Opt., 27:2396-2404.

Table 9. Indices of Refraction for the O-Ray of Quartz. The numbers in parentheses in the k columns are the power of 10 following the value of k (if no value given, then the previous power of 10 is implied)

WAVELENGTH (μm)	INDEX OF REFRACTION		WAVELENGTH (μm)	INDEX OF REFRACTION	
	n	k		n	k
0.200	1.649	1.00(-8)	8.500	0.114	1.26(0)
0.250	1.606	1.00	8.700	0.131	1.41
0.300	1.584	1.00	9.000	0.176	2.61
0.337	1.568	1.00	9.200	0.633	4.55
0.400	1.559	1.00	9.500	4.497	3.92(-1)
0.488	1.550	1.00	9.800	3.014	8.69(-2)
0.515	1.548	1.00	10.000	2.663	5.17
0.550	1.546	1.00	10.591	2.188	2.22
0.633	1.542	1.00	11.000	2.013	1.73
0.694	1.541	1.00	11.500	1.833	1.88
0.860	1.537	1.00	12.500	1.587	2.27(0)
1.060	1.534	1.00	13.000	2.174	5.19(-2)
1.300	1.531	1.00	14.000	1.768	3.48
1.536	1.538	1.00	14.800	1.831	2.29
1.800	1.524	1.00	15.000	1.785	1.54
2.000	1.520	1.00	16.400	1.580	9.75(-3)
2.250	1.516	1.00	17.200	1.456	1.20(-2)
2.500	1.511	4.99(-7)	18.000	1.289	1.77
2.700	1.506	7.20	18.500	1.142	2.52
3.000	1.499	2.67(-5)	20.000	0.106	7.66(-1)
3.200	1.493	6.77(-6)	21.300	0.194	2.57(0)
3.392	1.487	6.40	22.500	5.709	9.41(-1)
3.500	1.483	8.31	25.000	0.679	1.85(0)
3.750	1.473	5.95(-5)	27.900	2.729	2.16(-2)
4.000	1.462	7.12	30.000	2.500	1.08
4.500	1.442	5.06(-4)	35.000	2.305	4.98(-3)
5.000	1.417	5.62(-3)	40.000	2.228	3.29
5.500	1.371	5.51	50.000	2.214	2.86
6.000	1.325	6.74	60.000	2.175	2.24
6.200	1.293	7.82	80.000	2.148	3.69
6.500	1.246	5.80	100.000	2.132	9.55(-4)
7.200	1.065	1.24(-2)	150.000	2.120	8.72
7.900	0.585	8.49	200.000	2.111	7.96
8.200	0.141	5.38(-1)	300.000	2.109	7.96

Table 10. Indices of Refraction for the E-Ray of Quartz. The numbers in parentheses in the k columns are the power of 10 following the value of k (if no value given, the the previous power of 10 is implied)

WAVELENGTH (μm)	INDEX OF REFRACTION		WAVELENGTH (μm)	INDEX OF REFRACTION	
	n	k		n	k
0.200	1.649	1.00(-8)	8.500	0.085	1.22(0)
0.250	1.606	1.00	8.700	0.096	1.72
0.300	1.584	1.00	9.000	0.231	3.05
0.337	1.568	1.00	9.200	1.689	6.41
0.400	1.559	1.00	9.500	3.899	2.29(-1)
0.488	1.550	1.00	9.800	2.860	6.91(-2)
0.515	1.548	1.00	10.000	2.571	4.40
0.550	1.546	1.00	10.591	2.156	2.05
0.633	1.542	1.00	11.000	1.999	1.59
0.694	1.541	1.00	11.500	1.849	1.53
0.860	1.537	1.00	12.500	1.260	1.30(-1)
1.060	1.534	1.00	13.000	2.625	3.18
1.300	1.531	1.00	14.000	1.821	1.65(-2)
1.536	1.528	1.00	14.800	1.670	1.21
1.800	1.524	1.00	15.000	1.636	1.21
2.000	1.520	1.00	16.400	1.361	1.92
2.250	1.516	1.00	17.200	1.093	3.77
2.500	1.511	7.48(-7)	18.000	0.425	2.12(-1)
2.700	1.506	1.14(-6)	18.500	0.197	9.73
3.000	1.499	8.47	20.000	1.270	4.98(0)
3.200	1.493	4.03	21.300	3.041	1.02(-1)
3.392	1.487	5.70	22.500	2.366	4.38(-2)
3.500	1.483	8.31	25.000	1.451	9.99
3.750	1.473	3.68(-5)	27.900	4.905	8.60(-1)
4.000	1.462	7.12	30.000	2.959	5.93(-2)
4.500	1.442	3.58(-4)	35.000	2.464	1.25
5.000	1.417	4.46(-3)	40.000	2.337	6.75(-3)
5.500	1.371	5.20	50.000	2.262	1.71
6.000	1.325	4.80	60.000	2.223	1.08
6.200	1.293	7.82	80.000	2.190	6.35(-4)
6.500	1.246	7.30	100.000	2.176	4.77
7.200	1.063	1.46(-2)	150.000	2.163	2.40
7.900	0.564	8.61	200.000	2.159	1.59
8.200	0.123	5.86(-1)	300.000	2.156	6.20(-5)

- 1) Gray³⁹ and Peterson and Weinman⁴⁰ for the visible and near IR regime
- 2) Drummond⁴¹ for the region from 2.3 to 7.0 μm
- 3) Spitzer and Kleinman⁴² for the region 7.0 to 40.0 μm
- 4) Philipp⁴³ for the region 40 to 300 μm .

Figure 5 gives these indices of refraction in pictorial form.

Indices of refraction for hematite are listed in Table 11 and shown in Figure 6. The values are based on the work from four researchers:

- 1) Galuza et al.⁴⁴ for the 0.2 to 0.4 μm region
- 2) Kerker et al.⁴⁵ for the 0.4 to 0.8 μm region
- 3) Steyer⁴⁶ for the 4 to 20 μm region

-
39. Gray, D. C. (1963), American Institute of Physics Handbook, McGraw-Hill, New York, NY, 1963, 2nd Edition.
 40. Peterson, J. T. and Weinman, J. A. (1969) Optical properties of quartz dust particles at infrared wavelengths, J. Geophys. Res., 74:6947-6957.
 41. Drummond, D. G. (1936) Absorption coefficients of crystal quartz in the infrared, Proc. Roy. Soc. (London)-Series A, 153:328-338.
 42. Spitzer, W. G. and Kleinman, D. A. (1961) Infrared lattice bands of quartz, Phys. Rev., 121:1324-1335.
 43. Philipp, H. R. (1985) Silicon dioxide (SiO_2), type- α (crystalline), in Handbook of Optical Constants of Solids, Edited by E. D. Palik, 719-747.
 44. Galuza, A. I., Eremenko, V. V. and Kirichenko, A. P. (1979) Analysis of hematite reflection spectrum by the Kramers-Kronig method, Sov. Phys. Solid State, 21:654-656.
 45. Kerker, M., Scheiner, P., Cooke, D. D. and Kratochvil, J. P. (1979) Absorption index and color of colloidal hematite, J. Colloid. Interface Sci., 71:176-187.
 46. Steyer, T. R. (1974) Infrared optical properties of some solids of possible interest in astronomy and atmospheric physics, Ph.D. Thesis, Department of Physics, University of Arizona.

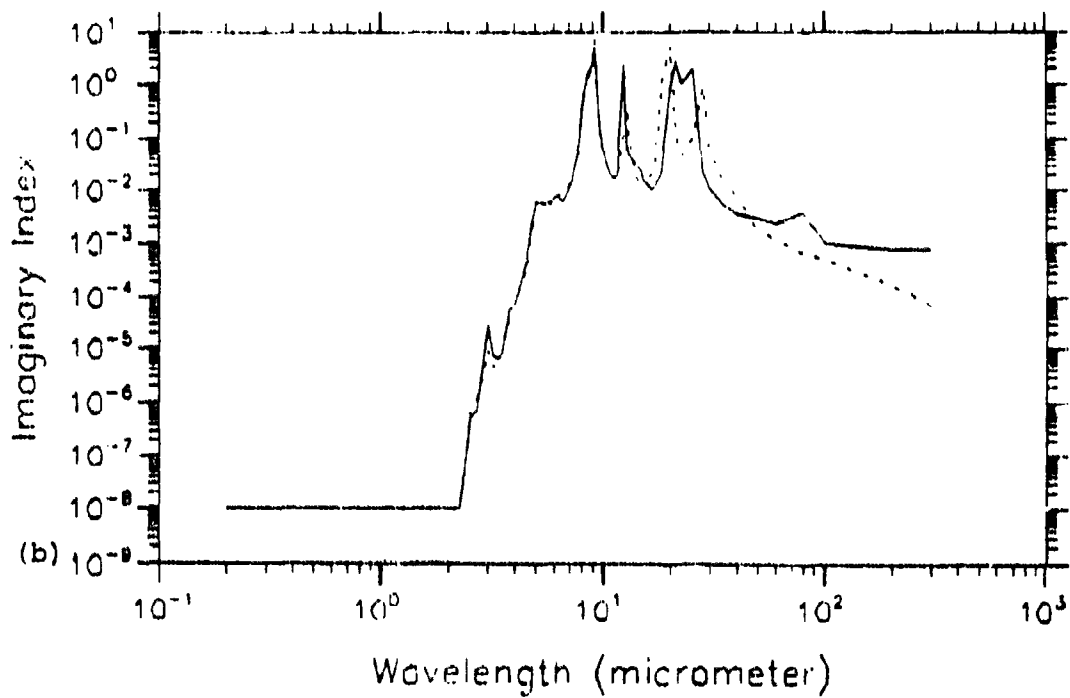
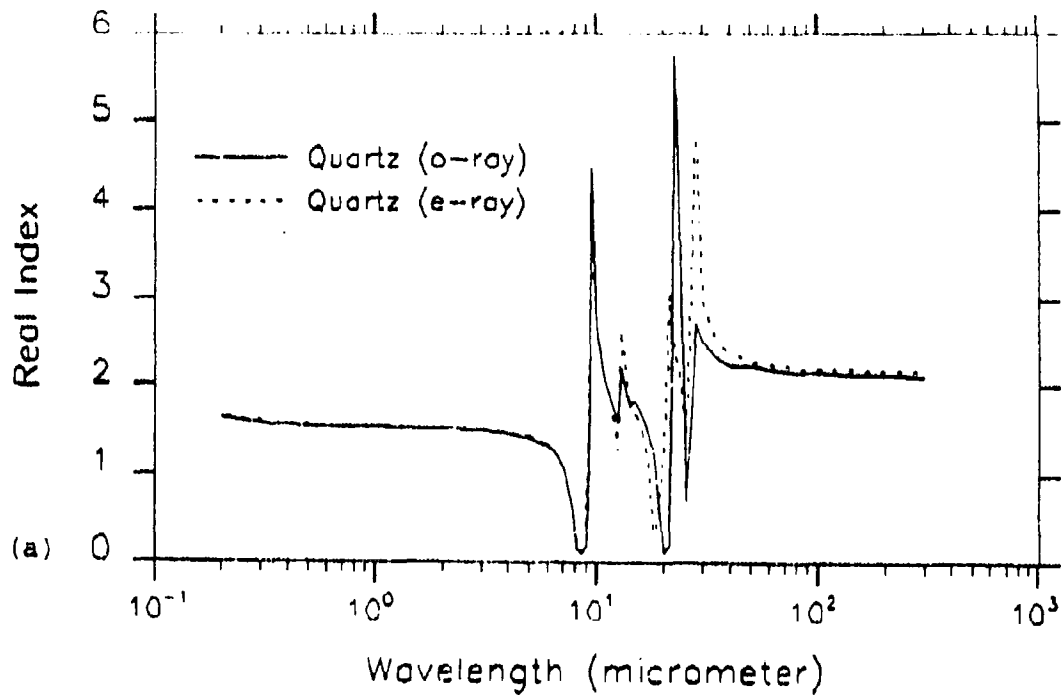


Figure 5. Indices of Refraction of Quartz, (a) Real part and (b) Imaginary Part

Table 11. Indices of Refraction for Hematite. The numbers in parentheses in the k columns are the power of 10 following the value of k (if no value given, then the previous power of 10 is implied)

WAVELENGTH (μm)	INDEX OF REFRACTION		WAVELENGTH (μm)	INDEX OF REFRACTION	
	n	k		n	k
0.200	1.560	1.28(0)	8.500	2.363	3.10(-3)
0.250	2.070	1.33	8.700	2.343	4.07
0.300	2.320	1.18	9.000	2.317	5.00
0.337	2.430	1.09	9.200	2.290	5.93
0.400	2.674	5.23(-1)	9.500	2.253	7.33
0.488	3.074	2.10	9.800	2.217	8.73
0.515	3.104	1.58	10.000	2.197	9.67
0.550	3.102	9.25(-2)	10.591	2.103	1.39(-2)
0.633	3.007	9.74(-3)	11.000	2.027	1.67
0.694	2.920	1.00	11.500	1.945	2.13
0.660	2.730	4.00	12.500	1.746	3.66
1.060	2.660	3.00(-5)	13.000	1.636	4.75
1.300	2.640	1.00	14.000	1.246	8.01
1.536	2.630	5.50(-6)	14.800	0.769	2.17(-1)
1.800	2.620	4.00	15.000	0.592	3.07
2.000	2.610	4.50	16.400	0.244	1.64(0)
2.250	2.610	5.00	17.200	0.350	2.38
2.500	2.610	6.00	18.000	0.711	3.35
2.700	2.610	8.00	18.500	1.468	4.14
3.000	2.610	1.00(-5)	20.000	2.812	1.47
3.200	2.610	1.10	21.300	1.643	2.57
3.392	2.610	1.10	22.500	2.940	4.29
3.500	2.610	1.20	25.000	2.644	1.02
3.750	2.610	1.20	27.900	0.558	2.68
4.000	2.603	4.90	30.000	0.583	4.96
4.500	2.593	4.63	35.000	13.862	1.01(1)
5.000	2.580	4.77	40.000	7.370	3.87(-1)
5.500	2.567	4.23(-4)	50.000	6.059	1.12
6.000	2.547	8.12	60.000	5.474	5.93(-2)
6.200	2.537	1.01(-3)	80.000	5.108	3.28
6.500	2.520	1.14	100.000	4.976	2.33
7.200	2.473	1.22	150.000	4.861	1.39
7.900	2.427	1.23	200.000	4.824	1.01
8.200	2.390	2.17	300.000	4.799	6.56(-3)

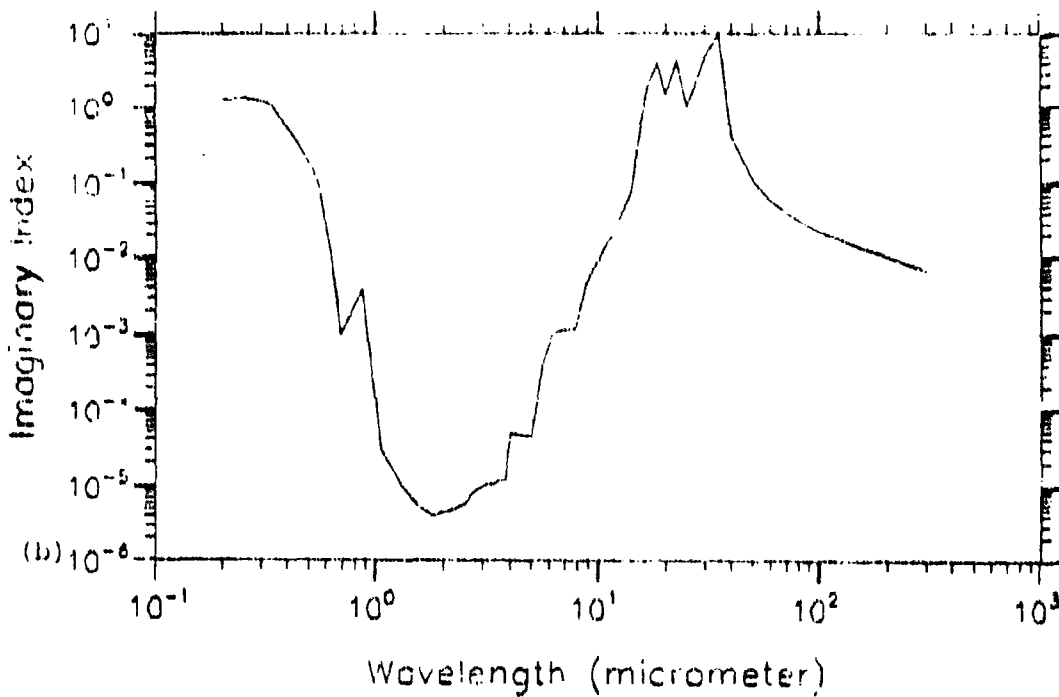
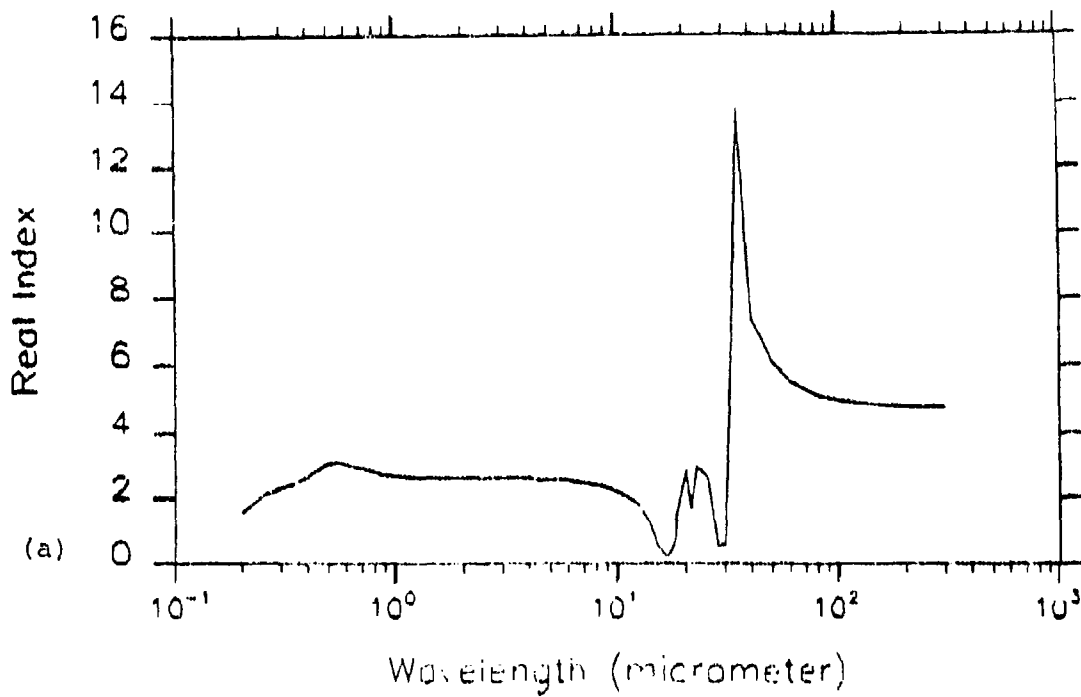


Figure 6. Indices of Refraction of Hematite, (a) Real part and (b) Imaginary Part

4) Onari et al.⁴⁷ for the 10 to 300 μm region
 In Table 11, the values for the 0.8 to 4 μm region are estimates because indices of refraction are not available. Also the values beyond 4 μm represent average indices of refraction since hematite, like quartz, is anisotropic in this region. The average indices of refraction are calculated using

$$m_{\text{avg}} = 2m_{\text{o-ray}}/3 + m_{\text{e-ray}}/3 \quad (9)$$

where the 2/3 to 1/3 ratio is used because two of the optical axes of hematite are the same. (Although it is not correct to average indices of refraction, the resulting values are sufficient for use in Eqs. 6 - 8. That is, for small concentrations of hematite, the anisotropic effects from quartz dominate those of the hematite.) For the 10 to 20 μm region, the measurements by Steyer⁴⁶ and Onari et al.⁴⁷ have been averaged together before applying Eq. 9. The weighting scheme is given by

$$m(\lambda) = w(\lambda)m_S(\lambda) + (1 - w(\lambda))m_O(\lambda) \quad (10)$$

where m_S and m_O are the complex indices of refraction from Steyer and Onari et al. and

$$w(\lambda) = \begin{cases} 1, & \lambda \leq 10 \\ (\lambda - 20)^2(2\lambda - 10)/1000, & 10 \leq \lambda \leq 20 \\ 0, & 20 \leq \lambda \end{cases} \quad (11)$$

47. Onari, S., Arai, T. and Kudo, K. (1977) Infrared lattice vibrations and dielectric dispersion in $\alpha\text{-Fe}_2\text{O}_3$, Phys. Rev. B, 16:1717-1721.

Table 12. Indices of Refraction for Sand Having a Volume Fraction of Hematite of 5%. The numbers in parentheses in the k columns are the power of 10 following the value of k (if no value given, then the previous power of 10 is implied)

WAVELENGTH (μm)	(O-RAY)		(E-RAY)		WAVELENGTH (μm)	(O-RAY)		(E-RAY)	
	n	k	n	k		n	k	n	k
0.200	1.657	7.36(-2)	1.657	7.36(-2)	8.500	0.220	1.52(0)	0.153	1.47(0)
0.250	1.646	5.80	1.646	5.80	8.700	0.425	1.80	1.037	1.03
0.300	1.630	4.45	1.630	4.45	9.000	0.199	2.33	0.241	2.80
0.337	1.617	3.84	1.617	3.84	9.200	0.622	4.31	1.639	6.13
0.400	1.607	1.66	1.607	1.66	9.500	4.385	3.74(-1)	3.816	2.18(-1)
0.488	1.608	5.39(-3)	1.608	5.39(-3)	9.800	2.973	8.29(-2)	2.827	6.60(-2)
0.515	1.607	3.98	1.607	3.98	10.000	2.639	4.95	2.552	4.22
0.550	1.605	2.33	1.605	2.33	10.591	2.104	2.18	2.153	2.02
0.633	1.598	2.57(-4)	1.598	2.57(-4)	11.000	2.014	1.73	2.001	1.59
0.694	1.595	2.76(-5)	1.595	2.76(-5)	11.500	1.839	1.89	1.854	1.56
0.860	1.586	1.22(-4)	1.586	1.22(-4)	12.500	1.576	2.14(0)	1.283	1.26(-1)
1.060	1.580	9.54(-7)	1.580	9.54(-7)	13.000	2.147	5.17(-2)	2.575	3.05
1.300	1.577	3.27	1.577	3.27	14.000	1.741	3.71	1.792	1.97(-2)
1.538	1.574	1.85	1.574	1.85	14.800	1.778	3.05	1.625	2.08
1.800	1.569	1.37	1.569	1.37	15.000	1.727	2.52	1.584	2.28
2.000	1.565	1.53	1.565	1.53	16.000	1.360	1.22(-1)	1.146	2.57(-1)
2.250	1.561	1.69	1.561	1.69	17.000	1.748	2.98	1.744	9.09(-2)
2.500	1.556	6.76	1.556	9.19	18.000	1.433	5.23(-2)	0.457	2.30(-1)
2.700	1.551	8.54	1.551	1.36(-6)	18.500	1.242	4.20	0.213	1.04(0)
3.000	1.545	2.64(-5)	1.545	0.58	20.000	0.125	8.25(-1)	1.330	4.78
3.200	1.539	6.95(-6)	1.539	4.28	21.000	0.270	2.58(0)	2.948	2.77(-1)
3.392	1.533	6.59	1.533	5.91	22.500	5.540	1.15	2.531	1.66
3.500	1.529	8.49	1.529	8.49	25.000	0.812	1.84	1.505	1.26
3.750	1.519	5.85(-5)	1.519	3.63(-5)	27.900	2.442	2.04(-1)	4.651	8.88
4.000	1.508	7.11	1.508	7.11	30.000	2.953	1.62	3.605	6.48
4.500	1.488	4.86(-4)	1.488	3.52(-4)	31.000	2.477	1.43(-2)	2.647	7.43(-2)
5.000	1.464	5.51(-3)	1.464	4.37(-3)	40.000	2.358	6.89(-3)	2.470	1.08
5.500	1.418	5.42	1.418	5.12	50.000	2.329	4.46	2.377	3.36(-3)
6.000	1.372	6.65	1.372	4.74	60.000	2.280	3.24	2.329	2.11
6.200	1.340	7.73	1.340	7.73	80.000	2.247	4.31	2.289	1.27
6.500	1.294	5.75	1.294	7.24	100.000	2.226	1.40	2.272	9.42(-4)
7.200	1.113	1.74(-2)	1.113	1.46(-2)	150.000	2.214	1.15	2.257	5.27
7.500	0.623	8.25	0.601	8.99	200.000	2.204	9.97(-4)	2.252	1.69
8.200	0.157	5.84(-1)	0.139	6.38(-1)	300.000	2.202	8.27	2.249	2.00

Table 13. Indices of Refraction for Sand Having a Volume Fraction of Hematite of 10%. The numbers in parentheses in the k columns are the power of 10 following the value of k (if no value given, then the previous power of 10 is implied)

WAVELENGTH (μm)	(O-RAY)		(E-RAY)		WAVELENGTH (μm)	(O-RAY)		(E-RAY)	
	n	k	n	k		n	k	n	k
0.200	1.665	1.47(-1)	1.665	1.47(-1)	8.500	0.356	1.83(0)	0.239	1.74(0)
0.250	1.666	1.17	1.666	1.17	8.700	0.854	2.19	1.557	7.09(-1)
0.300	1.677	9.00(-2)	1.677	9.00(-2)	9.000	0.221	2.06	0.251	2.56(0)
0.337	1.665	7.78	1.665	7.78	9.200	0.612	4.07	1.580	5.85
0.400	1.656	3.35	1.656	3.35	9.500	4.274	3.56(-1)	3.733	2.07(-1)
0.488	1.667	1.09	1.667	1.09	9.800	2.933	7.89(-2)	2.794	6.29(-2)
0.515	1.666	8.09(-3)	1.666	8.09(-3)	10.000	2.615	4.74	2.533	4.05
0.550	1.664	4.74	1.664	4.74	10.591	2.180	2.14	2.151	1.98
0.633	1.655	5.22(-4)	1.655	5.22(-4)	11.000	2.015	1.72	2.003	1.60
0.694	1.650	5.61(-5)	1.650	5.61(-5)	11.500	1.844	1.90	1.859	1.59
0.860	1.635	2.46(-4)	1.635	2.46(-4)	12.500	1.564	2.02(0)	1.305	1.23(-1)
1.060	1.627	1.92(-6)	1.627	1.92(-6)	13.000	2.113	5.15(-2)	2.524	2.91
1.300	1.623	6.51(-7)	1.623	6.51(-7)	14.000	1.715	3.94	1.762	2.29(-2)
1.536	1.620	3.63	1.620	3.63	14.800	1.727	3.81	1.585	2.93
1.800	1.615	2.67	1.615	2.67	15.000	1.669	3.48	1.533	3.33
2.000	1.611	3.00	1.611	3.00	16.400	1.163	2.37(-1)	0.955	4.81(-1)
2.250	1.607	3.31	1.607	3.31	17.200	2.011	6.55	1.404	1.53
2.500	1.602	8.58	1.602	1.09(-6)	18.000	1.584	9.12(-2)	0.489	2.49
2.700	1.597	1.19(-6)	1.597	1.59	18.500	1.346	6.03	0.279	1.10(0)
3.000	1.591	2.60(-5)	1.591	8.69	20.000	0.145	8.86(-1)	1.389	4.57
3.200	1.585	7.13(-6)	1.585	4.53	21.300	0.346	2.59(0)	2.653	4.48(-1)
3.392	1.579	6.78	1.579	6.17	22.500	5.370	1.35	2.698	2.95
3.500	1.576	8.66	1.576	8.66	25.000	0.346	1.84	1.559	1.54
3.750	1.567	5.75(-5)	1.566	3.58(-5)	27.900	2.162	3.82(-1)	4.400	9.15
4.000	1.555	7.10	1.555	7.10	30.000	1.446	3.53	4.196	1.41(0)
4.500	1.535	4.86(-4)	1.535	3.45(-4)	35.000	2.655	2.43(-2)	2.836	3.69(-2)
5.000	1.511	5.39(-3)	1.511	4.27(-3)	40.000	2.491	1.07	2.606	1.51
5.500	1.466	5.33	1.466	5.03	50.000	2.446	6.11(-3)	2.495	5.09(-3)
6.000	1.420	6.56	1.420	4.68	60.000	2.388	4.28	2.436	3.19
6.500	1.389	7.64	1.389	7.64	80.000	2.347	4.94	2.389	1.92
6.500	1.342	5.71	1.342	7.17	100.000	2.326	1.87	2.370	1.43
7.200	1.161	1.24(-2)	1.160	1.46(-2)	150.000	2.310	1.43	2.352	8.24(-4)
7.900	0.662	9.22	0.634	9.38	200.000	2.299	1.21	2.347	5.88
8.200	0.175	6.32(-1)	0.155	6.93(-1)	300.000	2.296	1.36	2.343	3.43

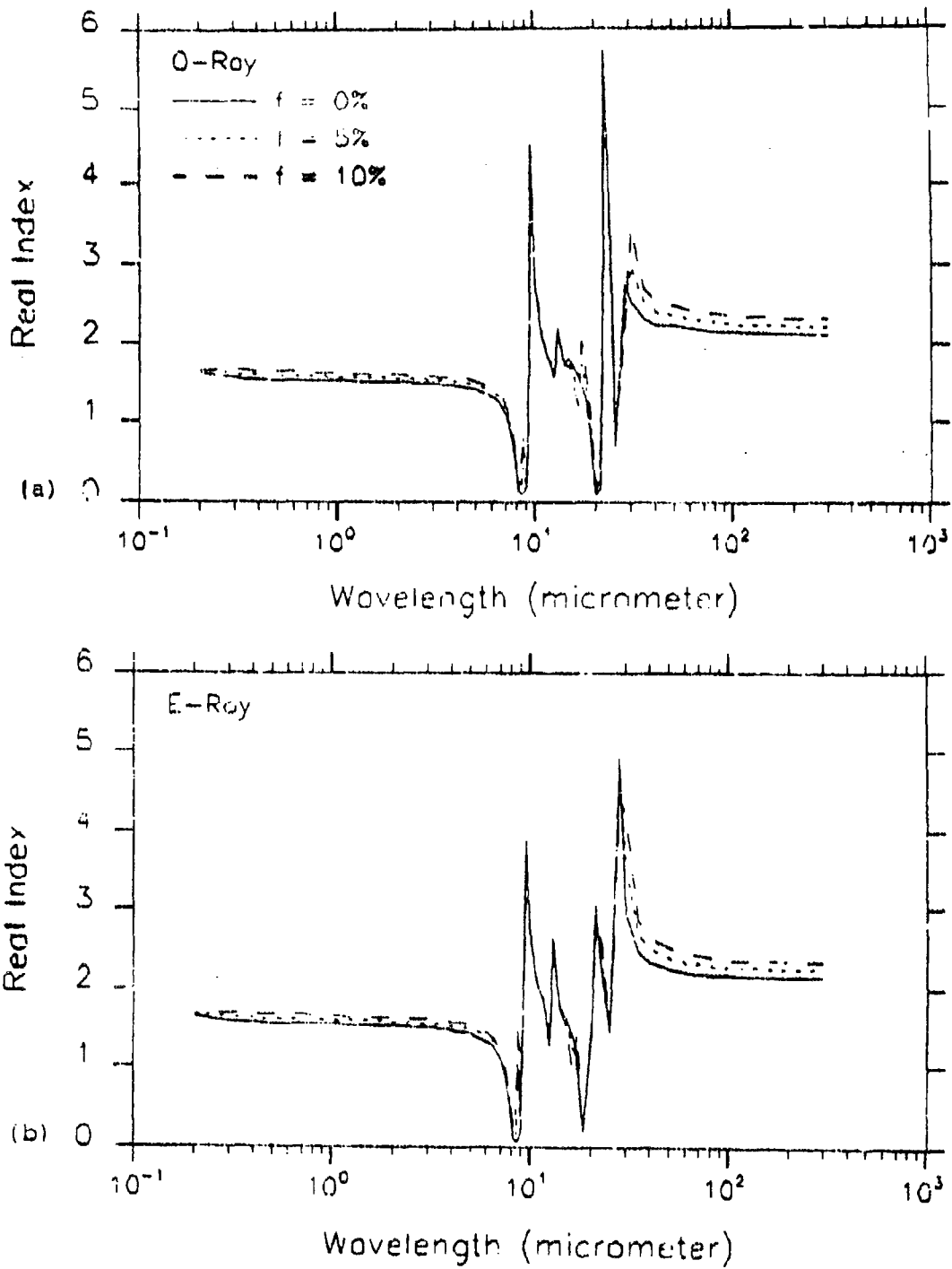


Figure 7. Real Part of the Index of Refraction for Sand Having Hematite Concentrations of 0, 5 and 10%, (a) O-Ray and (b) E-Ray

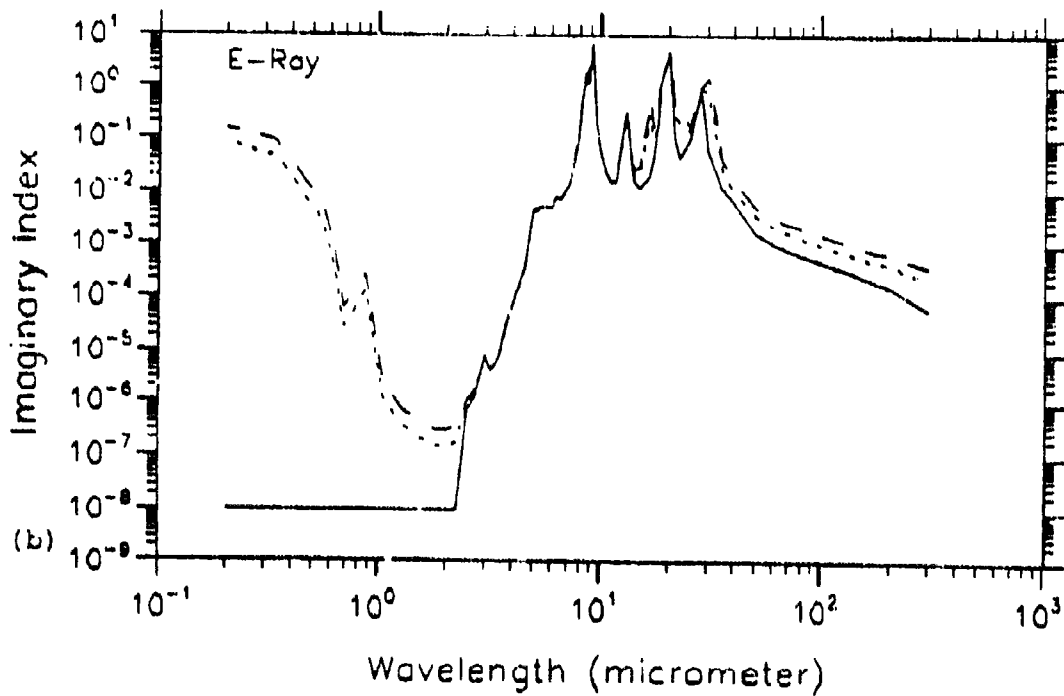
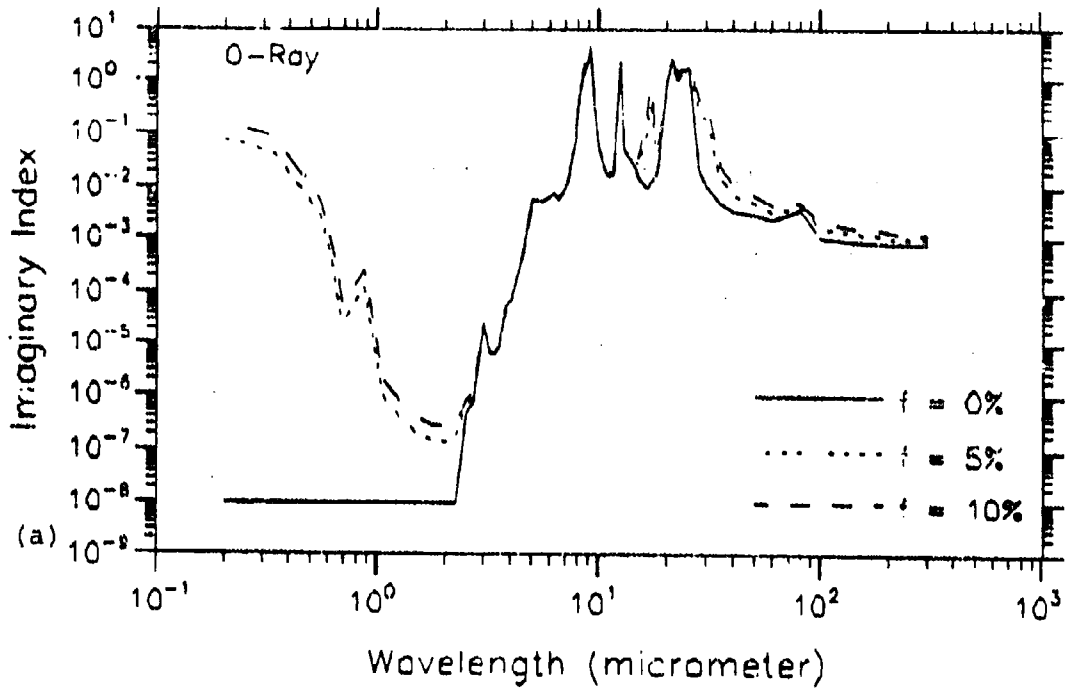


Figure 8. Imaginary Part of the Index of Refraction for Sand Having Hematite Concentrations of 0, 5 and 10%, (a) O-Ray and (b) E-Ray

where the weighting function has the properties that: $w(10) = 1$, $w(20) = 0$ and the derivative of $w(\lambda)$ goes to zero for $\lambda = 10, 20$.

Equations 6 - 8 and the data in Tables 9 - 11 have been used to obtain indices of refraction for sand having hematite concentrations of 5 and 10%. The results are listed in Tables 12 and 13, and are shown in Figures 7 and 8. These volume fractions, along with $f = 0\%$ (pure quartz), encompass the range of hematite concentrations in sand^{7,48}.

Tables 12 and 13 suggest that the concentration of hematite in the sand component will strongly affect the radiative properties of the aerosol as a whole. This is especially true for the 0.2 - 0.6 μm wavelength region where the imaginary index varies from 10^{-8} to 10^{-1} . Therefore, Mie calculations were performed for sand having hematite concentrations of 0, 5 and 10%. The results and implications of these calculations will be discussed in Section 4.1.

It should be mentioned that for each hematite concentration, separate Mie calculations were performed for the o-ray and e-ray. The radiative properties for a given concentration of hematite are then obtained as two thirds of the o-ray values plus one third of the e-ray values. The two-thirds to one-third ratio is used because, like hematite, two of the three optical axes of quartz are the same. (Note in this case, Mie calculations are being averaged, not indices of re-

48. Egan, W. G. (1985) Photometry and Polarization in Remote Sensing, Elsevier Science Publishing, New York, pp. 398-399.

fraction.) Dealing with birefringent materials in this manner is, strictly speaking, only valid for particles that are small compared with the wavelength. Since our sand particles approach the geometric optics limit, the approach may not be truly applicable.

3.3.3 Discussion of the Indices of Refraction

The use of a separate set of optical constants for each mode of the size distribution is the main difference between the present model and the previous desert aerosol models of Shettle¹ and of d'Almeida³⁴. (They both use only one set of optical constants for all particles making up the aerosol.) The distinction between the two approaches is subtle, but important. In the present model, the indices of refraction for each component are based on measurements of pure substances while the Shettle and d'Almeida models use average indices of refraction which attempt to characterize the complex mixture of discrete particles comprising the desert aerosol. Because they have different physical meanings, it is difficult to make a direct comparison between the average indices of refraction used by Shettle and by d'Almeida, which are based on those in the literature, and the ones used in the present model. However, the advantage of using optical constants obtained from bulk measurements is that they tend to be more accurate.

3.4 Method of Determining the Optical Properties of Multicomponent Mixtures

When performing the radiative calculations for each aerosol component, a number density of 1 particle cm^{-3} of air

was used for simplicity. The attenuation coefficients corresponding to 1 particle cm^{-3} were then converted to those having the absolute volumes given in Table 6. (The conversion factor is the actual volume of the aerosol component divided by the volume for 1 particle cm^{-3} .) These attenuation coefficients were then added together to obtain the volume-weighted attenuation coefficients. In turn, the single scattering albedo, w_0 , of the aerosol is equal to the volume-weighted scattering coefficient divided by the volume-weighted extinction coefficient.

By definition, the method of determining the volume-weighted asymmetry parameter, g , is different from that for the attenuation coefficients. Here, g represents the average cosine of the scattering angle for a fictitious 1 particle cm^{-3} of air. g is thus calculated using the following equation:

$$g(\lambda) = \frac{\sum g_i(\lambda) X_i(\lambda) N_i}{\sum X_i(\lambda) N_i} \quad (12)$$

where X_i is the scattering coefficient for 1 particle cm^{-3} and g_i is the asymmetry parameter for each component.

4. RESULTS

4.1 Results for Various Concentrations of Hematite in the Sand Component

An effort has been made to determine how the radiative properties of the desert aerosol are affected by the concentration of hematite in the sand component. (The presence of hematite is important because it is a selective absorber at visible wavelengths.) Seven cases have been investigated in this report, each representing a possible composition for the sand component. The cases are summarized in Table 14.

Table 14. Various Compositions of the Sand Component Investigated in this Report

Percentage of Particles Making Up the Sand Component			
Case No.	f = 0%	f = 5%	f = 10%
1	100	0	0
2	0	100	0
3	0	0	100
4	50	50	0
5	50	0	50
6	0	50	50
7	33.3	33.3	33.3

Cases 1 - 3 represent sand components that have hematite concentrations of 0, 5 and 10%, respectively. In Cases 4 - 6, the sand component is composed of two types of particles, each having its own hematite content. Here the two types of particles have the same size distribution as before, but have only 50% of the total number of sand particles. In Case 7, the size distribution of the sand component contains an equal number of particles having hematite contents of 0, 5 and 10%.

The radiative properties of the desert aerosol were determined using each of the sand components given in Table 14. A preliminary survey of the results showed that the extinction coefficients for Cases 1 - 7 are essentially the same. (This is expected since extinction is driven primarily by the size distribution.) Furthermore, Cases 2, 3, 6 and 7 gave similar values for the absorption coefficient which suggests that for our size distribution, the effects of hematite concentrations of 5 and 10% are about the same.

Figures 9(a) and 9(b) give absorption coefficients and single scattering albedos as a function of wavelength for a wind speed of 0 ms^{-1} . (Only Cases 1, 3 and 5 have been plotted because, as mentioned above, the effects of hematite concentrations of 5% and 10% are about the same.) In Figure 9(a), it can be seen that beyond about $1 \mu\text{m}$, absorption coefficients are similar for Cases 1, 3 and 5. At UV and visible wavelengths, the presence of hematite in the sand component gives increased absorption as expected. In Figure 9(b), the higher absorption for Cases 3 and 5 leads to lower single

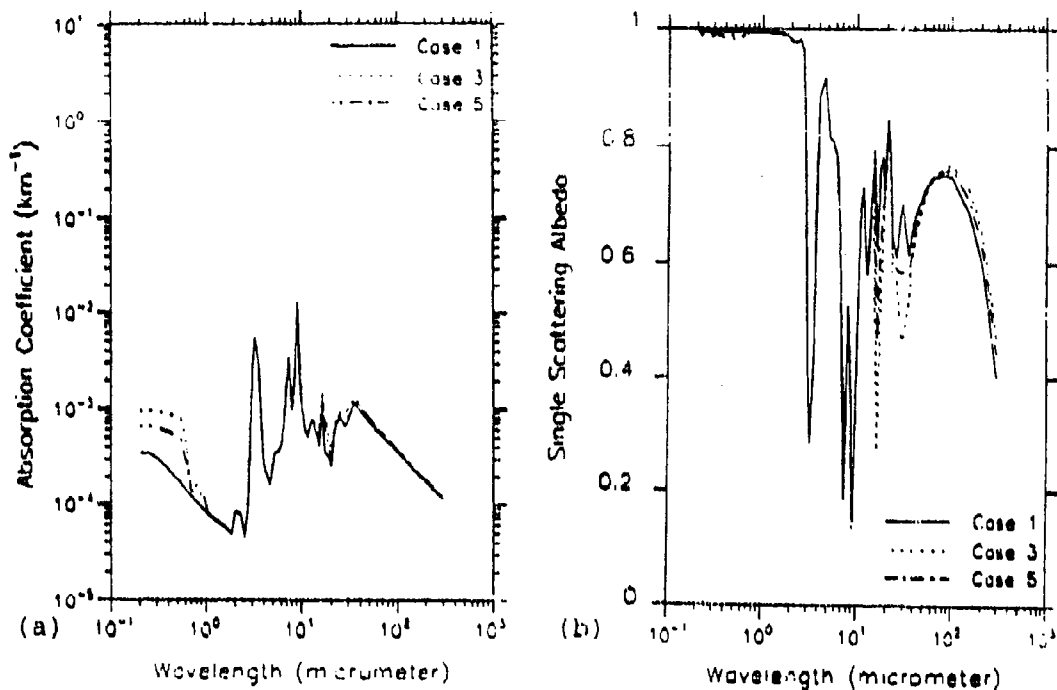


Figure 9. Desert Aerosol Model (a) Absorption Coefficients and (b) Single Scattering Albedos using Cases 1, 3 and 5 for the Sand Component with 0 ms⁻¹ Wind Speed Conditions

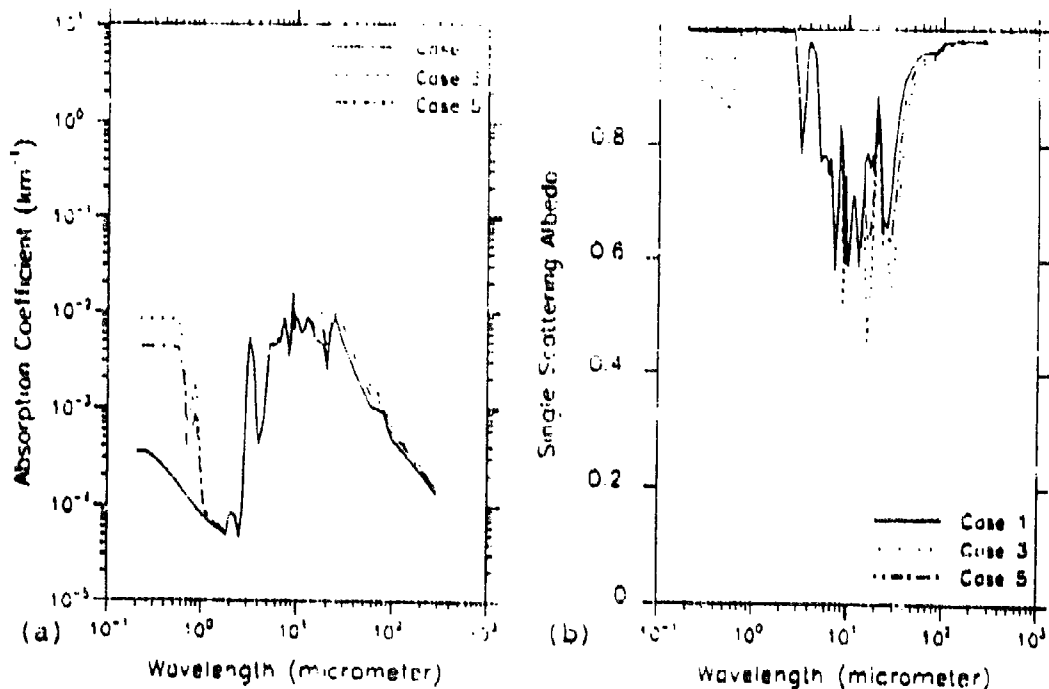


Figure 10. Desert Aerosol Model (a) Absorption Coefficients and (b) Single Scattering Albedos using Cases 1, 3 and 5 for the Sand Component with 10 ms⁻¹ Wind Speed Conditions

scattering albedos at UV and visible wavelengths. The minima near 16 and 30 μm for Cases 3 and 5 are directly related to the absorption bands of hematite at these wavelengths.

Similar plots of absorption coefficient and single scattering albedo are given in Figures 10 - 12 for wind speeds of 10, 20 and 30 ms^{-1} . The same observations can be made for Cases 1, 3 and 5, but the differences at UV and visible wavelengths become more pronounced as the wind speed increases.

4.2 Choosing a Sand Component for the Desert Aerosol Model

We have selected Case 5 to represent the sand component in the present desert aerosol model. Case 5 was chosen because it represents a "middle of the road" estimate of the absorption at UV and visible wavelengths. That is, Cases 1 and 3 give the extrema of absorption and, therefore, Case 5 best represents the range of the calculations. For reference, the results of the Mie calculations for Case 5, as well as for the carbonaceous and water soluble components, are given in Appendix B.

4.3 General Discussion of the Desert Aerosol Model

This section gives the results for the present desert aerosol model where, as discussed in Section 4.2, the sand component consists of quartz particles and quartz particles contaminated with a 10% concentration of hematite. Figures 13 through 16 give the attenuation coefficients as a function of wavelength for 0, 10, 20 and 30 ms^{-1} wind speed conditions. The 0 ms^{-1} and 30 ms^{-1} winds are meant to represent background

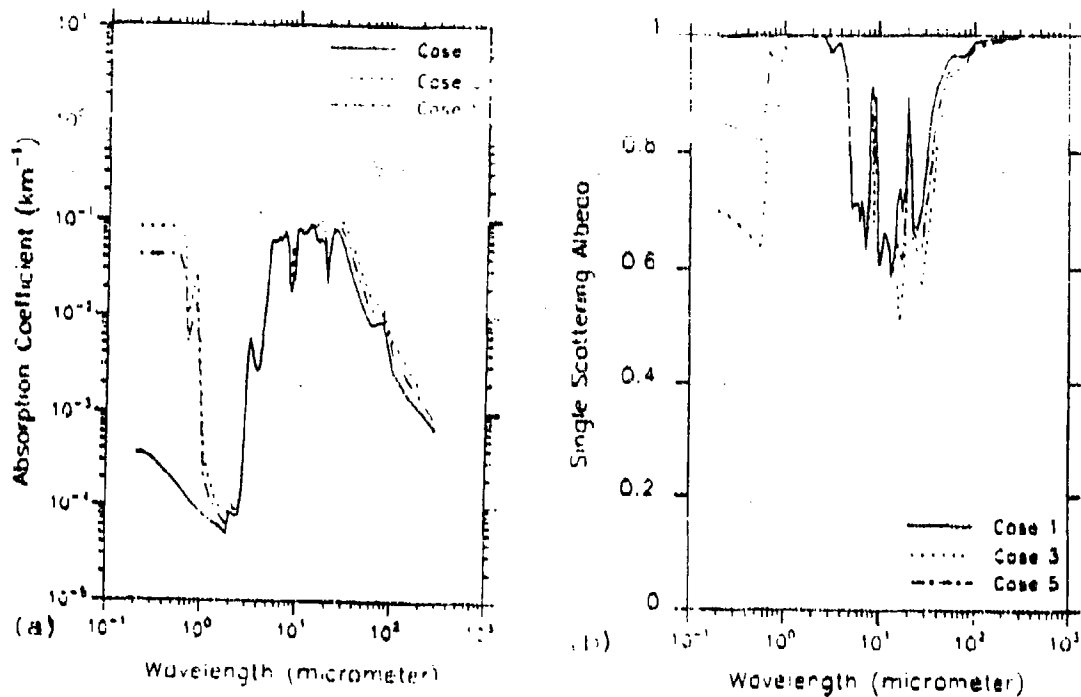


Figure 11. Desert Aerosol Model (a) Absorption Coefficients and (b) Single Scattering Albedos using Cases 1, 3 and 5 for the Sand Component with 20 ms⁻¹ Wind Speed Conditions

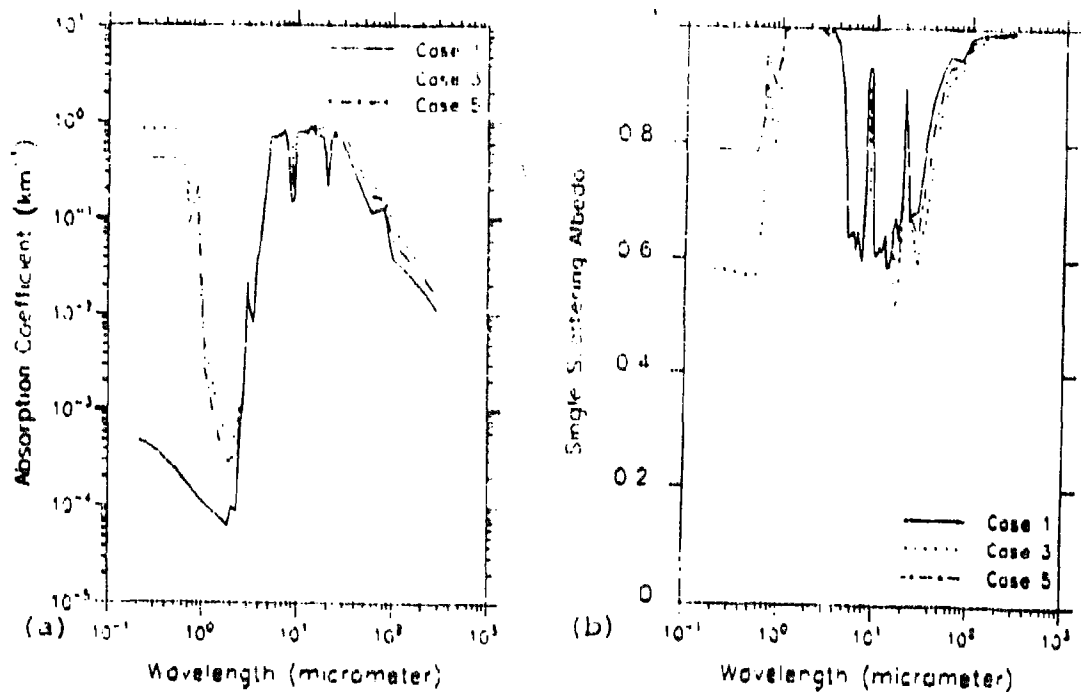


Figure 12. Desert Aerosol Model (a) Absorption Coefficients and (b) Single Scattering Albedos using Cases 1, 3 and 5 for the Sand Component with 30 ms⁻¹ Wind Speed Conditions

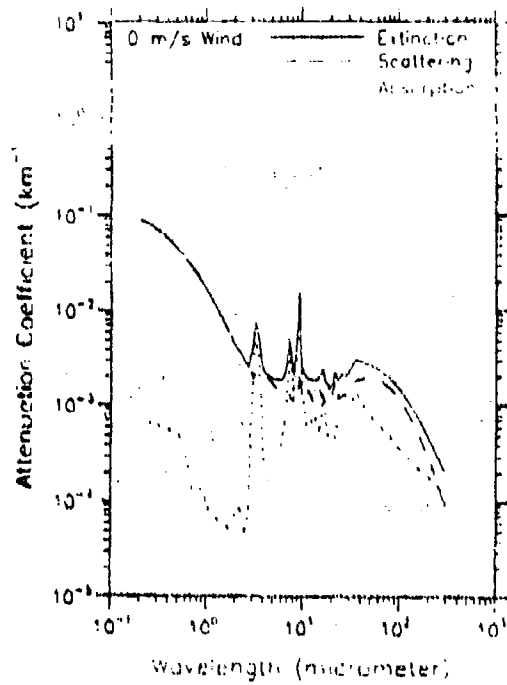


Figure 13. Desert Aerosol Model Attenuation Coefficients Versus Wavelength for 0 ms^{-1} Wind Speed Conditions

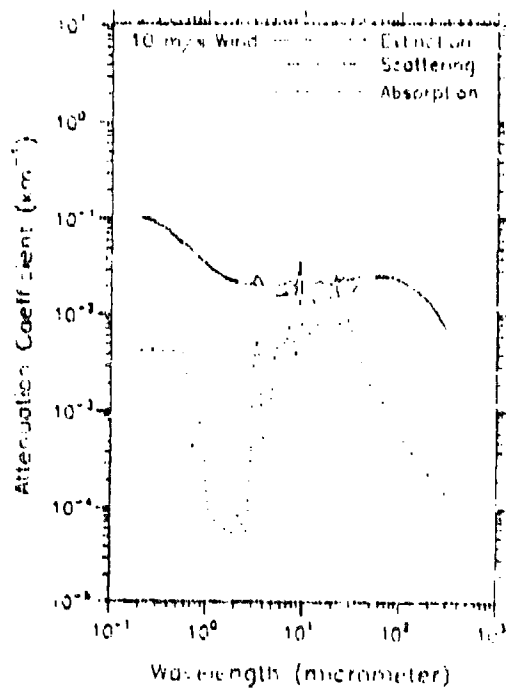


Figure 14. Desert Aerosol Model Attenuation Coefficients Versus Wavelength for 10 ms^{-1} Wind Speed Conditions

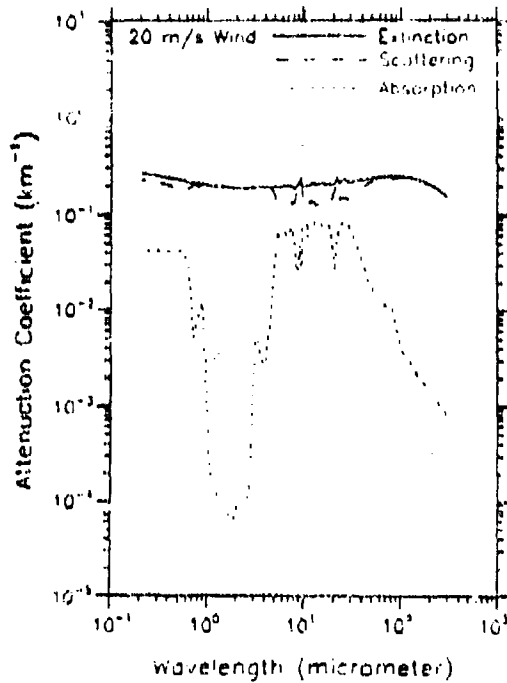


Figure 15. Desert Aerosol Model Attenuation Coefficients Versus Wavelength for 20 ms^{-1} Wind Speed Conditions

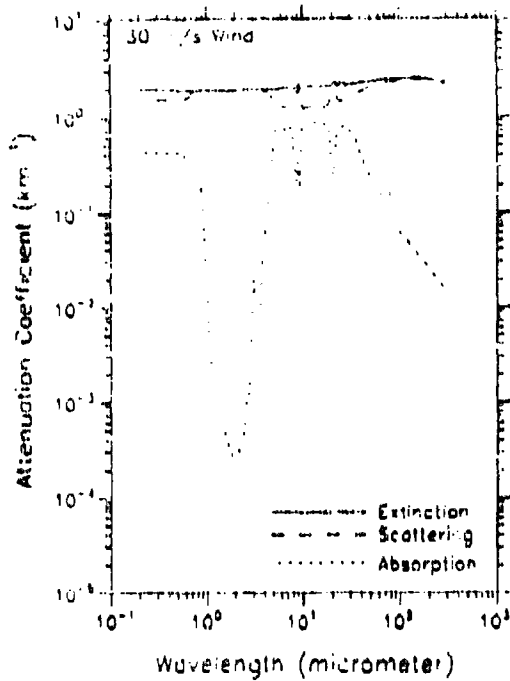


Figure 16. Desert Aerosol Model Attenuation Coefficients Versus Wavelength for 30 ms^{-1} Wind Speed Conditions

and severe dust storm conditions respectively. For reference, the values in Figures 13 - 16 have been tabulated in Appendix C.

A number of important features in Figures 13 - 16 are worth mentioning. First, there is selective absorption at visible wavelengths which becomes more pronounced as the wind speed increases. The selective absorption is due to the hematite in the sand component and will make the desert aerosol appear slightly reddish in color during dust storm conditions. The carbonaceous particles contribute very little to the total absorption of visible radiation primarily because their abundance is too small.

A second thing to observe in Figures 13 - 16 is the structure in the IR absorption. The peaks in the absorption near 3, 7 and 9 μm for 0 ms^{-1} wind speed conditions are primarily due to the strong absorption bands of ammonium sulfate. For dust storm conditions however, the absorption in the IR is dominated by the sand component. Interestingly, there are minima in the absorption and maxima in the scattering near 8 and 20 μm , which correspond to the centers of the strong crystal lattice absorption bands of quartz. It is believed that this phenomenon is a result of the quartz in the sand component acting as a reflector. To show this, consider an electromagnetic wave propagating in air as it encounters a plane boundary having a complex index of refraction, $m = n + ik$. For normal incidence, the reflectance is given by

$$\text{Reflectance} = \frac{(n - 1)^2 + k^2}{(n + 1)^2 + k^2} \quad (13)$$

When $n \ll 1$, $n \gg 1$ or $k \gg 1$ (as is the case for the absorption bands of quartz), the reflectance approaches 1.0. Thus the incident radiation is reflected and the absorption drops because the incident wave cannot penetrate the material to be absorbed.

Finally, it can be seen from Figures 13 - 16 that the extinction is wavelength dependent for winds of 0 ms^{-1} but nearly constant at 20 and 30 ms^{-1} . These differences are driven by the relative contributions of the aerosol components. For winds of 0 ms^{-1} , only the smaller water soluble particles with respect to the wavelength dominate the extinction at visible and near IR wavelengths and, therefore, a wavelength dependence exists. On the otherhand, in high wind speed conditions, the extinction is dominated by the much larger sand particles that approach the geometric optics regime.

Figure 17 gives the values of single scattering albedo for 0 ms and 30 ms^{-1} wind speed conditions. At the UV and shorter visible wavelengths, the single scattering albedos decrease significantly as the wind speed increases. This effect becomes less pronounced, however, for the longer visible and near IR wavelengths. In the middle IR region, single scattering albedos for 0 and 30 ms^{-1} winds exhibit a high degree of structure. Specifically, the sharp minima near 3, 7 and $9 \mu\text{m}$

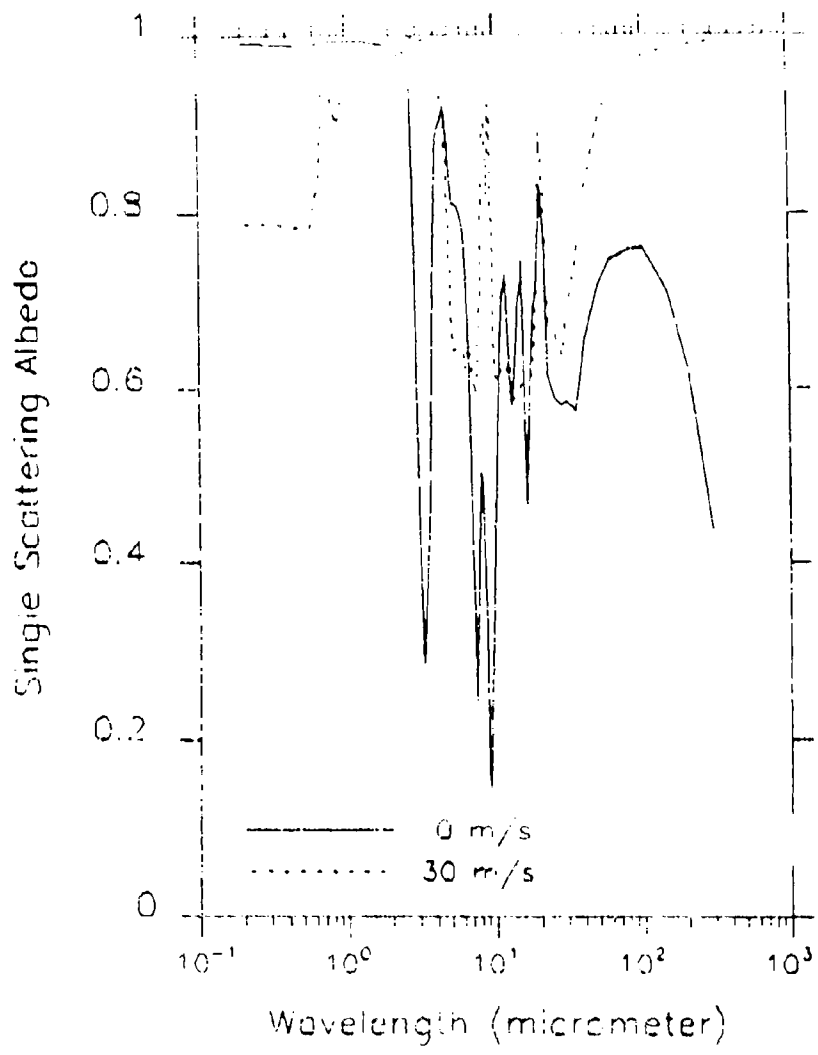


Figure 17. Desert Aerosol Model Single Scattering Albedo Versus Wavelength for 0 and 30 ms⁻¹ Wind Speed Conditions

can be attributed to the absorption by ammonium sulfate. For winds of 30 ms^{-1} , the large peaks near 9 and 20 μm relate to the excess scattering by the quartz in the sand component which was discussed earlier. Beyond about 40 μm , single scattering albedos for 0 ms^{-1} winds are much lower than those for 30 ms^{-1} winds. This should not be interpreted as significant absorption, however, because the magnitude of the absorption is small beyond 40 μm for 0 ms^{-1} winds.

Figure 18 gives the values of the asymmetry parameter as a function of wavelength for 0 and 30 ms^{-1} wind speed conditions. Generally speaking, the values for dust storm conditions are greater than those for background conditions throughout the 0.2 to 300 μm region. This should not be a surprise because the scattering for dust storm conditions is dominated by the large sand particles (with respect to the wavelength of radiation) which have their scattering peaked in the forward direction.

4.4 Comparison with Other Researchers

This section compares the present desert aerosol model with the models of Shettle¹ and d'Almeida³⁴. The comparisons are limited to the 0.4 - 40 μm wavelength region because the Shettle and d'Almeida models end at 40 μm . For reference, the number densities distributions of the present desert aerosol and the d'Almeida model are compared in Figure 19 and the area distributions are compared in Figure 20. The curves for the d'Almeida model are derived from the trimodal lognormal size distributions that d'Almeida used when performing his radia-

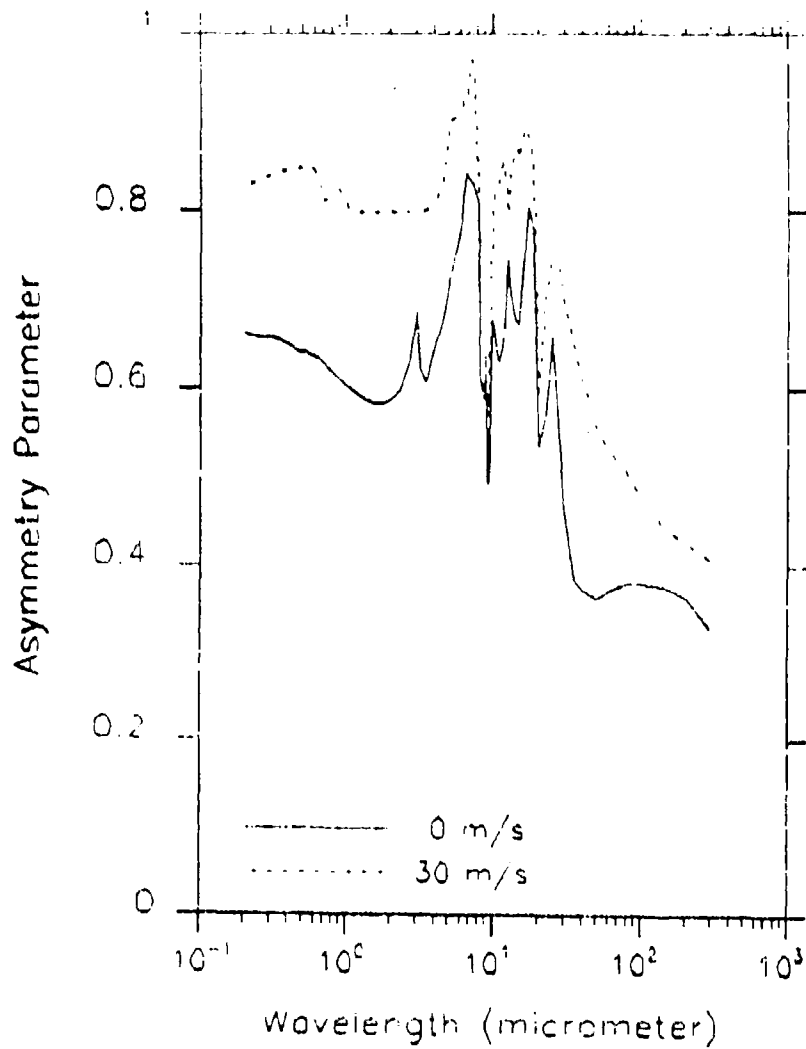


Figure 18. Desert Aerosol Model Asymmetry Parameter Versus Wavelength for 0 and 30 ms⁻¹ Wind Speed Conditions

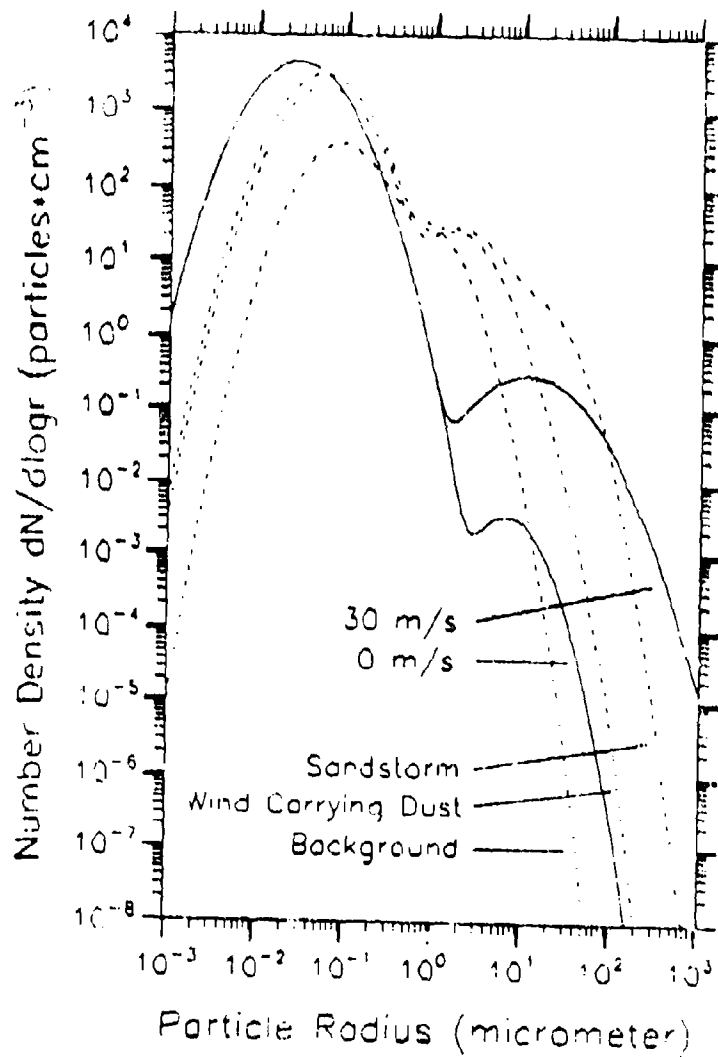


Figure 19. Number Density Distributions for the Present Desert Aerosol Model (solid lines) and Those of d'Almeida³⁴ (dashed lines)

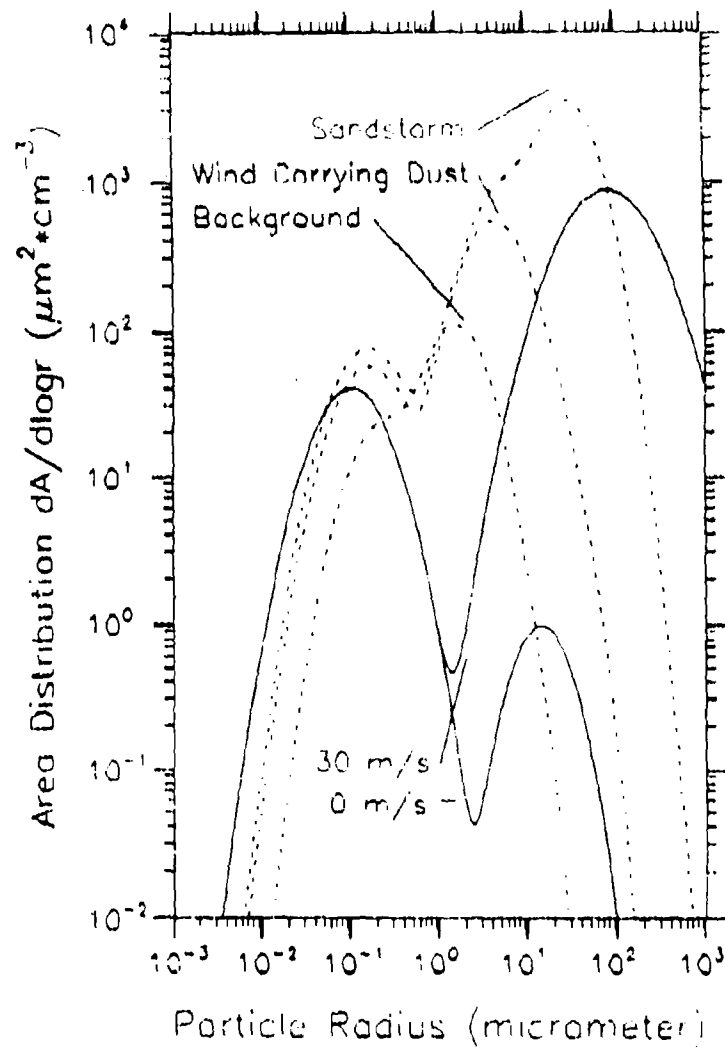


Figure 20. Area Distributions for the Present Desert Aerosol Model (solid lines) and Those of d'Almeida³⁴ (dashed lines)

tive transfer calculations, not the observed size distribution data. (d'Almeida's size distribution parameters for background, wind carrying dust and sandstorm conditions are based on data gathered when the horizontal visibility was greater than 8 km, between 2 to 7 km and less than 2 km, respectively.) The size distributions of the present desert aerosol model and the Shettle model are essentially the same.

Figures 21(a) and 21(b) compare the wavelength dependent extinction coefficients against those of Shettle and d'Almeida, respectively. The present model gives values that are close to those of Shettle because both models use similar size distributions. Figure 21(b) suggests that the values of d'Almeida for background conditions are much greater than ours. The differences appear to be a result of d'Almeida defining his background conditions in terms of "clear" visibility and not wind speed, and some mass loading due to the wind may be occurring. The extinction calculated by d'Almeida for sandstorm conditions show strong variations with wavelength while ours do not. The structure beyond about 1 μm arises because much of the mass loading in the d'Almeida model is from particles that are smaller than ours and not in the geometric optics limit. Figures 22(a) and 22(b) give comparisons of the scattering coefficients.

Figures 23(a) and 23(b) compare the values of absorption coefficient as a function of wavelength against those of Shettle and d'Almeida respectively. (To avoid cluttering the figures, only the values for 0 and 30 ms^{-1} have been plotted.)

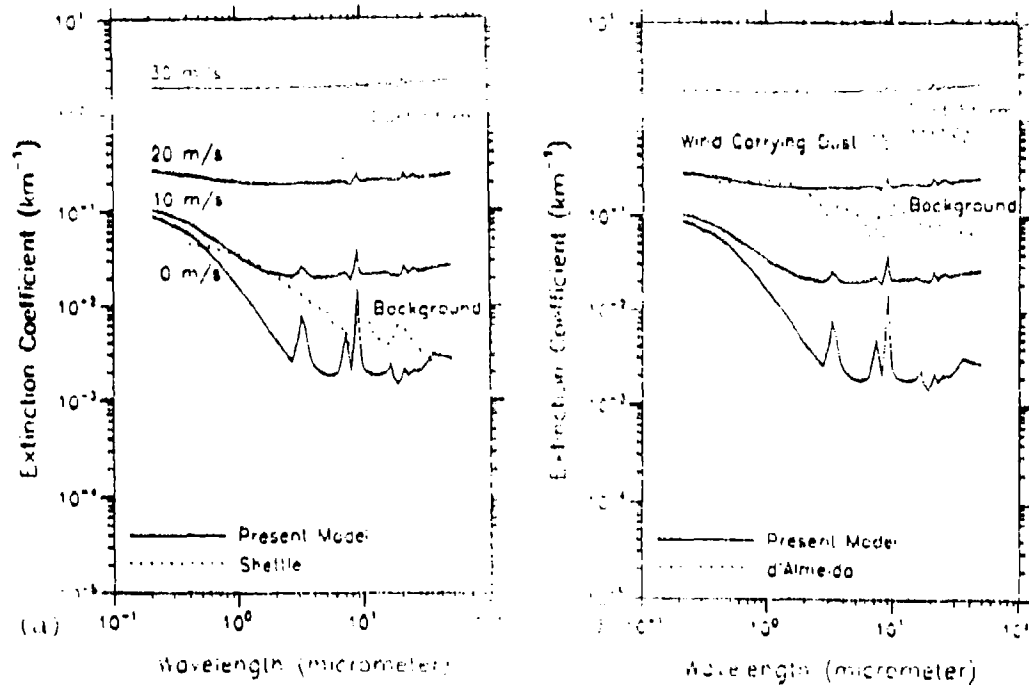


Figure 21. Comparison of Extinction Coefficients for the Desert Aerosol Model with Those of (a) Shettle¹ and (b) d'Almeida³⁴

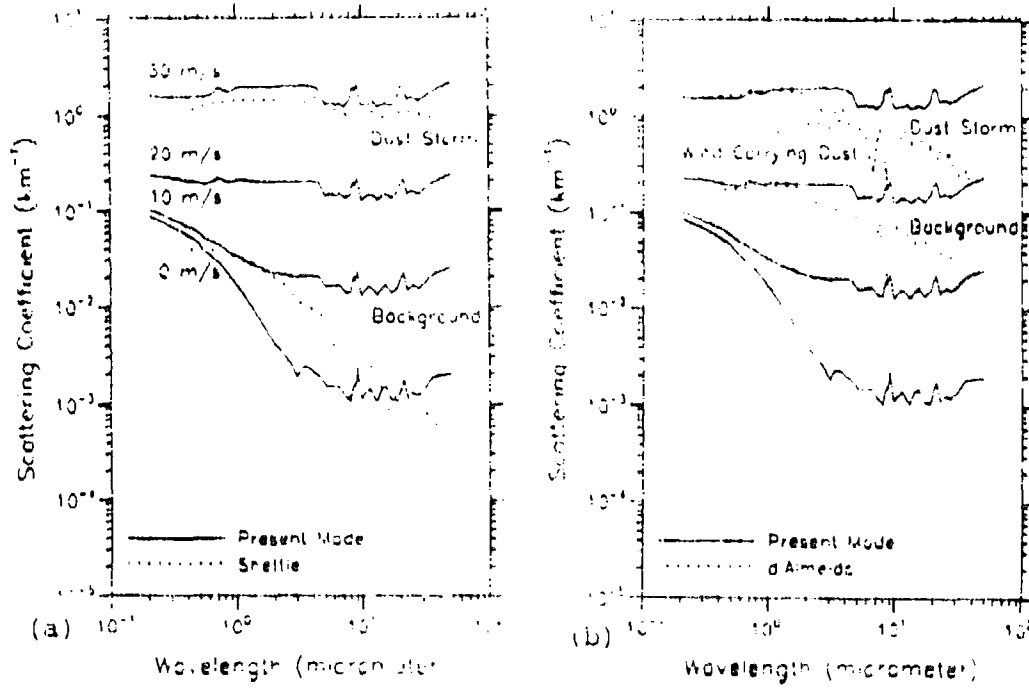


Figure 22. Comparison of Scattering Coefficients for the Desert Aerosol Model with Those of (a) Shettle¹ and (b) d'Almeida³⁴

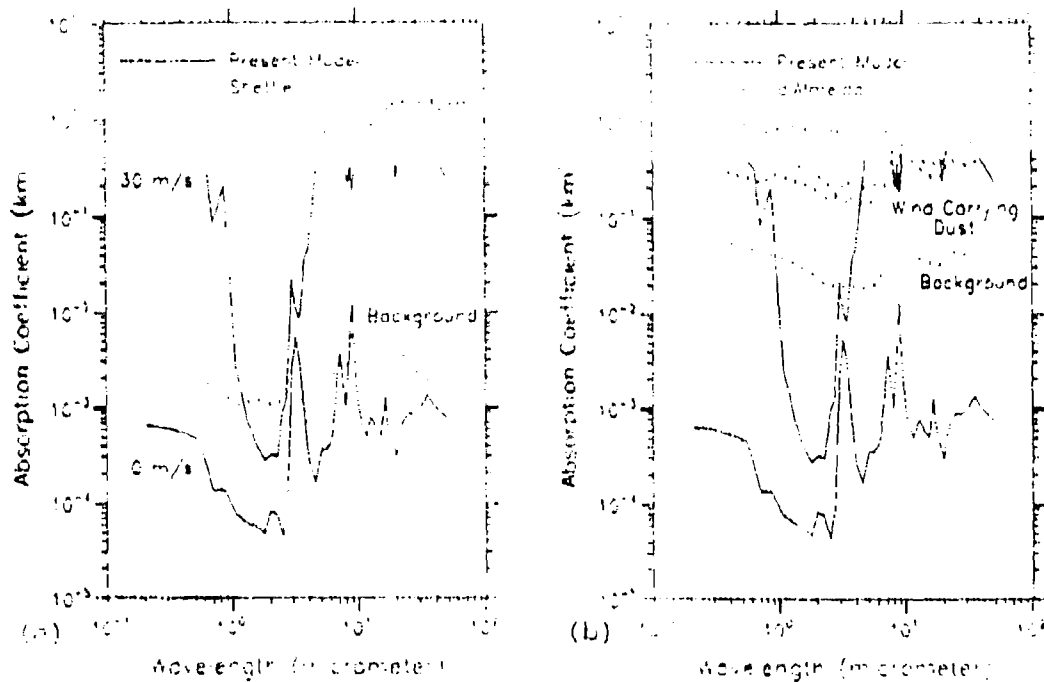


Figure 23. Comparison of Absorption Coefficients of the Desert Aerosol Model with (a) Those of Shettle and (b) Those of d'Almeida³⁴

In Figure 23(a), the magnitude of absorption for 0 ms^{-1} wind speeds is about one order less than the background model of Shettle. For dust storm conditions, the present and the Shettle models are similar in the middle IR region, but the present model gives far less absorption at the longer visible and the near IR wavelengths. Similar observations can be made about Figure 23(b). Absorption coefficients of the d'Almeida background model are about two orders of magnitude greater than ours and for dust storm conditions, the two models agree in the middle IR region. As with the Shettle model, the d'Almeida model for dust storm conditions predicts more absorption than the present model at longer visible and near IR

wavelengths. (This is the main difference between the three models and it is directly related to the way the present model deals with the index of refraction.)

Figure 24 compares single scattering albedos against those of Shettle and d'Almeida. In Figure 24(a), albedos for 0 ms^{-1} wind speeds are greater than the background models of Shettle and d'Almeida throughout the visible and near IR regime. The three models are in reasonable agreement between about 3 and $10 \mu\text{m}$, but significant differences exist beyond $20 \mu\text{m}$. In Figure 24(b), all three models show increasing albedos when going from UV to near IR wavelengths, but the absolute magnitudes differ from each other. Specifically, albedos for 30 ms^{-1} wind speeds are much higher than the dust storm models of Shettle and d'Almeida which is a direct consequence of the way the present model deals with the index of refraction. Also, Figure 24(b) suggests that the large peaks near 9 and $20 \mu\text{m}$ are not seen in the previous two models.

Comparisons of the asymmetry parameter as a function of wavelength are given in Figures 25(a) and 25(b) for background and for dust storm conditions, respectively. For background conditions, there is very little agreement between the three models, especially at visible and near IR wavelengths. In dust storm conditions, asymmetry parameters are similar for the three models. This should come as no surprise because the scattering for dust storm conditions is dominated by the large (with respect to the wavelength of radiation) sand particles which have their scattering peaked in the forward direction.

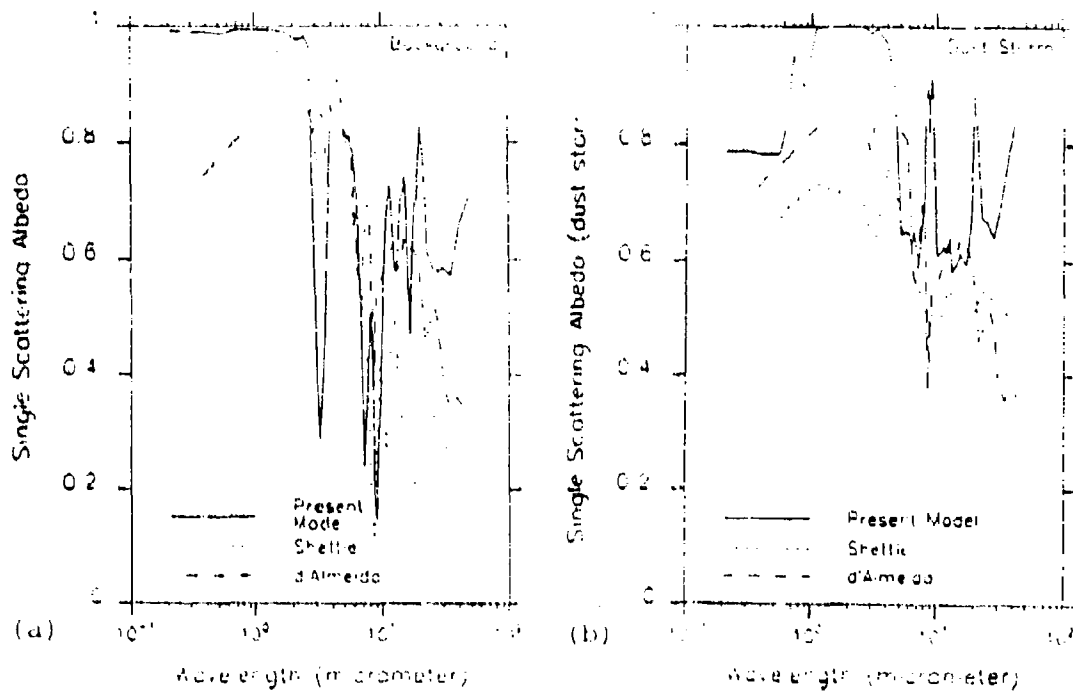


Figure 24. Comparison of Single Scattering Albedo for the Desert Aerosol Model with Those of Shettle¹ and d'Almeida³⁴, (a) Background and (b) Dust Storm Conditions

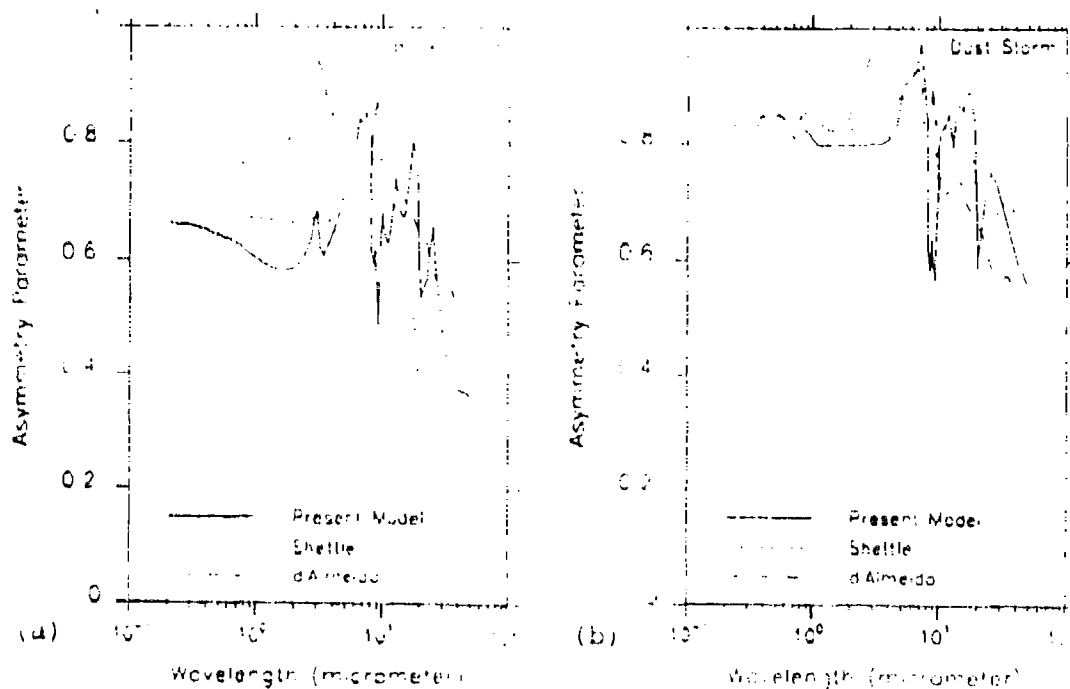


Figure 25. Comparison of Asymmetry Parameter for the Desert Aerosol Model with Those of Shettle¹ and d'Almeida³⁴, (a) Background and (b) Dust Storm Conditions

4.5 Comparison with Observations

In order to compare the three models with observed data, the extinction at 0.55 μm can be converted to visual ranges, V, using the formula

$$V = 3.912/\text{Extinction at } 0.55 \mu\text{m}.$$

Both the present and the Shettle background models yield visual ranges of about 80 km, while the d'Almeida background model yields a value close to 20 km. Measurements of visual range at White Sands, New Mexico by Pitchford and at Big Bend, Texas by Malm et al.⁵⁰ indicate that visibilities of 80 km occur frequently in desert and semi-desert areas which adds credibility to the present model. These measurements may also suggest that the extinction in the d'Almeida model may be too high for background conditions.

49. Pitchford, A., Pitchford, M., Malm, W., Flocchini, R., Cahill, T. and Walther, E. (1981) Regional Analysis of Factors Affecting Visual Air Quality, Atmospheric Environment, 15:2043-2054.

50. Malm, W. C., Walther, E. G., O'Dell, K. and Kleingardner, J. (1981) Visibility in the Southwestern United States from Summer 1978 to Spring 1979, Atmospheric Environment, 15:2031-2042.

5. SUMMARY AND CONCLUSIONS

A desert aerosol model that can be used to represent background and dust storm conditions has been presented. The model differs from previous desert aerosol models in that it treats the desert aerosol as being a three-component mixture, with each component having its own size distribution and set of indices of refraction. Mass loading during dust storms has been incorporated into the model also. Results from the present model for dust storm conditions indicate more selective absorption of visible and near IR radiation when compared with previous desert aerosol models. This should be of particular importance to those in the field of climate research.

References

1. Shettle, E. P. (1984) Optical and radiative properties of a desert aerosol model, IRS '84: Current Problems in Atmospheric Radiation, G. Fiocco, Ed., A. Deepak Publishing, Hampton, VA, 74-77.
2. World Climate Research Programme (1983) Report of the Experts Meeting on Aerosols and Their Climatic Effects, A. Deepak and H. F. Gerber, eds. World Climate Program Publication WCP-55, December 1983.
3. d'Almeida, G. and Schutz, L. (1983) Number, mass and volume distributions of mineral aerosol and soils of the Sahara, J. Climate and Appl. Meteor., 22:233-243.
4. Patterson, E.M., and Gillette, D. A. (1977) Commonalities in measured size distributions for aerosols having a soil-derived component, J. Geophys. Res., 82:2074-2082
5. Schutz, L. and Jaenicke, R. (1974) Particle number and mass distributions above 10^{-4} cm radius in sand and aerosols of the Sahara Desert, J. Appl. Meteor., 13:863-870.
6. Levin, Z., and Lindberg, J. A. (1979) Size distribution, chemical composition, and optical properties of urban and desert aerosols in Israel, J. Geophys. Res., 84:6941-6950.
7. Kushelevsky, A., Shani G., and Haccoun A. (1983) Effect of meteorologic conditions on total suspended particulate (TSP) levels and elemental concentration of aerosols in a semi-arid zone (Beer-Sheva, Israel), Tellus, 35B:55-64.
8. Cahill, T. A., Kusko, B. H., Ashbaugh, L. L., Barone, J. B, Eldred, R. A. and Walther, F. G. (1981) Regional and local determinations of particulate matter and visibility in the southwestern United States during June and July, 1979, Atmospheric Environment, 15:2011-2016.
9. Annegarn, H. J., Van Greiken, R. E., Bibby, D. M. and Von Blottnitz., F. (1983) Background aerosol composition in the Namib Desert, southwest Africa (Namibia), Atmospheric Environment, 17:2045-2053.
10. Pinnick, R. G., Jennings, S. G., and Fernandez, G. (1987) Volatility of aerosols in the arid southwestern United States, J. Atmos. Sci., 44:562-576.

11. Levin, Z., Joseph, J. H. and Mekler, Y. (1980) Properties of Sharav (Khamsin) Dust - Comparison of optical and direct sampling data, J. Atmos. Sci., 37:882-891.
12. Malm, W. C. and Johnson, C. E. (1984) Optical characteristics of fine and coarse particulates at Grand Canyon, Arizona, Atmospheric Environment, 18:1231-1237.
13. Otterman, J., Fraser, R. S., and Bahethi, O. P. (1982) Characterization of tropospheric desert aerosols at solar wavelengths by multispectral radiometry from Landsat, J. Geophys. Res., 87:1270-1278.
14. Junge, C. and Jaenicke, R. (1971) New results in background aerosols studies from the Atlantic expedition of the R. V. Meteor, Spring 1969, Aerosol Science, 2:305-314.
15. Savoie, D. L. and Prospero, J. M. (1977) Aerosol concentration statistics for the Northern Tropical Atlantic, J. Geophys. Res., 82:5954-5964.
16. Schmidt, M., Specht, H. and Fabian, P. (1978) Aerosol measurements at the Algarve Coast of Portugal, Tellus, 30:449-457.
17. Ganor, E. and Mamane, Y. (1982) Transport of Saharan dust across the Eastern Mediterranean, Atmospheric Environment, 16:581-587.
18. Chester, R., Sharples, E. J., Sanders, G. S. and Saydam, A. C. (1984) Saharan dust incursion over the Tyrrhenian Sea, Atmospheric Environment, 18:929-935.
19. Shaw, G. E. (1980) Transport of Asian desert aerosol to the Hawaiian Islands, J. Appl. Meteor., 19:1254-1259.
20. Jaenicke, R., and Schutz, L. (1978) A comprehensive study of physical and chemical properties of the surface aerosols in the Cape Verde Islands region, J. Geophys. Res., 83:3583-3598.
21. d'Almeida, G. A. and Jaenicke, R. (1981) The size distribution of mineral dust, J. Aerosol Sci., 12:160-162.
22. Gillette, D. A., Blifford, Jr., J. H. and Fryrear, D. W. (1974) The influence of wind velocity on the size distributions of aerosols generated by the wind erosion of soils, J. Geophys. Res., 79:4068-4075.
23. Gillette, D. A. (1978) Tests with a portable wind tunnel for determining wind erosion threshold velocities, Atmospheric Environment, 12:2309-2313.

24. Gillette, D. A., Blifford, Jr., J. H. and Fenster, C. R. (1972) Measurements of aerosol size distributions and vertical fluxes of aerosols in Badkhab, Iran, due to wind erosion, J. Appl. Meteor., 11:977-987.
25. Gillette, D. A. (1978) A wind tunnel simulation of the erosion of soil: Effect of soil texture, sandblasting, wind speed, and soil consolidation on dust production, Atmospheric Environment, 12:1735-1743.
26. Grams, G. W., Blifford, Jr., J. H., Gillette, D. A., and Russell, P. E. (1974) Complex index of refraction of airborne soil particles, J. Appl. Meteor., 13:439-471.
27. Bohren, C. F., Private Communication
28. Volz, F. E. (1973) Infrared optical constants of ammonium sulfate, Sahara dust, volcanic pumice and flyash, Appl. Opt., 12:564-568.
29. Patterson, E. M., Gillette, D. A. and Stockton, B. H. (1977) Complex index of refraction between 300 and 700 nm for Saharan aerosols, J. Geophys. Res., 82:3153-3160.
30. Carlson, T. N. and Benjamin, S. G. (1980) Radiative Heating Rates for Saharan Dust, J. Atmos. Sci., 37:193-213.
31. Bohren, C. F. and Huffman, D. (1983) Absorption and Scattering of Light by Small Particles, Wiley-Interscience, New York.
32. Guedalia, D., Estournel, C. and Vehil, R. (1984) Effects of Sahel dust layers upon nocturnal cooling of the atmosphere (ECHATS Experiment), J. Clim. Appl. Meteor., 23:644-650.
33. Jaenicke, R. (1984) Aerosol Physics and Chemistry, Meteorology Volume, Landolt-Boerstein Numerical Data and Functional Relationships in Science and Technology, to be published by Springer-Verlag.
34. d'Almeida, G. A. (1987) On the variability of desert aerosol radiative characteristics, J. Geophys. Res., 92:3017-3026.
35. Shettle, E. P., and Fenn, R. W. (1979) Models for the Aerosols of the Lower Atmosphere and the Effects of Humidity Variations on Their Optical Properties, AFGL-TR-79-0214, 20 Sept 1979, ADA085951.

36. Toon, O. B., Pollock, J. R. and Khare, B. N. (1976) The optical constants of several atmospheric aerosols species: Ammonium sulfate, aluminum oxide and sodium chloride, J. Geophys. Res., 81: 233-244.
37. Maxwell-Garnett, J. C. (1904) Colours in metal glasses and in metallic films, Philos. Trans. R. Soc., A203:385-420.
38. Chýlek, P., Srivastava, V., Pinnick, R. G. and Wang, R. T. (1986) Scattering of electromagnetic waves by composite spherical particles: experiment and effective medium approximations, Appl. Opt., 27:2396-2404.
39. Gray, D. C. (1963), American Institute of Physics Handbook, McGraw-Hill, New York, NY, 1963, 2nd Edition.
40. Peterson, J. T. and Weinman, J. A. (1969) Optical properties of quartz dust particles at infrared wavelengths, J. Geophys. Res., 74:6947-6957.
41. Drummond, D. G. (1936) Absorption coefficients of crystal quartz in the infrared, Proc. Roy. Soc. (London)-Series A, 153:328-338.
42. Spitzer, W. G., and Kleinman, D. A. (1961) Infrared lattice bands of quartz, Phys. Rev., 121:1324-1335.
43. Philipp, H. R. (1985) Silicon dioxide (SiO₂), type- α (crystalline), in Handbook of Optical Constants of Solids, Edited by E. D. Palik, 719-747.
44. Galuzza, A. I., Eremenko, V. V. and Kirichenko, A. P. (1979) Analysis of hematite reflection spectrum by the Kramers-Kronig method, Sov. Phys. Solid State, 21: 654-656.
45. Kerker, M., Scheiner, P., Cooke, D. D. and Kratochvil, J. P. (1979) Absorption index and color of colloidal hematite, J. Colloid. Interface Sci., 71: 176-187.
46. Steyer, T. R. (1974) Infrared optical properties of some solids of possible interest in astronomy and atmospheric physics, Ph.D. Thesis, Department of Physics, University of Arizona.
47. Onari, S., Arai, T. and Kudo, K. (1977) Infrared lattice vibrations and dielectric dispersion in α -Fe₂O₃, Phys. Rev. B, 16:1717-1721.

48. Egan, W. G. (1985) Photometry and Polarization in Remote Sensing, Elsevier Science Publishing, New York, pp. 398-399.
49. Pitchford, A., Pitchford, M., Malm, W., Fiocchini, R., Cahill, T. and Walther, E. (1981) Regional Analysis of Factors Affecting Visual Air Quality, Atmospheric Environment, 15:2043-2054.
50. Malm, W. C., Walther, E. G., O'Dell, K. and Kleine, M. (1981) Visibility in the Southwestern United States from Summer 1978 to Spring 1979, Atmospheric Environment, 15:2031:2042.

Appendix A

Aerosol Fractions by Volume as a Function of Wind Speed

The introduction of mass loading into our model means that the aerosol fraction by volume of each component, C_i , depends on wind speed, u . The C_i 's can be calculated in a straight forward manner because all extra mass loading due to the wind is assumed to be sand. The first step is to determine the mass of each component per unit volume of air for background conditions (i.e., $u = 0$). To do this, let m_1 , m_2 and m_3 be the mass of carbonaceous, water soluble and sand material per unit volume of air. Because the present desert aerosol model assumes that the mass of carbonaceous and water soluble material is independent of wind speed, these components will be called \bar{m}_1 and \bar{m}_2 , respectively. The mass of sand per unit volume of air depends on the wind speed (Eq. 5 of the text) and will be called $m_3(u)$. The total mass of the aerosol per unit volume of air, $M(u)$, is then given by

$$M(u) = \bar{m}_1 + \bar{m}_2 + m_3(u) \quad (\text{A-1})$$

which can be written in terms of the density, ρ , and volume concentration, v , of each component

$$M(u) = \rho_1 \bar{v}_1 + \rho_2 \bar{v}_2 + \rho_3 v_3(u) . \quad (\text{A-2})$$

The definition of aerosol fraction by volume, $C_i = v_i/V$ where V is the total aerosol volume per unit volume of air, is then substituted into Eq. A-2 and solved for V

$$V(u) = M(u) / (C_1(u)\rho_1 + C_2(u)\rho_2 + C_3(u)\rho_3) . \quad (\text{A-3})$$

The total aerosol volume for background conditions, $V(0)$, can be determined from Eq. A-3 using $M(0)$ (Eq. 5 of the text) plus $C_1(0)$ and ρ_1 from Table 4. It then follows that the mass, $m_1(0)$, and the volume concentration, $v_1(0)$, of each component is given by

$$m_1(0) = C_1(0)V(0)\rho_1 \quad (A-4)$$

and

$$v_1(0) = C_1(0)V(0) \quad (A-5)$$

where $i = 1$ to 3.

Having found \bar{v}_1 and \bar{v}_2 , the aerosol fractions by volume for each component can be computed for any wind speed. Specifically, Eq. A-2 is solved for $v_3(u)$ where $M(u)$ is obtained from Eq. 5 of the text. The volume concentrations of the aerosol components are then converted to an aerosol fractions by volume using

$$C_{1,2}(u) = \bar{v}_{1,2}/V(u) \quad (A-6)$$

and

$$C_3(u) = v_3(u)/V(u) \quad (A-7)$$

where $V(u)$ is the sum of \bar{v}_1 , \bar{v}_2 and $v_3(u)$.

Appendix B

Mie Scattering Calculations for the Three Components

This appendix gives the results of Mie calculations for the three components of the present desert aerosol model. Tables B-1 and B-2 give the results for the carbonaceous component and the water soluble component, respectively. In Tables B-3 through B-7, the results are given for the sand component at four wind speeds. Note that because of round-off, the radiative properties at some wavelengths are not internally consistent to the least significant digit. The calculations were performed using a number density of 1 particle per cm^3 of air and the size distribution parameters given in Table 5 of the text. For reference, Table B-7 gives the surface area and volume of the aerosol components that correspond to a number density of 1 particle per cm^3 of air.

Table B-1. Mie Scattering Results for the Carbonaceous Component Normalized to 1 Particle cm^{-3} . The numbers in parentheses in the attenuation columns are the power of 10 following the value of attenuation (if no value given, then the previous power of 10 is implied)

WAVELENGTH (μm)	ATTENUATION COEFFICIENTS (km^{-1})				
	Extinction	Scattering	Absorption	w_0	g
0.200	1.39(-6)	4.52(-7)	9.35(-7)	0.326	0.581
0.250	1.36	4.17	9.38	0.308	0.502
0.300	1.21	3.79	8.33	0.313	0.454
0.337	1.07	3.16	7.52	0.296	0.429
0.400	8.61(-7)	2.30	6.31	0.267	0.396
0.488	6.59	1.52	5.07	0.231	0.358
0.515	6.14	1.35	4.79	0.220	0.348
0.550	5.54	1.16	4.38	0.209	0.336
0.633	4.50	8.19(-8)	3.68	0.182	0.311
0.694	3.97	6.48	3.32	0.163	0.293
0.860	2.97	3.61	2.60	0.122	0.253
1.060	2.29	1.96	2.10	0.085	0.214
1.300	1.80	1.06	1.69	0.059	0.179
1.536	1.49	6.21(-9)	1.43	0.042	0.153
1.800	1.27	3.77	1.23	0.030	0.131
2.000	1.14	2.65	1.11	0.023	0.117
2.250	1.01	1.77	9.91(-8)	0.018	0.103
2.500	9.08(-8)	1.23	8.96	0.014	0.091
2.700	8.44	9.44(-10)	8.34	0.011	0.083
3.000	7.74	6.54	7.68	0.008	0.072
3.200	7.11	5.23	7.06	0.007	0.067
3.392	6.75	4.27	6.70	0.006	0.062
3.500	6.58	3.86	6.54	0.006	0.060
3.750	6.12	3.04	6.09	0.005	0.055
4.000	5.72	2.43	5.69	0.004	0.050
4.500	5.06	1.58	5.04	0.003	0.043
5.000	4.49	1.08	4.48	0.002	0.037
5.500	4.07	7.56(-11)	4.06	0.002	0.032
6.000	3.68	5.51	3.67	0.001	0.028
6.200	3.55	4.89	3.55	0.001	0.027
6.500	3.38	4.10	3.38	0.001	0.025
7.200	3.08	2.80	3.08	0.001	0.021
7.900	2.74	2.04	2.74	0.001	0.018
8.200	2.65	1.78	2.65	0.001	0.017
8.500	2.55	1.57	2.54	0.001	0.016
8.700	2.47	1.44	2.46	0.001	0.015

Table B-1. (cont.)

ATTENUATION COEFFICIENTS (km^{-1})					
WAVELENGTH (μm)	Extinction	Scattering	Absorption	w_o	g
9.000	2.39(-8)	1.27(-11)	2.39(-8)	0.001	0.015
9.200	2.32	1.17	2.32	0.001	0.014
9.500	2.26	1.04	2.25	0.000	0.013
9.800	2.18	9.29(-12)	2.18	0.000	0.013
10.000	2.13	8.64	2.13	0.000	0.012
10.591	2.02	6.94	2.02	0.000	0.011
11.000	1.93	5.99	1.93	0.000	0.010
11.500	1.85	5.07	1.85	0.000	0.009
12.500	1.68	3.70	1.68	0.000	0.008
13.000	1.62	3.20	1.62	0.000	0.007
14.000	1.49	2.43	1.49	0.000	0.007
14.800	1.41	1.98	1.41	0.000	0.006
15.000	1.39	1.87	1.39	0.000	0.006
16.400	1.26	1.34	1.26	0.000	0.005
17.200	1.20	1.12	1.20	0.000	0.004
18.000	1.13	9.45(-13)	1.13	0.000	0.004
18.500	1.10	8.52	1.10	0.000	0.004
20.000	1.00	6.39	1.00	0.000	0.003
21.300	9.42(-9)	5.01	9.42(-9)	0.000	0.003
22.500	8.85	4.07	8.85	0.000	0.003
25.000	7.92	2.72	7.92	0.000	0.002
27.900	7.05	1.78	7.05	0.000	0.002
30.000	6.51	1.36	6.51	0.000	0.002
35.000	5.50	7.58(-14)	5.50	0.000	0.001
40.000	4.70	4.56	4.70	0.000	0.001
50.000	3.76	1.87	3.76	0.000	0.001
60.000	3.13	9.00(-15)	3.13	0.000	0.000
80.000	2.35	2.85	2.35	0.000	0.000
100.000	1.88	1.17	1.88	0.000	0.000
150.000	1.25	2.30(-16)	1.25	0.000	0.000
200.000	9.39(-10)	7.29(-17)	9.39(-10)	0.000	0.000
300.000	6.26	1.44	6.26	0.000	0.000

Table B-2. Mie Scattering Results for the Water Soluble Component Normalized to 1 Particle cm^{-3} . The numbers in parentheses in the attenuation columns are the power of 10 following the value of attenuation (if no value given, then the previous power of 10 is implied)

WAVELENGTH (μm)	ATTENUATION COEFFICIENTS (km^{-1})			w_0	g
	Extinction	Scattering	Absorption		
0.200	2.33(-5)	2.33(-5)	2.36(-11)	1.000	0.658
0.250	2.13	2.13	1.84	1.000	0.654
0.300	1.89	1.89	1.47	1.000	0.656
0.337	1.74	1.74	1.32	1.000	0.652
0.400	1.51	1.51	1.04	1.000	0.645
0.488	1.23	1.23	9.18(-12)	1.000	0.635
0.515	1.14	1.14	7.51	1.000	0.637
0.550	1.05	1.05	7.20	1.000	0.633
0.633	8.52(-6)	8.52(-6)	5.70	1.000	0.627
0.694	7.47	7.47	5.04	1.000	0.620
0.860	5.31	5.31	5.64	1.000	0.600
1.060	3.55	3.55	5.03(-11)	1.000	0.580
1.300	2.29	2.29	3.57(-10)	1.000	0.556
1.536	1.54	1.54	1.28(-9)	0.999	0.534
1.800	1.03	1.03	1.02	0.999	0.510
2.000	7.72(-7)	7.61(-7)	1.16(-8)	0.985	0.493
2.250	5.53	5.42	1.10	0.980	0.473
2.500	3.81	3.78	3.06(-9)	0.992	0.454
2.700	2.83	2.67	1.60(-8)	0.944	0.440
3.000	7.69	9.88(-8)	6.70(-7)	0.129	0.391
3.200	1.71(-6)	2.00(-7)	1.51(-6)	0.117	0.343
3.392	1.14	2.40	9.05(-7)	0.210	0.355
3.500	9.49(-7)	2.24	7.25	0.236	0.356
3.750	3.67	1.87	1.80	0.510	0.362
4.000	2.11	1.45	6.60(-8)	0.687	0.353
4.500	1.16	8.55(-8)	3.07	0.736	0.330
5.000	7.70(-8)	5.23	2.47	0.679	0.307
5.500	5.87	3.07	2.80	0.523	0.284
6.000	5.96	1.69	4.27	0.283	0.261
6.200	7.02	1.19	5.83	0.169	0.250
6.500	1.64(-7)	3.95(-9)	1.60(-7)	0.024	0.223
7.200	9.95	5.29(-8)	9.43	0.053	0.190
7.900	1.90	6.96(-9)	1.83	0.037	0.198
8.200	3.14	1.80	3.12	0.006	0.168
8.500	8.04	3.53	8.00	0.004	0.126
8.700	2.63(-6)	1.89(-8)	2.01(-6)	0.009	0.091

Table B-2. (cont.)

WAVELENGTH (μm)	ATTENUATION COEFFICIENTS (km^{-1})			w_0	g
	Extinction	Scattering	Absorption		
9.000	3.62(-6)	1.08(-7)	3.51(-6)	0.030	0.046
9.200	1.42	6.55(-8)	1.35	0.046	0.067
9.500	4.72(-7)	4.09	4.32(-7)	0.087	0.185
9.800	2.41	3.03	2.11	0.125	0.217
10.000	1.59	2.36	1.36	0.148	0.215
10.591	7.94(-8)	1.45	6.49(-8)	0.183	0.201
11.000	6.17	1.13	5.04	0.182	0.191
11.500	4.02	8.59(-9)	3.16	0.214	0.181
12.500	2.81	5.21	2.29	0.185	0.162
13.000	2.67	4.19	2.25	0.157	0.153
14.000	2.46	2.65	2.20	0.108	0.137
14.800	2.83	1.65	2.66	0.058	0.122
15.000	3.05	1.42	2.91	0.046	0.118
16.400	2.21(-7)	5.97	2.15(-7)	0.027	0.134
17.200	3.81(-8)	2.93	3.51(-8)	0.077	0.141
18.000	2.01	1.50	1.86	0.075	0.114
18.500	1.63	1.19	1.51	0.073	0.107
20.000	1.55	7.48(-10)	1.48	0.048	0.093
21.300	1.84	5.28	1.79	0.029	0.083
22.500	2.27	3.82	2.23	0.017	0.075
25.000	3.30	2.12	3.28	0.006	0.061
27.900	5.95	9.97(-11)	5.94	0.002	0.048
30.000	1.07(-7)	5.60	1.07(-7)	0.001	0.039
35.000	2.96	1.03(-10)	2.96	0.000	0.027
40.000	2.39	1.83	2.39	0.001	0.028
50.000	1.91	7.53(-11)	1.91	0.000	0.020
60.000	1.59	3.63	1.59	0.000	0.015
80.000	1.19	1.14	1.19	0.000	0.009
100.000	9.53(-8)	4.67(-12)	9.53(-8)	0.000	0.006
150.000	6.35	9.18(-13)	6.35	0.000	0.003
200.000	4.76	2.90	4.76	0.000	0.002
300.000	3.17	5.71(-14)	3.17	0.000	0.001

Table B-3. Mie Scattering Results for the Sand Component With a 0 ms^{-1} Wind Normalized to $1 \text{ Particle cm}^{-3}$. The numbers in parentheses in the attenuation columns are the power of 10 following the value of attenuation (if no value given, then the previous power of 10 is implied)

WAVELENGTH (μm)	ATTENUATION COEFFICIENTS (km^{-1})			w_{ext}	g
	Extinction	Scattering	Absorption		
0.200	5.62(-1)	4.38(-1)	1.24(-1)	0.780	0.784
0.250	5.64	4.40	1.24	0.780	0.794
0.300	5.65	4.40	1.25	0.780	0.798
0.337	5.66	4.41	1.25	0.779	0.802
0.400	5.68	4.41	1.26	0.778	0.802
0.488	5.70	4.45	1.25	0.780	0.803
0.515	5.71	4.48	1.23	0.785	0.802
0.550	5.71	4.57	1.14	0.801	0.802
0.633	5.73	5.37	3.60(-2)	0.937	0.801
0.694	5.74	5.70	4.58(-3)	0.992	0.801
0.860	5.78	5.63	1.51(-2)	0.974	0.798
1.060	5.82	5.82	1.19(-4)	1.000	0.795
1.300	5.86	5.86	3.72(-5)	1.000	0.790
1.536	5.91	5.91	1.59	1.000	0.788
1.800	5.95	5.95	1.25	1.000	0.784
2.000	6.00	6.00	1.19	1.000	0.778
2.250	6.04	6.04	1.16	1.000	0.775
2.500	6.08	6.08	4.56	1.000	0.771
2.700	6.11	6.11	6.18	1.000	0.769
3.000	6.15	6.14	1.04(-3)	0.998	0.768
3.200	6.17	6.17	2.69(-4)	1.000	0.767
3.392	6.21	6.20	2.99	1.000	0.766
3.500	6.23	6.22	3.49	0.999	0.763
3.750	6.26	6.24	1.97(-3)	0.997	0.764
4.000	6.30	6.28	2.51	0.996	0.763
4.500	6.38	6.25	1.33(-2)	0.979	0.766
5.000	6.48	5.48	9.99	0.846	0.802
5.500	6.61	5.65	9.60	0.855	0.811
6.000	6.76	5.79	9.74	0.856	0.830
6.200	6.84	5.71	1.13(-1)	0.835	0.852
6.500	6.98	6.07	9.09(-2)	0.870	0.877
7.200	5.26	4.05	1.20(-1)	0.758	0.980
7.900	5.49	4.12	1.37	0.750	0.804
8.200	6.16	5.36	8.03(-2)	0.870	0.611
8.500	7.45	6.39	1.06(-1)	0.861	0.574
8.700	7.48	5.95	1.63	0.776	0.583

Table B-3. (cont.)

WAVELENGTH (μm)	ATTENUATION COEFFICIENTS (km^{-1})			w_0	g
	Extinction	Scattering	Absorption		
9.000	8.36(-1)	7.52(-1)	8.34(-2)	0.900	0.576
9.200	7.08	6.41	6.68	0.906	0.552
9.500	6.52	4.14	2.38(-1)	0.635	0.695
9.800	6.67	4.08	2.59	0.611	0.727
10.000	6.74	4.33	2.41	0.642	0.705
10.591	6.87	5.07	1.79	0.739	0.653
11.000	6.98	5.41	1.57	0.776	0.644
11.500	7.12	5.53	1.59	0.777	0.661
12.500	7.11	4.35	2.76	0.607	0.753
13.000	7.06	4.28	2.78	0.606	0.716
14.000	7.46	5.47	1.99	0.734	0.669
14.800	7.57	5.80	1.77	0.766	0.642
15.000	7.62	6.01	1.61	0.789	0.638
16.400	6.49	4.50	1.99	0.652	0.724
17.200	6.54	4.32	2.22	0.638	0.813
18.000	6.35	4.60	1.75	0.731	0.809
18.500	5.76	4.21	1.54	0.727	0.810
20.000	6.81	5.86	9.44(-2)	0.862	0.527
21.300	8.92	7.12	1.81(-1)	0.780	0.533
22.500	7.19	4.63	2.55	0.645	0.545
25.000	8.27	5.16	3.11	0.622	0.654
27.900	7.61	4.93	2.68	0.645	0.454
30.000	7.76	5.48	2.28	0.701	0.412
35.000	8.24	7.28	9.66(-2)	0.882	0.385
40.000	8.34	7.85	4.92	0.941	0.387
50.000	8.12	7.90	2.21	0.973	0.386
60.000	7.53	7.40	1.26	0.984	0.395
80.000	6.04	5.95	9.34(-3)	0.985	0.404
100.000	4.64	4.61	2.54	0.995	0.404
150.000	2.33	2.33	9.06(-4)	0.996	0.396
200.000	1.20	1.20	4.02	0.997	0.378
300.000	3.72(-2)	3.71(-2)	1.45	0.996	0.330

Table B-4. Mie Scattering Results for the Sand Component With a 10 ms^{-1} Wind Normalized to $1 \text{ Particle cm}^{-3}$. The numbers in parentheses in the attenuation columns are the power of 10 following the value of attenuation (if no value given, then the previous power of 10 is implied)

WAVELENGTH (μm)	ATTENUATION COEFFICIENTS (km^{-1})				w_0	g
	Extinction	Scattering	Absorption			
0.200	1.22(0)	9.55(-1)	2.69(-1)	0.780	0.785	
0.250	1.23	9.57	2.69	0.780	0.796	
0.300	1.23	9.59	2.71	0.780	0.801	
0.337	1.23	9.59	2.72	0.779	0.805	
0.400	1.23	9.61	2.73	0.779	0.806	
0.488	1.24	9.65	2.73	0.780	0.807	
0.515	1.24	9.67	2.71	0.782	0.808	
0.550	1.24	9.78	2.62	0.789	0.807	
0.633	1.24	1.13(0)	1.18	0.905	0.808	
0.694	1.24	1.23	1.80(-2)	0.986	0.806	
0.860	1.25	1.20	5.50	0.956	0.804	
1.060	1.26	1.26	4.53(-4)	1.000	0.803	
1.300	1.26	1.26	1.31	1.000	0.802	
1.536	1.27	1.27	6.54(-5)	1.000	0.798	
1.800	1.28	1.28	3.93	1.000	0.795	
2.000	1.28	1.28	3.98	1.000	0.796	
2.250	1.29	1.29	3.94	1.000	0.793	
2.500	1.30	1.30	1.64(-4)	1.000	0.791	
2.700	1.30	1.30	2.19	1.000	0.792	
3.000	1.31	1.31	3.54(-3)	0.998	0.790	
3.200	1.31	1.31	1.06	0.999	0.789	
3.392	1.32	1.32	1.02	0.999	0.785	
3.500	1.32	1.32	1.32	0.999	0.789	
3.750	1.32	1.32	7.46	0.994	0.789	
4.000	1.33	1.32	9.55	0.993	0.788	
4.500	1.34	1.29	4.83(-2)	0.964	0.799	
5.000	1.35	1.05	3.02(-1)	0.777	0.846	
5.500	1.37	1.07	2.93	0.785	0.851	
6.000	1.38	1.09	2.99	0.784	0.862	
6.200	1.39	1.05	3.40	0.756	0.878	
6.500	1.41	1.12	2.88	0.796	0.890	
7.200	1.29	9.19(-1)	3.71	0.711	0.986	
7.900	1.23	9.11	3.22	0.739	0.807	
8.200	1.33	1.16(0)	1.67	0.875	0.614	
8.500	1.50	1.31	1.83	0.880	0.574	
8.700	1.50	1.20	3.01	0.796	0.580	

Table B-4. (cont.)

WAVELENGTH (μm)	ATTENUATION COEFFICIENTS (km^{-1})			w_0	g
	Extinction	Scattering	Absorption		
9.000	1.66(0)	1.51(0)	1.53(-1)	0.908	0.581
9.200	1.49	1.35	1.37	0.908	0.564
9.500	1.37	8.93(-1)	4.78	0.651	0.712
9.800	1.39	8.48	5.45	0.609	0.769
10.000	1.40	8.69	5.35	0.619	0.766
10.591	1.42	9.71	4.50	0.683	0.734
11.000	1.43	1.02(0)	4.10	0.714	0.726
11.500	1.45	1.03	4.19	0.711	0.743
12.500	1.49	9.23(-1)	5.65	0.617	0.774
13.000	1.45	8.55	5.95	0.590	0.783
14.000	1.49	9.93	4.99	0.666	0.752
14.800	1.51	1.05(0)	4.61	0.695	0.721
15.000	1.52	1.09	4.30	0.717	0.709
16.400	1.40	9.26(-1)	4.77	0.641	0.758
17.200	1.42	9.06	5.09	0.631	0.836
18.000	1.42	9.88	4.35	0.698	0.826
18.500	1.37	9.85	3.89	0.716	0.833
20.000	1.46	1.28(0)	1.83	0.876	0.561
21.300	1.79	1.43	3.53	0.787	0.598
22.500	1.48	9.68(-1)	5.12	0.655	0.624
25.000	1.70	1.08(0)	6.16	0.634	0.704
27.900	1.55	9.97(-1)	5.55	0.643	0.554
30.000	1.57	1.09(0)	4.76	0.694	0.517
35.000	1.64	1.39	2.59	0.841	0.461
40.000	1.69	1.54	1.49	0.911	0.444
50.000	1.73	1.66	7.52(-2)	0.957	0.421
60.000	1.74	1.69	4.86	0.972	0.415
80.000	1.67	1.63	4.21	0.975	0.413
100.000	1.54	1.53	1.36	0.991	0.409
150.000	1.18	1.18	6.03(-3)	0.995	0.409
200.000	8.67(-1)	8.64(-1)	3.31	0.996	0.407
300.000	4.76	4.74	1.46	0.997	0.401

Table B-5. Mie Scattering Results for the Sand Component with a 20 ms^{-1} wind Normalized to $1 \text{ particle cm}^{-3}$. The numbers in parentheses in the attenuation columns are the power of 10 following the value of attenuation (if no value given, then the previous power of 10 is implied)

WAVELENGTH (μm)	ATTENUATION COEFFICIENTS (km^{-1})			w_0	g
	Extinction	Scattering	Absorption		
0.200	2.61(0)	2.03(0)	5.73(-1)	0.780	0.787
0.250	2.61	2.04	5.73	0.780	0.798
0.300	2.61	2.04	5.75	0.780	0.803
0.337	2.62	2.04	5.77	0.780	0.80
0.400	2.62	2.04	5.80	0.779	0.809
0.488	2.63	2.05	5.79	0.780	0.810
0.515	2.63	2.05	5.78	0.780	0.811
0.550	2.63	2.06	5.70	0.784	0.811
0.633	2.63	2.29	3.44	0.870	0.811
0.694	2.64	2.57	6.86(-2)	0.974	0.811
0.860	2.65	2.46	1.87(-1)	0.930	0.810
1.060	2.66	2.65	1.85(-3)	1.000	0.809
1.300	2.67	2.66	5.28(-4)	1.000	0.807
1.536	2.68	2.68	2.53	1.000	0.807
1.800	2.69	2.69	1.62	1.000	0.806
2.000	2.69	2.69	1.63	1.000	0.804
2.250	2.70	2.70	1.58	1.000	0.804
2.500	2.71	2.71	6.43	1.000	0.804
2.700	2.72	2.72	8.50	1.000	0.803
3.000	2.73	2.72	1.41(-2)	0.995	0.804
3.200	2.73	2.73	4.01(-3)	0.998	0.805
3.392	2.75	2.74	4.00	0.999	0.803
3.500	2.75	2.74	5.18	0.998	0.804
3.750	2.76	2.73	2.76(-2)	0.990	0.807
4.000	2.76	2.73	3.60	0.987	0.810
4.500	2.78	2.60	1.73(-1)	0.938	0.825
5.000	2.80	1.98	8.22	0.706	0.883
5.500	2.82	2.01	8.09	0.713	0.887
6.000	2.83	2.01	8.21	0.710	0.895
6.200	2.85	1.94	9.08	0.681	0.909
6.500	2.87	2.06	8.08	0.718	0.913
7.200	2.81	1.82	9.90	0.648	0.988
7.900	2.66	1.94	7.16	0.730	0.808
8.200	2.78	2.44	3.43	0.877	0.613
8.500	3.00	2.67	3.27	0.892	0.570
8.700	3.01	2.45	5.65	0.811	0.573

Table B-5. (cont.)

WAVELENGTH (μm)	ATTENUATION COEFFICIENTS (km^{-1})			w_0	g
	Extinction	Scattering	Absorption		
9.000	3.25(0)	2.98(0)	2.71(-1)	0.917	0.576
9.200	3.06	2.78	2.75	0.910	0.567
9.500	2.84	1.88	9.57	0.663	0.721
9.800	2.87	1.76	1.11(0)	0.613	0.789
10.000	2.88	1.75	1.12	0.610	0.802
10.591	2.90	1.86	1.04	0.642	0.795
11.000	2.92	1.93	9.88(-1)	0.661	0.791
11.500	2.94	1.93	1.01(0)	0.655	0.807
12.500	3.03	1.91	1.12	0.628	0.784
13.000	2.95	1.73	1.23	0.584	0.821
14.000	3.00	1.85	1.14	0.618	0.817
14.800	3.02	1.93	1.09	0.640	0.790
15.000	3.03	1.99	1.04	0.657	0.777
16.400	2.91	1.82	1.09	0.619	0.805
17.200	2.95	1.82	1.13	0.613	0.867
18.000	2.96	1.96	9.97(-1)	0.666	0.842
18.500	2.96	2.05	9.13	0.692	0.843
20.000	3.02	2.67	3.54	0.883	0.576
21.300	3.51	2.83	6.75	0.794	0.629
22.500	3.01	2.00	1.02(0)	0.664	0.673
25.000	3.37	2.19	1.18	0.646	0.732
27.900	3.12	1.99	1.13	0.640	0.631
30.000	3.14	2.16	9.86(-1)	0.686	0.608
35.000	3.24	2.59	6.55	0.797	0.543
40.000	3.32	2.91	4.17	0.874	0.517
50.000	3.42	3.20	2.27	0.934	0.485
60.000	3.49	3.34	1.51	0.957	0.469
80.000	3.56	3.42	1.41	0.961	0.453
100.000	3.54	3.49	5.13(-2)	0.986	0.434
150.000	3.28	3.25	2.67	0.992	0.422
200.000	2.92	2.91	1.72	0.994	0.417
300.000	2.22	2.21	9.46(-3)	0.996	0.411

Table B-6. Mie Scattering Results for the Sand Component With a 30 ms^{-1} Wind Normalized to $1 \text{ Particle cm}^{-3}$. The numbers in parentheses in the attenuation columns are the power of 10 following the value of attenuation (if no value given, then the previous power of 10 is implied)

ATTENUATION COEFFICIENTS (km^{-1})					
WAVELENGTH (μm)	Extinction	Scattering	Absorption	w_0	g
0.200	5.60(0)	4.37(0)	1.23(0)	0.780	0.788
0.250	5.61	4.38	1.23	0.780	0.799
0.300	5.61	4.38	1.24	0.780	0.804
0.337	5.62	4.38	1.24	0.780	0.808
0.400	5.62	4.38	1.24	0.779	0.810
0.488	5.63	4.39	1.24	0.780	0.812
0.515	5.63	4.39	1.24	0.780	0.813
0.550	5.64	4.40	1.23	0.781	0.813
0.633	5.65	4.72	9.21(-1)	0.837	0.814
0.694	5.65	5.40	2.55	0.955	0.813
0.860	5.66	5.07	5.92	0.896	0.813
1.060	5.68	5.67	7.60(-3)	0.998	0.813
1.300	5.69	5.69	2.11	1.000	0.813
1.536	5.70	5.70	1.03	1.000	0.812
1.800	5.72	5.72	6.58(-4)	1.000	0.811
2.000	5.74	5.74	6.80	1.000	0.812
2.250	5.75	5.75	6.58	1.000	0.812
2.500	5.77	5.76	2.61(-3)	1.000	0.812
2.700	5.77	5.77	3.52	0.999	0.813
3.000	5.79	5.73	5.59(-2)	0.990	0.814
3.200	5.80	5.78	1.62	0.997	0.814
3.392	5.81	5.80	1.60	0.997	0.814
3.500	5.81	5.79	2.07	0.997	0.815
3.750	5.83	5.72	1.09(-1)	0.961	0.820
4.000	5.84	5.70	1.41	0.976	0.824
4.500	5.86	5.25	6.15	0.895	0.845
5.000	5.89	3.79	2.09(0)	0.644	0.912
5.500	5.91	3.83	2.08	0.649	0.917
6.000	5.94	3.83	2.11	0.645	0.923
6.200	5.95	3.69	2.25	0.622	0.935
6.500	5.97	3.88	2.10	0.649	0.936
7.200	5.98	3.54	2.44	0.592	0.990
7.900	5.72	4.14	1.58	0.724	0.808
8.200	5.89	5.17	7.18(-1)	0.878	0.610
8.500	6.16	5.55	6.18	0.900	0.565
8.700	6.19	5.09	1.10(0)	0.821	0.566

Table B-6. (cont.)

ATTENUATION COEFFICIENTS (km^{-1})					
WAVELENGTH (μm)	Extinction	Scattering	Absorption	w_0	g
9.000	6.53(0)	6.04(0)	4.87(-1)	0.925	0.566
9.200	6.36	5.80	5.55	0.912	0.564
9.500	5.97	4.01	1.96(0)	0.673	0.724
9.800	6.01	3.72	2.29	0.619	0.799
10.000	6.02	3.66	2.36	0.609	0.819
10.591	6.06	3.73	2.33	0.615	0.833
11.000	6.08	3.80	2.29	0.624	0.835
11.500	6.10	3.75	2.34	0.616	0.855
12.500	6.26	4.00	2.25	0.638	0.788
13.000	6.12	3.59	2.54	0.586	0.842
14.000	6.18	3.64	2.54	0.589	0.864
14.800	6.22	3.75	2.47	0.603	0.843
15.000	6.23	3.82	2.41	0.614	0.833
16.400	6.09	3.64	2.45	0.595	0.852
17.200	6.18	3.67	2.51	0.593	0.899
18.000	6.17	3.93	2.23	0.641	0.860
18.500	6.24	4.17	2.07	0.668	0.850
20.000	6.31	5.61	7.03(-1)	0.889	0.581
21.300	6.99	5.69	1.30(0)	0.804	0.640
22.500	6.24	4.19	2.05	0.672	0.703
25.000	6.77	4.49	2.28	0.659	0.747
27.900	6.41	4.08	2.33	0.637	0.689
30.000	6.44	4.34	2.10	0.674	0.680
35.000	6.59	4.96	1.64	0.751	0.620
40.000	6.70	5.54	1.16	0.827	0.591
50.000	6.88	6.19	6.87(-1)	0.900	0.553
60.000	7.01	6.53	4.78	0.932	0.534
80.000	7.24	6.79	4.50	0.938	0.512
100.000	7.35	7.18	1.73	0.977	0.483
150.000	7.41	7.31	1.04	0.986	0.456
200.000	7.22	7.15	7.17(-2)	0.990	0.442
300.000	6.53	6.49	4.25	0.994	0.427

Table B-7. Surface Area and Volume of Each Aerosol Component of the Desert Aerosol Model per Unit Volume of Air for a Number Density of 1 Particle cm^{-3}

Aerosol Component	Surface Area ($\mu\text{m}^2 \text{ cm}^{-3}$ of Air)	Volume ($\mu\text{m}^3 \text{ cm}^{-3}$ of Air)
Carbonaceous	1.14×10^{-3}	5.97×10^{-5}
Water Soluble	9.35×10^{-3}	1.80×10^{-3}
Sand: 0 ms^{-1} Wind	2.76×10^2	6.30×10^3
Sand: 10 ms^{-1} Wind	6.04×10^2	2.66×10^4
Sand: 20 ms^{-1} Wind	1.29×10^3	1.12×10^5
Sand: 30 ms^{-1} Wind	2.78×10^3	4.76×10^5

Appendix C

Radiative Properties of the Desert Aerosol Model as a Function of Wind Speed

This appendix gives the tabulated radiative properties of the present desert aerosol model. Tables C-1 through C-4 give values for wind speeds of 0, 10, 20 and 30 ms^{-1} respectively. As discussed in the main text, these results were obtained using sand component that is a mixture of quartz particles and quartz particles contaminated with hematite. Note because of round-off, the radiative properties at some wavelengths are not internally consistent to the least significant digit.

For reference, Tables C-5 through C-7 give the angular scattering, P , of the desert aerosol model for wavelengths of 0.55, 1.06 and 10.591 μm respectively. Figures C-1 through C-3 present these results in pictorial form. The method of determining the angular scattering for a multicomponent mixture of particles is similar to that for the asymmetry parameter which was described in Section 3.4 of the main text. The values have been normalized so that

$$\frac{1}{4\pi} \int P(\theta) d\theta = 1 \quad (\text{C-1})$$

where θ is the solid angle.

Table C-1. Radiative Properties of the Desert Aerosol for 0 ms^{-1} Wind Speed Conditions. The numbers in parentheses in the attenuation columns are the power of 10 following the value of attenuation (if no value given, then the previous power of 10 is implied)

WAVELENGTH (μm)	ATTENUATION COEFFICIENTS (km^{-1})			ν_0	g
	Extinction	Scattering	Absorption		
0.200	8.73(-2)	8.67(-2)	6.49(-4)	0.993	0.660
0.250	7.99	7.93	6.51	0.992	0.657
0.300	7.13	7.07	6.14	0.991	0.658
0.337	6.58	6.52	5.86	0.991	0.655
0.400	5.70	5.65	5.43	0.990	0.649
0.488	4.68	4.63	4.94	0.989	0.640
0.515	4.33	4.28	4.79	0.989	0.642
0.550	4.01	3.96	4.42	0.989	0.638
0.633	3.28	3.26	2.25	0.993	0.634
0.694	2.90	2.88	1.34	0.995	0.628
0.860	2.10	2.09	1.33	0.994	0.612
1.060	1.45	1.45	7.81(-5)	0.995	0.600
1.300	9.90(-3)	9.84(-3)	6.41	0.994	0.588
1.536	7.16	7.10	5.76	0.992	0.583
1.800	5.27	5.22	4.93	0.991	0.583
2.000	4.35	4.26	8.38	0.981	0.587
2.250	3.55	3.47	7.70	0.978	0.597
2.500	2.92	2.88	4.45	0.985	0.613
2.700	2.57	2.48	8.96	0.965	0.632
3.000	4.36	1.87	2.49(-3)	0.429	0.685
3.200	7.83	2.25	5.58	0.287	0.620
3.392	5.75	2.40	3.34	0.418	0.607
3.500	5.03	2.35	2.69	0.467	0.613
3.750	2.91	2.22	6.88(-4)	0.763	0.631
4.000	2.34	2.07	2.69	0.885	0.648
4.500	2.01	1.85	1.64	0.919	0.682
5.000	1.89	1.54	3.52	0.813	0.730
5.500	1.85	1.50	3.53	0.809	0.757
6.000	1.89	1.48	4.09	0.784	0.787
6.200	1.95	1.44	5.05	0.741	0.812
6.500	2.33	1.50	8.21	0.647	0.842
7.200	4.95	1.19	3.76(-3)	0.240	0.830
7.900	2.05	1.04	1.02	0.505	0.811
8.200	2.67	1.32	1.35	0.494	0.614
8.500	4.79	1.58	3.20	0.330	0.593
8.700	9.28	1.50	7.78	0.162	0.617

Table C-1. (cont.)

WAVELENGTH (μm)	ATTENUATION COEFFICIENTS (km^{-1})			w_0	g
	Extinction	Scattering	Absorption		
9.000	1.54(-2)	2.24(-3)	1.31(-2)	0.146	0.489
9.200	6.94(-3)	1.81	5.13(-3)	0.261	0.492
9.500	3.34	1.17	2.18	0.349	0.633
9.800	2.53	1.11	1.42	0.439	0.676
10.000	2.25	1.15	1.10	0.511	0.666
10.591	1.98	1.30	6.86(-4)	0.654	0.633
11.000	1.95	1.37	5.76	0.704	0.630
11.500	1.90	1.39	5.13	0.730	0.650
12.500	1.86	1.09	7.68	0.586	0.747
13.000	1.84	1.06	7.72	0.580	0.711
14.000	1.93	1.35	5.74	0.702	0.678
14.800	1.97	1.43	5.38	0.726	0.671
15.000	1.99	1.48	5.06	0.745	0.675
16.400	2.41	1.13	1.28(-3)	0.467	0.754
17.200	1.75	1.07	6.78(-4)	0.612	0.805
18.000	1.64	1.14	5.02	0.693	0.788
18.500	1.48	1.04	4.38	0.703	0.780
20.000	1.73	1.44	2.90	0.833	0.531
21.300	2.26	1.75	5.12	0.773	0.552
22.500	1.85	1.14	7.12	0.615	0.570
25.000	2.15	1.27	8.86	0.588	0.658
27.900	2.09	1.21	8.79	0.579	0.533
30.000	2.30	1.35	9.55	0.585	0.470
35.000	3.11	1.79	1.32(-3)	0.574	0.385
40.000	2.93	1.93	1.00	0.658	0.372
50.000	2.69	1.94	7.56(-4)	0.719	0.363
60.000	2.43	1.82	6.16	0.747	0.369
80.000	1.92	1.46	4.61	0.760	0.379
100.000	1.49	1.13	3.56	0.761	0.380
150.000	8.06(-4)	5.71(-4)	2.36	0.708	0.377
200.000	4.70	2.94	1.76	0.625	0.364
300.000	2.08	9.09(-5)	1.17	0.437	0.328

Table C-2. Radiative Properties of the Desert Aerosol for 10 ms^{-1} Wind Speed Conditions. The numbers in parentheses in the attenuation columns are the power of 10 following the value of attenuation (if no value given, then the previous power of 10 is implied)

WAVELENGTH (μm)	ATTENUATION COEFFICIENTS (km^{-1})				w_0	g
	Extinction	Scattering	Absorption			
0.200	1.04(-1)	9.98(-2)	4.36(-3)	0.958	0.684	
0.250	9.68(-2)	9.25	4.36	0.955	0.683	
0.300	8.83	8.39	4.34	0.951	0.688	
0.337	8.27	7.84	4.33	0.948	0.688	
0.400	7.40	6.97	4.30	0.942	0.687	
0.488	6.39	5.96	4.25	0.933	0.687	
0.515	6.03	5.61	4.21	0.930	0.692	
0.550	5.71	5.31	4.06	0.929	0.692	
0.633	5.00	4.81	1.89	0.962	0.694	
0.694	4.61	4.57	3.91(-4)	0.992	0.690	
0.860	3.82	3.73	9.16	0.976	0.697	
1.060	3.18	3.17	8.46(-5)	0.997	0.705	
1.300	2.73	2.72	6.59	0.998	0.717	
1.536	2.46	2.46	5.85	0.998	0.728	
1.800	2.29	2.28	4.99	0.998	0.738	
2.000	2.20	2.19	8.44	0.996	0.747	
2.250	2.13	2.12	7.75	0.996	0.752	
2.500	2.07	2.07	4.68	0.998	0.757	
2.700	2.04	2.03	9.27	0.995	0.763	
3.000	2.23	1.98	2.54(-3)	0.886	0.770	
3.200	2.59	2.03	5.59	0.784	0.760	
3.392	2.38	2.05	3.36	0.859	0.757	
3.500	2.31	2.04	2.70	0.883	0.759	
3.750	2.11	2.03	7.94(-4)	0.962	0.762	
4.000	2.06	2.02	4.06	0.980	0.765	
4.500	2.04	1.96	8.51	0.958	0.778	
5.000	2.05	1.59	4.60(-3)	0.775	0.829	
5.500	2.06	1.61	4.49	0.782	0.836	
6.000	2.08	1.62	4.62	0.778	0.846	
6.200	2.10	1.57	5.30	0.748	0.862	
6.500	2.16	1.67	4.89	0.774	0.871	
7.200	2.29	1.39	8.99	0.607	0.952	
7.900	1.91	1.56	5.47	0.713	0.829	
8.200	2.09	1.73	3.64	0.826	0.620	
8.500	2.53	1.96	5.67	0.775	0.595	
8.700	2.98	1.80	1.19(-2)	0.602	0.642	

Table C-2. (cont.)

WAVELENGTH (μm)	ATTENUATION COEFFICIENTS (km^{-1})			w_0	g
	Extinction	Scattering	Absorption		
9.000	3.80(-2)	2.28(-2)	1.52(-2)	0.601	0.578
9.200	2.73	2.03	7.00(-3)	0.744	0.562
9.500	2.22	1.35	8.72	0.607	0.711
9.800	2.16	1.27	8.90	0.589	0.765
10.000	2.15	1.30	8.47	0.606	0.761
10.591	2.15	1.45	6.95	0.676	0.731
11.000	2.16	1.53	6.30	0.708	0.725
11.500	2.17	1.54	6.37	0.707	0.742
12.500	2.23	1.38	8.50	0.618	0.778
13.000	2.17	1.27	8.95	0.587	0.785
14.000	2.23	1.48	7.52	0.663	0.762
14.800	2.26	1.56	6.96	0.692	0.748
15.000	2.27	1.62	6.52	0.713	0.745
16.400	2.17	1.38	7.90	0.636	0.809
17.200	2.12	1.35	7.72	0.636	0.841
18.000	2.13	1.47	6.55	0.692	0.823
18.500	2.05	1.47	5.85	0.715	0.811
20.000	2.18	1.90	2.78	0.872	0.567
21.300	2.67	2.14	5.33	0.800	0.612
22.500	2.21	1.44	7.72	0.651	0.643
25.000	2.55	1.62	9.30	0.635	0.711
27.900	2.33	1.49	8.48	0.636	0.628
30.000	2.38	1.63	7.48	0.685	0.574
35.000	2.56	2.06	4.95	0.807	0.477
40.000	2.60	2.29	3.10	0.881	0.442
50.000	2.65	2.47	1.82	0.931	0.409
60.000	2.65	2.52	1.31	0.951	0.398
80.000	2.53	2.43	1.07	0.958	0.392
100.000	2.33	2.28	5.52(-4)	0.976	0.385
150.000	1.78	1.75	3.23	0.982	0.384
200.000	1.31	1.29	2.24	0.983	0.383
300.000	7.20(-3)	7.06(-3)	1.38	0.981	0.380

Table C-3. Radiative Properties of the Desert Aerosol for 20 ms⁻¹ Wind Speed Conditions. The numbers in parentheses in the attenuation columns are the power of 10 following the value of attenuation (if no value given, then the previous power of 10 is implied)

WAVELENGTH (μm)	ATTENUATION COEFFICIENTS (km^{-1})			ω_0	η
	Extinction	Scattering	Absorption		
0.200	2.73(-1)	2.32(-1)	4.26(-2)	0.848	0.772
0.250	2.66	2.25	4.15	0.844	0.778
0.300	2.58	2.16	4.17	0.838	0.786
0.337	2.53	2.11	4.18	0.835	0.791
0.400	2.44	2.02	4.19	0.828	0.796
0.488	2.34	1.92	4.18	0.821	0.802
0.515	2.31	1.89	4.17	0.819	0.806
0.550	2.28	1.87	4.11	0.819	0.808
0.633	2.21	1.96	2.49	0.887	0.799
0.694	2.17	2.12	5.06(-3)	0.977	0.780
0.860	2.10	1.96	1.35(-2)	0.936	0.795
1.060	2.04	2.04	2.11(-4)	0.999	0.783
1.300	2.00	2.00	1.02	1.000	0.785
1.536	1.98	1.98	7.57(-5)	1.000	0.787
1.800	1.97	1.97	6.09	1.000	0.788
2.000	1.97	1.97	9.55	1.000	0.788
2.250	1.96	1.96	8.84	1.000	0.789
2.500	1.97	1.26	9.06	1.000	0.789
2.700	1.97	1.96	1.51(-4)	0.999	0.789
3.000	1.99	1.96	3.50(-3)	0.982	0.791
3.200	2.03	1.97	5.87	0.971	0.791
3.392	2.02	1.98	3.63	0.982	0.788
3.500	2.01	1.98	3.06	0.985	0.790
3.750	2.00	1.97	2.67	0.987	0.793
4.000	1.99	1.97	2.85	0.986	0.795
4.500	2.00	1.88	1.26(-2)	0.937	0.810
5.000	2.01	1.42	5.92	0.706	0.873
5.500	2.03	1.44	5.83	0.712	0.877
6.000	2.04	1.45	5.92	0.710	0.884
6.200	2.05	1.40	6.55	0.681	0.898
6.500	2.07	1.48	5.87	0.716	0.900
7.200	2.06	1.31	7.47	0.637	0.970
7.900	1.92	1.39	5.22	0.728	0.832
8.200	2.01	1.75	2.58	0.872	0.620
8.500	2.19	1.92	2.64	0.879	0.590
8.700	2.24	1.76	4.80	0.786	0.642

Table C-3. (cont.)

WAVELENGTH (μm)	ATTENUATION COEFFICIENTS (km^{-1})			w_0	g
	Extinction	Scattering	Absorption		
9.000	2.47(-1)	2.15(-1)	3.24(-2)	0.869	0.580
9.200	2.25	2.00	2.47	0.890	0.570
9.500	2.06	1.36	7.04	0.658	0.725
9.800	2.07	1.27	8.06	0.611	0.790
10.000	2.07	1.26	8.12	0.609	0.801
10.591	2.09	1.34	7.51	0.641	0.794
11.000	2.10	1.39	7.12	0.661	0.790
11.500	2.12	1.39	7.30	0.655	0.807
12.500	2.18	1.37	8.06	0.630	0.789
13.000	2.12	1.24	8.83	0.584	0.824
14.000	2.16	1.33	8.24	0.618	0.826
14.800	2.17	1.39	7.83	0.640	0.814
15.000	2.18	1.43	7.49	0.657	0.809
16.400	2.10	1.31	7.89	0.624	0.855
17.200	2.12	1.31	8.14	0.616	0.869
18.000	2.13	1.41	7.18	0.663	0.847
18.500	2.13	1.47	6.77	0.692	0.829
20.000	2.17	1.92	2.55	0.883	0.582
21.300	2.52	2.04	4.86	0.807	0.639
22.500	2.17	1.44	7.31	0.663	0.684
25.000	2.42	1.57	8.50	0.649	0.740
27.900	2.24	1.43	8.11	0.638	0.694
30.000	2.26	1.55	7.13	0.685	0.650
35.000	2.34	1.86	4.82	0.794	0.568
40.000	2.40	2.09	3.09	0.871	0.524
50.000	2.47	2.30	1.70	0.931	0.479
60.000	2.52	2.40	1.15	0.954	0.458
80.000	2.57	2.46	1.06	0.959	0.438
100.000	2.55	2.51	4.04(-3)	0.984	0.417
150.000	2.36	2.34	2.15	0.991	0.401
200.000	2.10	2.09	1.41	0.993	0.394
300.000	1.59	1.59	7.97(-4)	0.995	0.387

Table C-4. Radiative Properties of the Desert Aerosol for 30 ms⁻¹ Wind Speed Conditions. The numbers in parentheses in the attenuation columns are the power of 10 following the value of attenuation (if no value given, then the previous power of 10 is implied).

ATTENUATION COEFFICIENTS (km ⁻¹)					
WAVELENGTH (μm)	Extinction Scattering Absorption			w_0	g
	0.200	1.98(0)	1.57(0)		
0.250	1.98	1.56	4.17	0.789	0.836
0.300	1.97	1.55	4.19	0.788	0.841
0.337	1.97	1.55	4.20	0.787	0.844
0.400	1.96	1.54	4.21	0.785	0.847
0.488	1.95	1.53	4.21	0.784	0.849
0.515	1.95	1.53	4.21	0.784	0.850
0.550	1.95	1.53	4.18	0.785	0.850
0.633	1.94	1.63	3.12	0.839	0.838
0.694	1.94	1.86	8.65(-2)	0.955	0.809
0.860	1.94	1.74	2.01(-1)	0.896	0.825
1.060	1.94	1.94	2.65(-3)	0.999	0.799
1.300	1.94	1.94	7.90(-4)	1.000	0.799
1.536	1.94	1.94	4.08	1.000	0.799
1.800	1.94	1.94	2.72	1.000	0.799
2.000	1.95	1.95	3.14	1.000	0.799
2.250	1.95	1.95	3.00	1.000	0.799
2.500	1.95	1.95	9.30	1.000	0.799
2.700	1.96	1.96	1.28(-3)	0.999	0.800
3.000	1.96	1.94	2.14(-2)	0.989	0.802
3.200	1.97	1.96	1.11	0.994	0.801
3.392	1.97	1.97	8.76(-3)	0.996	0.801
3.500	1.97	1.96	9.69	0.995	0.803
3.750	1.98	1.94	3.77(-2)	0.981	0.808
4.000	1.98	1.93	4.79	0.976	0.812
4.500	1.99	1.78	2.08(-1)	0.895	0.833
5.000	1.99	1.29	7.09	0.644	0.905
5.500	2.00	1.30	7.04	0.648	0.908
6.000	2.01	1.30	7.14	0.645	0.915
6.200	2.01	1.25	7.63	0.621	0.927
6.500	2.02	1.31	7.11	0.649	0.926
7.200	2.03	1.20	8.30	0.591	0.978
7.900	1.94	1.40	5.36	0.724	0.832
8.200	2.00	1.75	2.45	0.878	0.617
8.500	2.09	1.88	2.12	0.899	0.583
8.700	2.10	1.72	3.81	0.819	0.638

Table C-4. (cont.)

WAVELENGTH (μm)	ATTENUATION COEFFICIENTS (km^{-1})			w_0	g
	Extinction	Scattering	Absorption		
9.000	2.22(0)	2.05(0)	1.78(-1)	0.920	0.571
9.200	2.18	1.97	1.93	0.911	0.567
9.500	2.02	1.36	6.64	0.672	0.729
9.800	2.04	1.26	7.77	0.619	0.801
10.000	2.04	1.24	7.99	0.608	0.820
10.591	2.05	1.26	7.90	0.615	0.822
11.000	2.06	1.29	7.75	0.624	0.835
11.500	2.07	1.27	7.94	0.616	0.855
12.500	2.12	1.36	7.63	0.640	0.794
13.000	2.07	1.22	8.59	0.586	0.845
14.000	2.10	1.23	8.61	0.589	0.871
14.800	2.11	1.27	8.36	0.603	0.862
15.000	2.11	1.29	8.16	0.613	0.859
16.400	2.07	1.23	8.31	0.597	0.892
17.200	2.09	1.24	8.49	0.594	0.892
18.000	2.09	1.33	7.56	0.638	0.867
18.500	2.12	1.41	7.01	0.668	0.841
20.000	2.14	1.90	2.38	0.889	0.587
21.300	2.37	1.93	4.42	0.813	0.649
22.500	2.11	1.42	6.95	0.671	0.708
25.000	2.29	1.52	7.74	0.663	0.756
27.900	2.17	1.38	7.90	0.637	0.738
30.000	2.18	1.47	7.11	0.674	0.702
35.000	2.23	1.68	5.56	0.751	0.649
40.000	2.27	1.88	3.93	0.827	0.602
50.000	2.33	2.10	2.33	0.900	0.553
60.000	2.38	2.21	1.63	0.932	0.528
80.000	2.45	2.30	1.53	0.938	0.502
100.000	2.49	2.43	5.88(-2)	0.976	0.471
150.000	2.51	2.48	3.56	0.986	0.440
200.000	2.45	2.42	2.45	0.990	0.423
300.000	2.21	2.20	1.45	0.993	0.406

Table C-7. Normalized Angular Scattering Function for the Desert Aerosol Model as a Function of Wind Speed for a Wavelength of 0.55 μm

NORMALIZED ANGULAR SCATTERING FUNCTION				
AZIMUTH ANGLE (degrees)	0 ms^{-1}	10 ms^{-1}	20 ms^{-1}	30 ms^{-1}
0.00	8.10(1)	3.41(3)	4.54(4)	3.29(5)
2.00	1.27(0)	2.65(0)	4.10(0)	3.04(0)
4.00	9.15(-1)	9.69(-1)	8.65(-1)	6.06(-1)
6.00	8.39	7.51	4.86	3.48
8.00	7.79	6.65	3.86	2.84
10.00	7.22	6.06	3.41	2.37
12.00	6.67	5.56	3.11	2.20
14.00	6.14	5.11	2.84	2.11
16.00	5.63	4.69	2.63	1.93
18.00	5.16	4.30	2.49	1.78
20.00	4.71	3.94	2.29	1.71
22.00	4.30	3.60	2.11	1.64
24.00	3.92	3.29	1.94	1.51
26.00	3.56	3.00	1.84	1.36
28.00	3.24	2.73	1.67	1.29
30.00	2.94	2.49	1.55	1.16
32.00	2.67	2.27	1.43	1.10
34.00	2.43	2.06	1.30	3.90(-2)
36.00	2.20	1.88	1.21	9.57
38.00	2.00	1.70	1.09	8.71
40.00	1.81	1.55	9.66(-2)	7.98
50.00	1.13	9.65(-2)	6.20	5.07
60.00	7.17(-2)	6.13	3.90	3.01
70.00	4.71	3.98	2.39	1.84
80.00	3.23	2.69	1.51	1.04
90.00	2.34	1.88	8.91(-3)	5.15(-3)
100.00	1.81	1.45	6.58	3.67
110.00	1.53	1.22	5.63	3.33
120.00	1.40	1.12	5.35	3.20
125.00	1.38	1.12	5.57	3.72
130.00	1.39	1.12	5.48	3.48
135.00	1.43	1.15	5.48	3.42
140.00	1.49	1.19	5.48	3.18
145.00	1.58	1.25	5.64	3.17
150.00	1.68	1.33	5.87	3.24
155.00	1.78	1.42	6.31	3.33
160.00	1.91	1.80	1.33(-2)	8.41
165.00	2.09	2.64	3.71	4.08(-2)
170.00	2.33	2.83	3.71	4.09
175.00	2.80	3.70	5.40	5.82
180.00	3.06	4.01	5.63	6.37

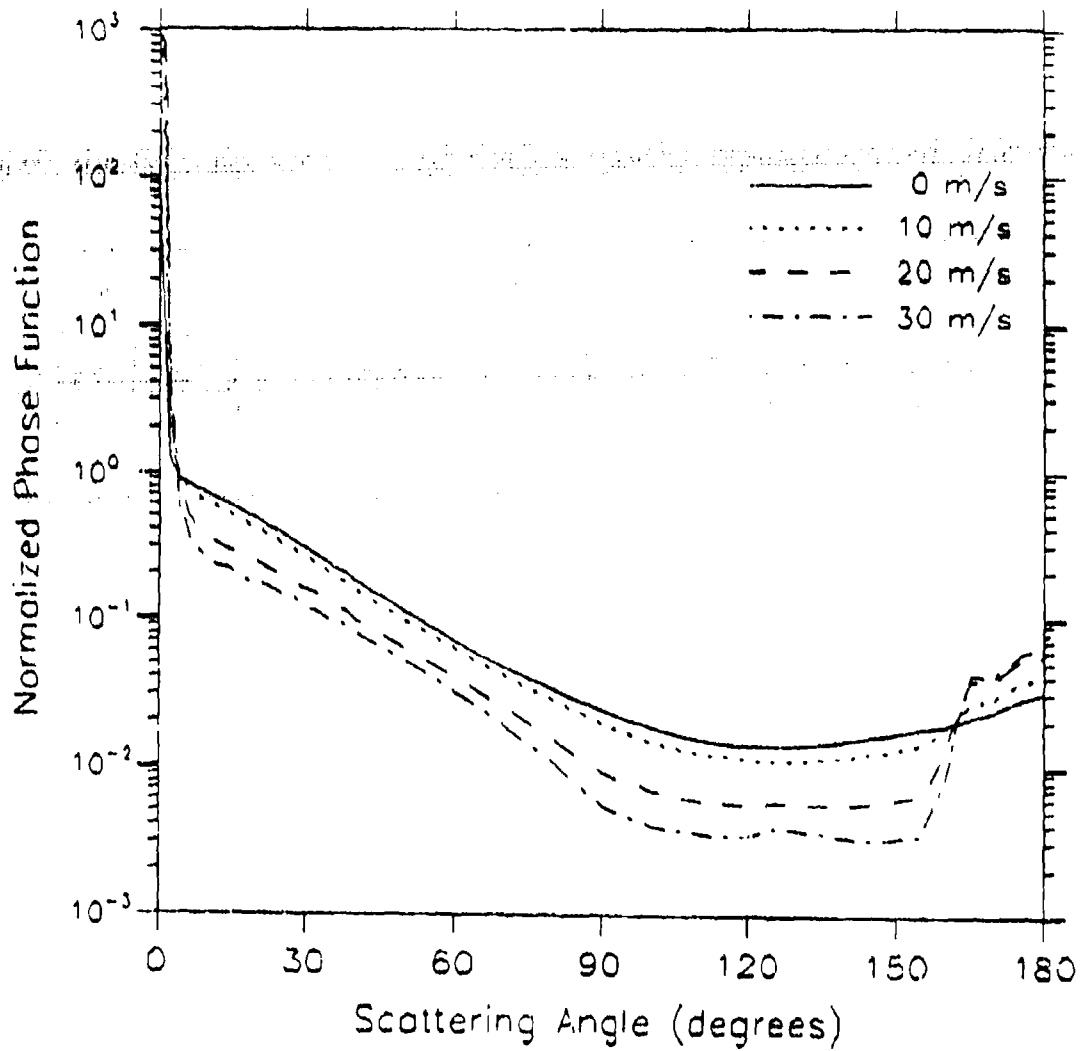


Figure C-1. Normalized Angular Scattering Function of the Desert Aerosol for a Wavelength of $0.55 \mu\text{m}$

Table C-6. Normalized Angular Scattering Function for the Desert Aerosol Model as a Function of Wind Speed for a Wavelength of 1.06 μm .

AZIMUTH ANGLE (degrees)	NORMALIZED ANGULAR SCATTERING FUNCTION			
	0 ms^{-1}	10 ms^{-1}	20 ms^{-1}	30 ms^{-1}
0.00	6.14(1)	1.56(3)	1.13(4)	4.90(4)
2.00	2.91(0)	7.87(0)	7.28(0)	4.69(0)
4.00	1.07	1.40	1.18	8.63(-1)
6.00	8.56(-1)	7.65(-1)	5.75(-1)	4.59
8.00	7.67	5.93	4.20	3.64
10.00	7.02	5.12	3.53	3.04
12.00	6.45	4.60	3.20	2.91
14.00	5.93	4.21	2.91	2.60
16.00	5.44	3.88	2.72	2.47
18.00	4.98	3.57	2.59	2.35
20.00	4.55	3.28	2.43	2.21
22.00	4.15	3.03	2.28	2.07
24.00	3.79	2.78	2.06	1.97
26.00	3.45	2.57	1.93	1.86
28.00	3.14	2.36	1.79	1.71
30.00	2.85	2.16	1.70	1.59
32.00	2.59	1.98	1.55	1.49
34.00	2.36	1.82	1.41	1.37
36.00	2.14	1.66	1.33	1.28
38.00	1.95	1.52	1.22	1.20
40.00	1.77	1.40	1.16	1.10
50.00	1.10	8.88(-2)	7.57(-2)	7.25(-2)
60.00	7.00(-2)	5.57	4.68	4.46
70.00	4.60	3.63	2.90	2.70
80.00	3.13	2.24	1.51	1.36
90.00	2.24	1.43	7.81(-3)	6.13(-3)
100.00	1.72	1.02	4.58	3.35
110.00	1.44	8.19(-3)	3.55	2.52
120.00	1.32	7.44	3.34	2.57
125.00	1.30	7.39	3.29	2.53
130.00	1.31	7.39	3.18	2.44
135.00	1.35	7.62	3.26	2.49
140.00	1.41	7.95	3.30	2.44
145.00	1.49	8.58	3.71	2.77
150.00	1.59	9.34	4.36	3.24
155.00	1.71	1.07(-2)	5.02	3.82
160.00	2.00	2.53	3.12(-2)	3.44(-2)
165.00	2.37	3.57	3.82	3.62
170.00	3.21	7.25	9.36	9.39
175.00	3.75	8.47	1.15(-1)	1.17(-1)
180.00	5.00	2.12(-1)	5.12	9.40

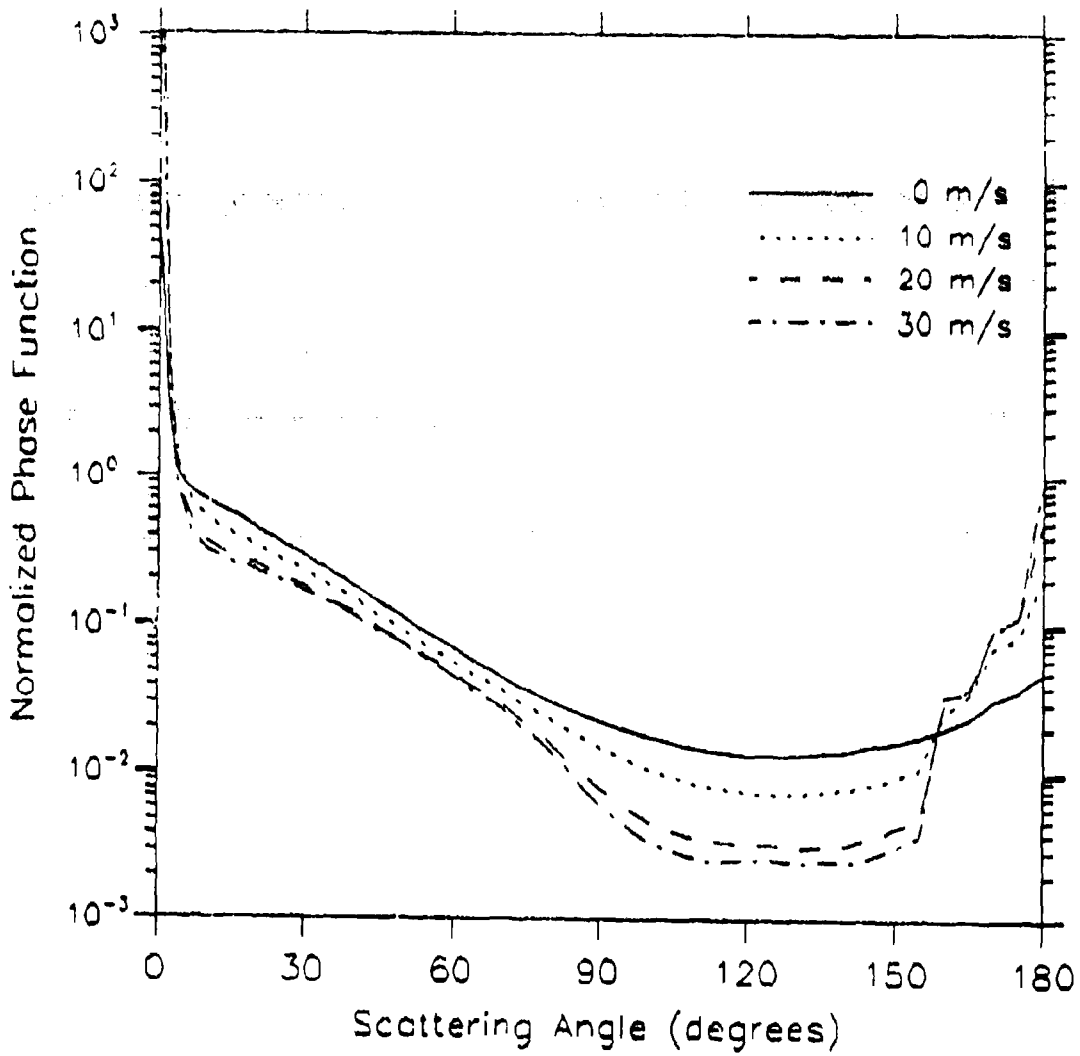


Figure C-2. Normalized Angular Scattering Function of the Desert Aerosol for a Wavelength of 1.06 μm

Table C-7. Normalized Angular Scattering Function for the Desert Aerosol Model as a Function of Wind Speed for a Wavelength of 10.591 μm

AZIMUTH ANGLE (degrees)	NORMALIZED ANGULAR SCATTERING FUNCTION			
	0 ms^{-1}	10 ms^{-1}	20 ms^{-1}	30 ms^{-1}
0.00	8.46(0)	3.89(1)	1.85(2)	7.89(2)
2.00	7.17	1.90	3.04(1)	3.31(1)
4.00	4.96	8.20(0)	8.64(0)	6.96(0)
6.00	3.30	4.03	3.45	2.47
8.00	2.20	2.20	1.68	1.14
10.00	1.50	1.31	9.37(-1)	6.19(-1)
12.00	1.05	8.31(-1)	5.75	3.78
14.00	7.57(-1)	5.60	3.82	2.52
16.00	5.61	3.98	2.69	1.80
18.00	4.27	2.95	2.00	1.35
20.00	3.34	2.27	1.55	1.06
22.00	2.68	1.81	1.25	8.63(-2)
24.00	2.20	1.49	1.03	7.23
26.00	1.84	1.25	8.79(-2)	6.21
28.00	1.58	1.08	7.63	5.44
30.00	1.37	9.45(-2)	6.73	4.84
32.00	1.21	8.40	6.03	4.36
34.00	1.08	7.58	5.47	3.98
36.00	9.76(-2)	6.90	5.02	3.67
38.00	8.90	6.35	4.64	3.40
40.00	8.18	5.89	4.32	3.18
50.00	5.80	4.33	3.24	2.43
60.00	4.43	3.42	2.60	1.99
70.00	3.55	2.80	2.17	1.69
80.00	2.94	2.35	1.85	1.48
90.00	2.49	2.01	1.61	1.32
100.00	2.17	1.76	1.43	1.20
110.00	1.96	1.58	1.30	1.11
120.00	1.83	1.46	1.21	1.06
125.00	1.79	1.42	1.18	1.03
130.00	1.79	1.40	1.16	1.02
135.00	1.80	1.39	1.15	1.01
140.00	1.87	1.42	1.15	1.01
145.00	1.99	1.40	1.18	1.02
150.00	2.22	1.60	1.24	1.05
155.00	2.57	1.80	1.34	1.10
160.00	3.14	2.14	1.52	1.18
165.00	4.06	2.74	1.85	1.35
170.00	5.48	3.73	2.42	1.64
175.00	7.26	5.12	3.29	2.10
180.00	8.27	6.07	3.95	2.48

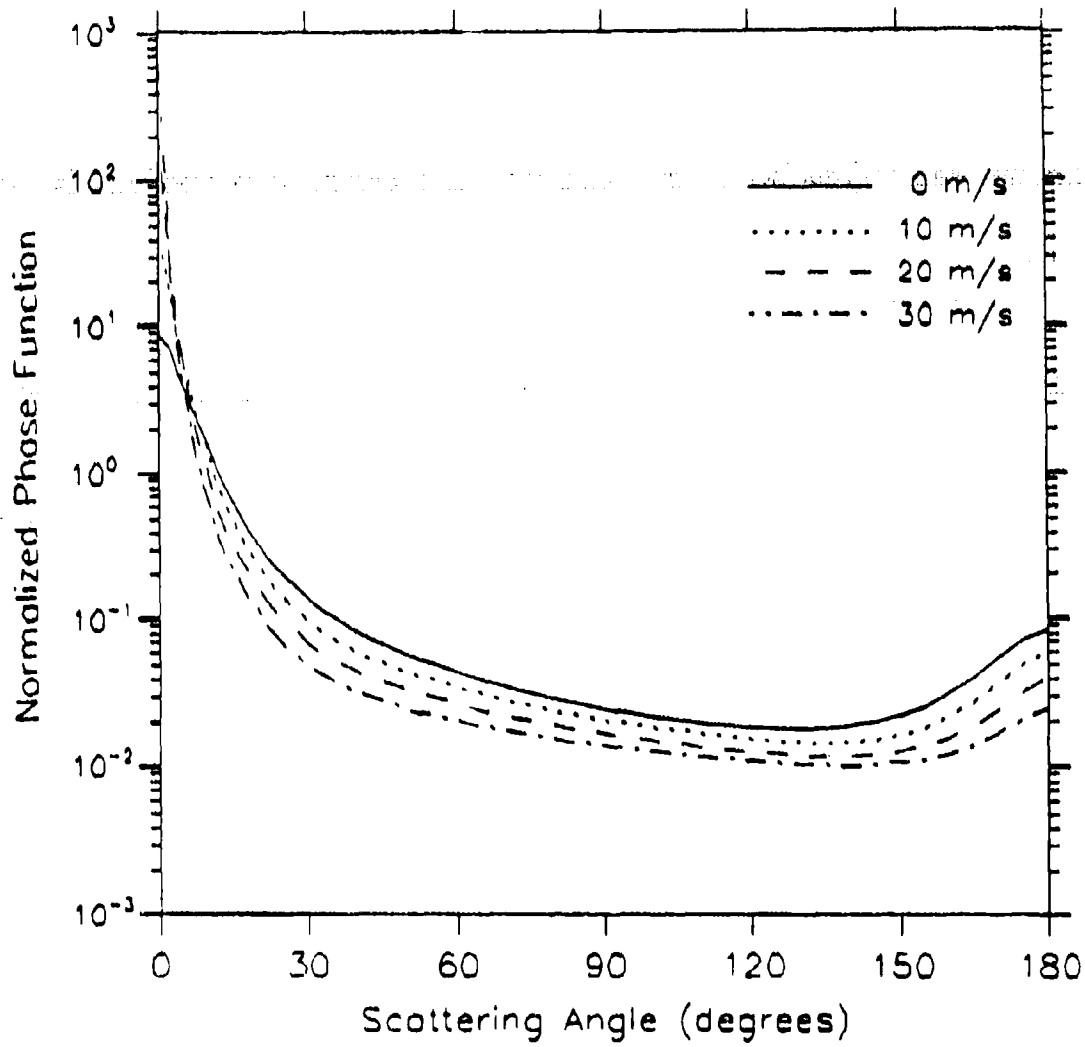


Figure C-3. Normalized Angular Scattering Function of the Desert Aerosol for a Wavelength of 10.591 μm